AD-A050 772 MISSION RESEARCH CORP LA JOLLA CA F/G 9/1
UGT NOISE MINIMIZATION TECHNIQUES.(U)
NOV 76 J B SMYTH, V A VAN LINT, M A MESSLER DNA001-76-C-0280
UNCLASSIFIED MRC/SD-R-7 DNA-4306F NL

1 OF 2
AD A050772

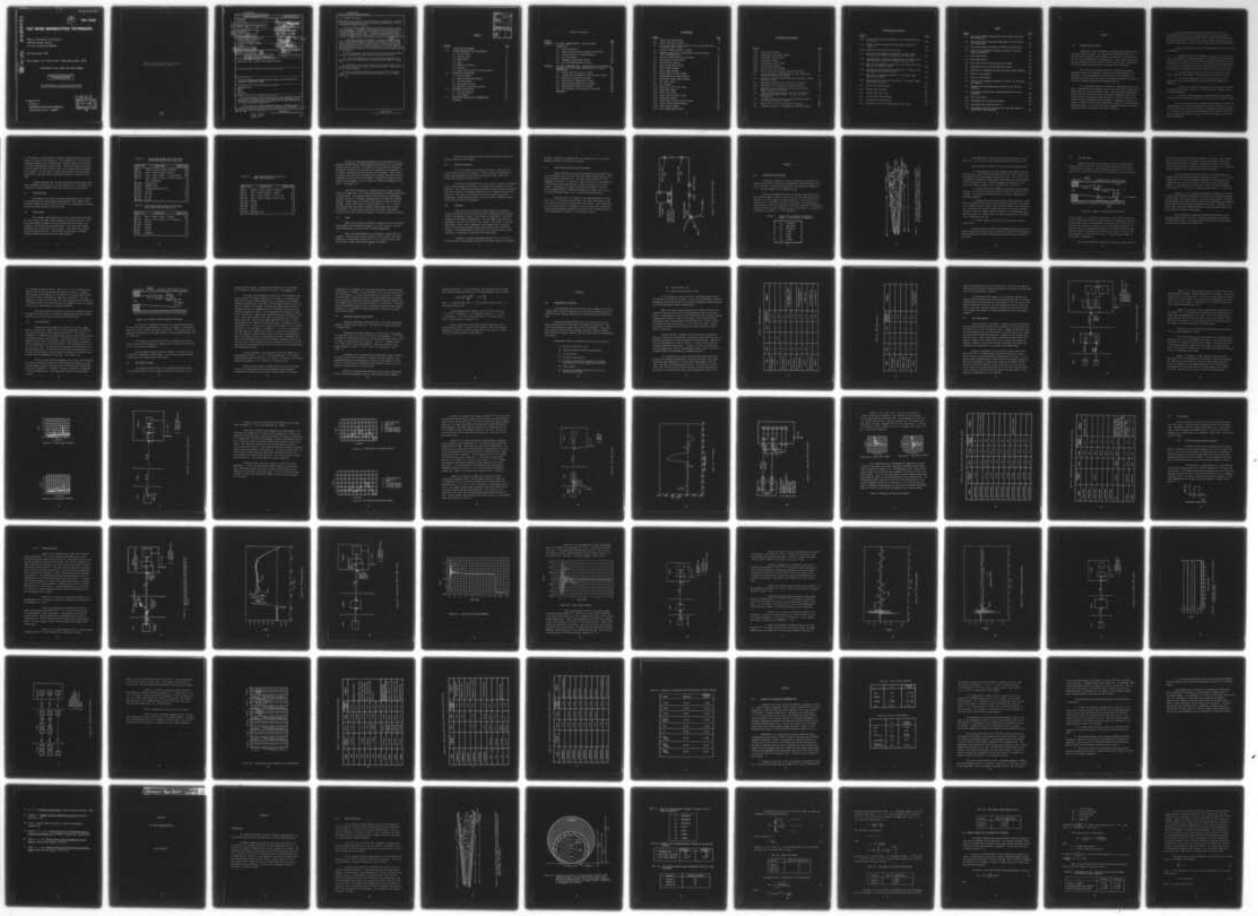

(12) B.S.

DNA 4306F

UGT NOISE MINIMIZATION TECHNIQUES

Mission Research Corporation
1150 Silverado Street
La Jolla, California 92037

30 November 1976

Final Report for Period April 1976—November 1976

CONTRACT No. DNA 001-76-C-0280

APPROVED FOR PUBLIC RELEASE;
DISTRIBUTION UNLIMITED.

THIS WORK SPONSORED BY THE DEFENSE NUCLEAR AGENCY
UNDER RDT&E RMSS CODE B345076462 J11AAXAX00439 H2590D.

Prepared for
Director
DEFENSE NUCLEAR AGENCY
Washington, D. C. 20305

Destroy this report when it is no longer needed. Do not return to sender.

UNCLASSIFIED

SECURITY CLASSIFICATION OF THIS PAGE *(When Data Entered)*

REPORT DOCUMENTATION PAGE

READ INSTRUCTIONS BEFORE COMPLETING FORM

1. REPORT NUMBER: DNA 4306F
2. GOVT ACCESSION NO.
3. RECIPIENT'S CATALOG NUMBER

4. TITLE *(and Subtitle)*: UGT NOISE MINIMIZATION TECHNIQUES

5. TYPE OF REPORT & PERIOD COVERED: Final Report, Apr [redacted]—Nov 76

6. PERFORMING ORG. REPORT NUMBER: MRC/SD-R-7

7. AUTHOR(s): John B. Smyth, Victor A. J. van Lint, Michael A. Messier

8. CONTRACT OR GRANT NUMBER(s): DNA 001-76-C-0280

9. PERFORMING ORGANIZATION NAME AND ADDRESS: Mission Research Corporation, 1150 Silverado Street, La Jolla, California 92037

10. PROGRAM ELEMENT, PROJECT, TASK AREA & WORK UNIT NUMBERS: NWET Subtask J11AAXAX004-39; PE 62710H

11. CONTROLLING OFFICE NAME AND ADDRESS: Director, Defense Nuclear Agency, Washington, D.C. 20305

12. REPORT DATE: 30 Nov [redacted] 76

13. NUMBER OF PAGES: ~~160~~ 158 pp.

14. MONITORING AGENCY NAME & ADDRESS *(if different from Controlling Office)*: DNA, SBIE

15. SECURITY CLASS *(of this report)*: UNCLASSIFIED

15a. DECLASSIFICATION/DOWNGRADING SCHEDULE

4306F, AD-E300 095

16. DISTRIBUTION STATEMENT *(of this Report)*

Approved for public release; distribution unlimited.

17. DISTRIBUTION STATEMENT *(of the abstract entered in Block 20, if different from Report)*

18. SUPPLEMENTARY NOTES

This work sponsored by the Defense Nuclear Agency under RDT&E RMSS Code B345076462 J11AAXAX00439 H2590D.

19. KEY WORDS *(Continue on reverse side if necessary and identify by block number)*

Underground Test
Noise
EMP
Grounding

20. ABSTRACT *(Continue on reverse side if necessary and identify by block number)*

The high-intensity radiation delivered by a nuclear explosion during an underground test produces large, fast current pulses on conductors and in the earth as a direct result of the interaction of the fast radiation pulse with the earth and test configuration.

These currents can produce transient voltages in experiment measuring circuits that interfere seriously with the experiments to be performed.

DD FORM 1 JAN 73 1473 EDITION OF 1 NOV 65 IS OBSOLETE

UNCLASSIFIED

SECURITY CLASSIFICATION OF THIS PAGE *(When Data Entered)*

392 797

20. ABSTRACT (Continued)

Experimenters have dealt with such interference by combinations of electrical and radiation shielding, grounding or electrical isolation, filtering, modulating and demodulating, etc.

This report addresses UGT-induced electrical noise in typical instrumentation systems. It addresses theoretically various potential radiation and electromagnetic interaction chains between the radiation output and interfering signals on data lines. It inspects many experimental records to check the observed noise signals against the predicted disturbances. It concludes that the following grounding and cabling practices are preferred:

1. Whether the sensors are grounded to the pipe or not, the cables from a given experiment should be enclosed in a conducting shield (zipper tube or pipe) until the cable run escapes from the radiation field and the electric field induced in the tunnel air and wall. This shield should be earth grounded at its end. The cable shields should be shorted together at this point, and more frequently as determined by the upper frequency response of the channel.

(2) The uphole cables should have their outer shields shorted together at the gas seal bulkhead, alcove splice rack and mesa splice rack.

(3) The transfer impedance for low-noise experiments should be minimized by using solid-shield cables and conducting foil bridges over connectors.

(4) Electrically pulsing the transmission line between cable shields and enclosing shield (e.g., zipper) is an effective means of quality control on the transfer impedance.

(5) The direct photon-induced cable currents should be minimized by using radiation shielding and solid-dielectric cables in the irradiated region.

CONTENTS

Contents (continued)

ILLUSTRATIONS

ILLUSTRATIONS (continued)

ILLUSTRATIONS (continued)

TABLES

SECTION 1

1.0 INTRODUCTION AND SUMMARY

Underground nuclear explosions are valuable experimental vehicles for nuclear effects studies. The high-intensity radiation delivered by a nuclear explosion produces strong effects on exposed test items as well as the rest of the underground test configuration. Large, fast current pulses flow on conductors and in the earth as a direct result of the interaction of the fast radiation pulse with the earth and test configuration.

These currents can produce transient voltages in experiment measuring circuits that interfere seriously with the measurements to be performed. Various experimenters have dealt with such interference by combinations of electrical and radiation shielding, grounding or electrical isolation, filtering, modulating and demodulating, etc.

To a significant degree, the practice of underground nuclear test (UGT) instrumentation has developed as an intuitive art based on qualitative appreciation of various interference terms. Each experienced experimenter has his favorite cassette and cable shielding and grounding scheme, with which he has had satisfactory experience and he is loath to vary from this scheme for fear of jeopardizing his experiment. Sometimes a scheme is applied in a regime (time and signal amplitude) for which it's not appropriate, leading to grief. It is also likely that considerable resources are being expended to satisfy unnecessary individual variations.

This report addresses UGT-induced electrical noise in typical instrumentation systems. We will address theoretically various potential radiation and electromagnetic interaction chains between the radiation output and interfering signals on data lines. We will inspect various experimental records to check the observed noise signals against the predicted disturbances.

Finally, we conclude that the following grounding and cabling practices are preferred.

1. Whether the sensors are grounded to the pipe or not, the cables from a given experiment should be enclosed in a conducting shield (zipper tube or pipe) until the cable run escapes from the radiation field and the electric field induced in the tunnel air and wall. This shield should be earth grounded at its end. The cable shields should be shorted together at this point, and more frequently as determined by the upper frequency response of the channel.

2. The uphole cables should have their outer shields shorted together at the gas seal bulkhead, alcove splice rack and mesa splice rack.

3. The transfer impedance for low-noise experiments should be minimized by using solid-shield cables and conducting foil bridges over connectors.

4. Electrically pulsing the transmission line between cable shields and enclosing shield (e.g., zipper) is an effective means of quality control on transfer impedance.

5. The direct photon-induced cable currents should be minimized by using radiation shielding and solid-dielectric cables in the irradiated region.

Section 2 of this report will summarize the parameters of typical UGT configurations. In Section 3, we summarize the results of theoretical calculations, the details of which are presented in Appendices A and B and Reference 1. In Section 4, we present typical experimental noise records for fast and slow, low-level data channels. Section 5 presents a discussion, conclusions and recommendations.

SECTION 2

2.0 TYPICAL UNDERGROUND TEST CONFIGURATION

2.1 Physical Layout

A typical underground test configuration is shown in Figure 2.1.[2,3] There are usually two horizontal tunnels that are essentially parallel (within $\sim 5°$) for about 75 percent of the length of their paths from the portal area. The bypass drift (tunnel) bends away from the main tunnel then loops around the source or Working Point (W.P.) and closes on the main tunnel (drift).

A pipe is placed in the main [line-of-sight (LOS)] drift. This pipe consists of two (or more) discrete conical frusta with a test chamber (T.C.) at the base of each cone. The aperture of the pipe is about 6 inches at its beginning, usually about 5 feet from the source. The pipe will diverge to a diameter of about 10 feet (at 65 - 80 percent of the total pipe length, depending upon the number of frusta) where the next conical section will begin. The diameter of any succeeding sections is typically 70 percent of the ending diameter of its preceding section. The test regions within the chambers are comprised of the remaining area, that is not the aperture for the next section.[2,4]

The pipe itself is supported above the railroad tracks which run the length of the tunnel. Adjustments are made to align the pipe with screw jacks that remain during the shot. There is a grounding rod

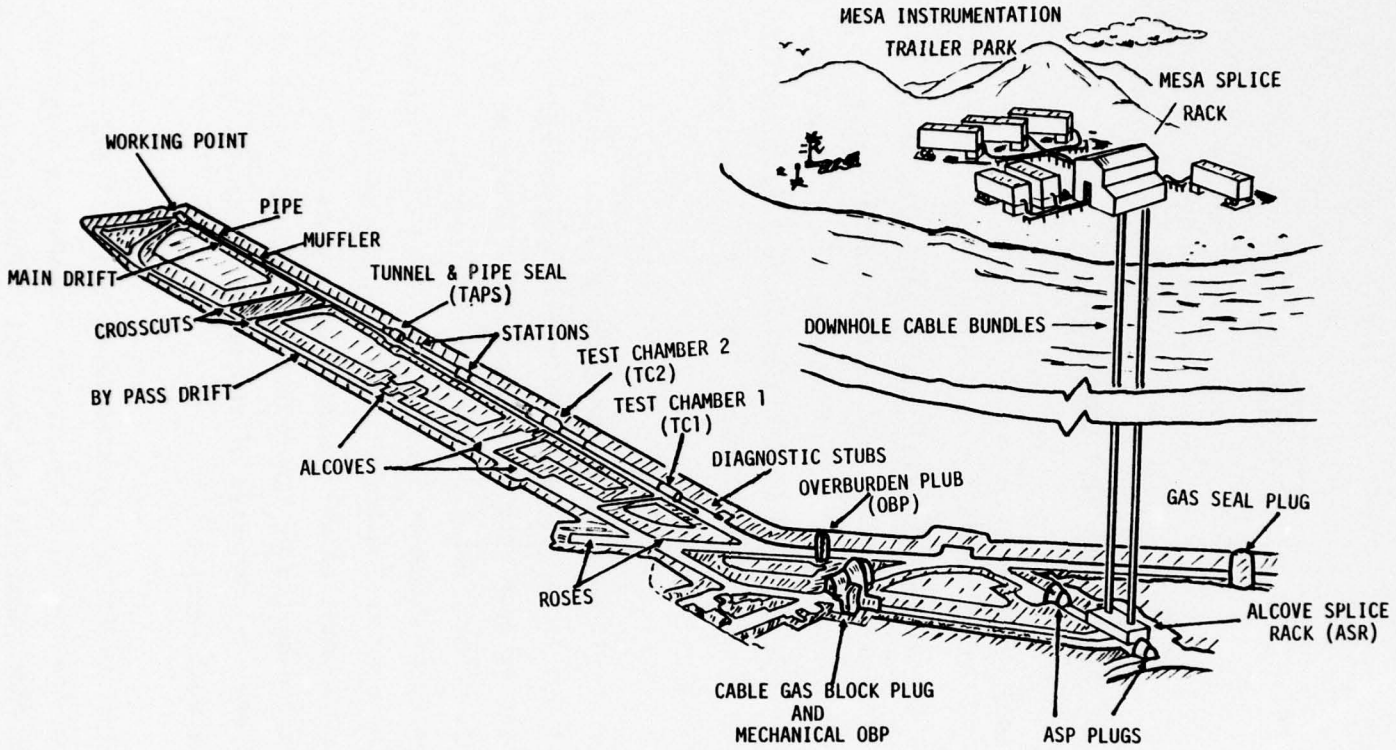

Figure 2.1. Typical UGT configuration.

(1 inch diameter, several strands of number 4 copper) which runs the entire length of the pipe on the tunnel wall. This grounding rod is electrically connected (bolted) to the railroad tracks, generally where the screw jacks are located (approximately every 20 feet). The pipe is sometimes in metal-to-metal contact with the railroad tracks, and in some places in intentionally grounded. In some cases, the screw jacks appear to sit on the damp ground next to the rails with no intentional electrical connection to the rails.

Stemming material fills the void between the main LOS pipe and the tunnel surfaces out to about 600 - 650 feet from the W.P. The bypass drift is filled to a distance about 75 feet less than that of the main drift.

2.2 Recording Areas

Recording of active data is usually accomplished in two locations: (1) Recording and Oscilloscope Sealed Environmental System (ROSES) within the tunnel complex (a special alcove or drift); (2) instrumentation trailers located some 1200-1400 feet on the mesa above.

2.3 Cable System

The permanent cable plant consists of an alcove splice rack (ASR) and a mesa splice rack (MSR) located about 1300 feet above the ASR. Cables are routed downhole through two 24-inch diameter cased drill holes from the MSR to the ASR and then filled with sand.[4] The splice racks connect the Rainier Mesa Trailer park with the tunnel. These cables are spliced at both the MSR and the ASR. A third cable hole 20 inches in diameter connects the HFR trailer park with the tunnel complex.[4]

Table 2.1 Cable usage between Alcove Splice Rack and Mesa Splice Rack (for Dining Car)

CABLE TYPE	DESCRIPTION	NUMBER USED
RG 22	Twinax, 2 inner Cu Cond. 2 Shields	133
RG 213	Coax, 1 inner Cu Cond. 1 Shield	168
RG 331	Coax, 1 inner Cu Cond. 1-.5" Al tube Sh.	84
RG 333	Coax, 1 inner Cu Cond., 1-7/8" Al tube Sh.	47
	3/8 " Foam Heliax	7
12 each	Conductor #16	5
26 each	Conductor #16	5
9 each	Twisted Shielded Pair #16	8
15 each	TSP #22	16
19 each	TSP #22	32
23 each	PR #19	3
50 each	PR #19	2

Table 2.2 Cable usage between tunnel and Dido Queen HFR Trailer Park (for Dining Car)

CABLE TYPE	DESCRIPTION	NUMBER USED
RG 213	Coax, 1 inner Cu Cond., 1 Shield	45
RG 331	Coax, 1 inner Cu Cond., 1-.5" Al tube Sh.	6
20 each	TSP #22	3
16 each	TSP #22	6
6 each	TSP #22	15
6 each	TSP #16	3
4 each	Conductor	2

Table 2.3 Cable usage between Experiment and ROSES (for Dining Car)

CABLE TYPE	DESCRIPTION	NUMBER USED
RG 22	Twinax, 2 inner Cu Cond., 2 Shields	7
RG 213	Coax, 1 inner Cu Cond., 1 Shield	22
RG 331	Coax, 1 inner Cu Cond., 1-.5" Al. Sh.	83
RG 333	Coax, 1 inner Cu Cond., 1-7/8" Al. Sh.	56
16 each	TSP #22	6
10 each	TSP #22	1
20 each	TSP #22	2
9 each	TSP #16	2
12 each	Conductors #16	1

On the mesa, matching multiconductor and coaxial cables are connected at the MSR and are routed through elevated metal trays to recording systems inside the trailers. The metal cable trays while not physically connected to the MSR or to the trailers are connected to earth ground. In the tunnel, cables are run from the ASR to the experiment. These cables, in general, are routed down the bypass drift, through a crosscut to the experimenter's alcove, and on to the sensor. Typical cable length from the trailer to Test Chamber 1 (TC-1) is 3850 feet (±300 feet depending on the shot). (See Figure 2.2)

Cables which penetrate the stemming materials are gas blocked within the stemmed area. All cables penetrating the overburden plugs (OBP's) are gas blocked. The standard design of the gas block is a feedthrough connector mounted in a fiberglass bulkhead which is backed with stemming material. Cables going to the mesa are gas blocked at both the ASR and the MSR. Typical cable usage is listed in Tables 2.1 - 2.3.[4] Some of the downhole cables are used to transmit timing signals from the Mesa Trailer Park to a tunnel timing and firing slave station (Red Shack). Cables from the slave station are routed to locations requiring the timing.

2.4 Power

Power for the trailers and ROSES is supplied by either the Nevada Power Company with isolation transformers or, in some cases, by on-site gasoline generators, which are usually isolated from ground.

Some of the experimenters use car batteries to power their experiments. The batteries, usually located in their trailers, have cables running to an alcove where they use D.C. to A.C. power inverters to run their alcove's signal conditioning equipment and sensors.

Power for the tunnel and for the timing and firing is again provided by the Nevada Power Company.

2.5 Radiation Shielding

It is not uncommon for shielding to be used to reduce the flux to the cassette as well as the cables.[5] Lead or sand (or a combination of the two) are sometimes used to shield the sensor and cables (until the cables reach the alcove) from the flux.[5]

One method of reducing the flux in the pipe is to place a perforated steel plate in the path of the beam. For example, such a plate was used on Husky Pup. This scattering plate contained holes on one half which transmitted 56% of the incident x-ray radiation and holes on the second half which transmitted 32%. The plate was 27 gauge steel (0.40 cm) and was essentially transparent to photon radiation above a few tens of keV. Additional details of this filter are given in Appendix A.

2.6 Grounding

There are two basic grounding schemes employed on these tests. The first is that the entire electrical system, including the trailer shell, "float" with respect to ground. The trailers are supported by a crushable honeycomb to withstand the groundshock. The only common point within one experimenter's system is the shell of his trailer. The system is isolated from ground, from all other experiments, and from the pipe. The second scheme is to ground the cassette and the cable shield at the cassette to the pipe. The instrumentation trailer shell is not tied directly to earth ground but is electrically connected to the cable shields.

In general, some pipe experiments performed at TC-1, TC-2, or TC-3 have their circuit ground isolated from the pipe; others are grounded to

the pipe. Experiments performed closer in (toward the W.P.) are usually grounded to earth or the pipe at the sensor.[6]

2.7 Signal Conditioning and Cable Equalizers

Signal conditioning is usually accomplished in the tunnel alcove. For slow-response, low-level data, the signal conditioning usually consists of an operational amplifier (i.e., Fairchild μA725) followed by a low-impedance line driver. In some cases, optical couplers have been employed in the signal conditioning package to isolate the sensor and recorder grounds. Multiplexing of signals within one experimenter's system is not an uncommon practice. Modulation-demodulation schemes are also used for medium frequency signals (e.g., strain or displacement gages).

Cable equalizers are inserted at the instrumentation end of the cable run to correct for the distortion of the signal introduced by long coax cable runs between the detector and the recording. Cable attenuation is an increasing function of frequency; an equalizer provides attenuation with an inverse frequency dependence to produce a total attenuation essentially independent of frequency in the region of interest.

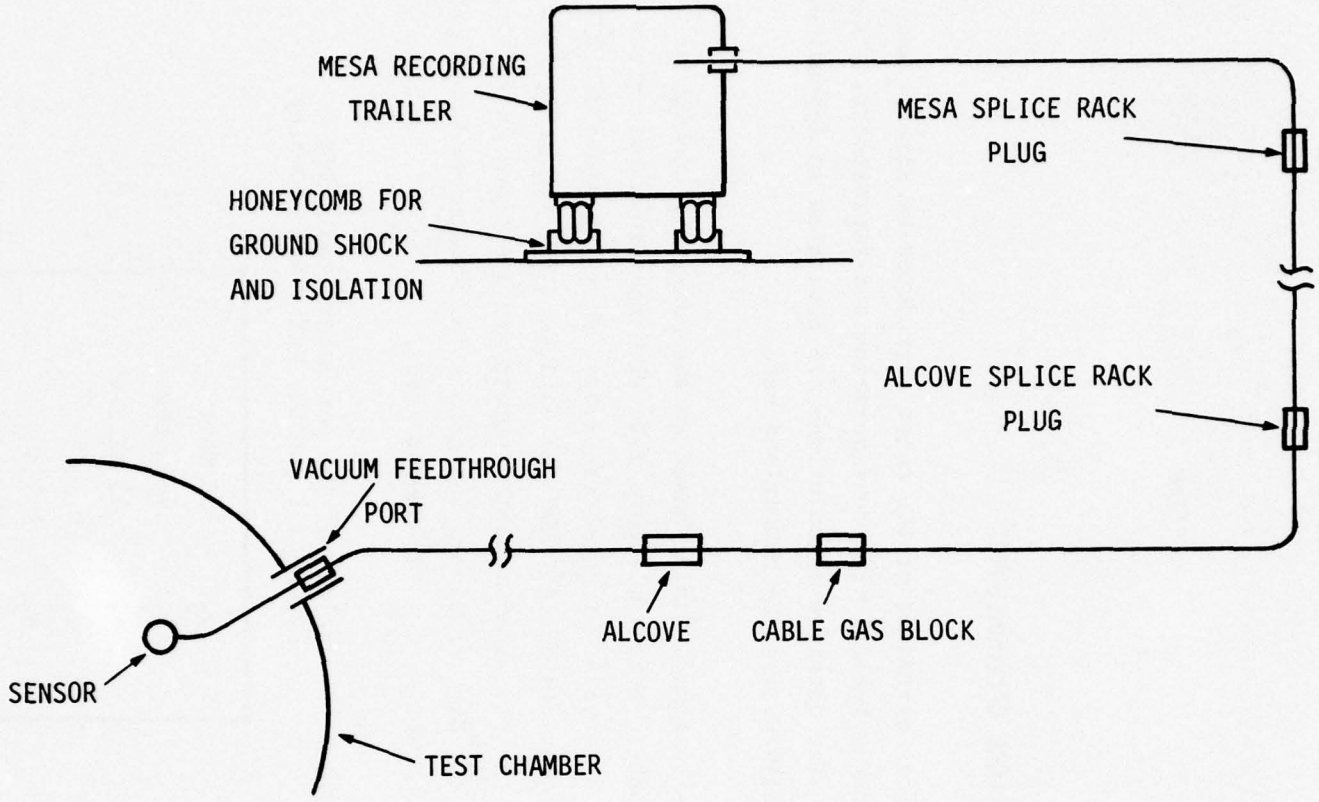

Figure 2.2 Typical cable path to mesa.

SECTION 3

3.0 THEORECTICAL CALCULATIONS

Theoretical estimates of the noise introduced by several mechanisms were made for a typical pipe configuration and representative x-ray and γ-ray yields. The detailed calculations are presented in Appendices 1 - 6. Only the results will be summarized here.

The pipe configuration is based on the Husky Pup configuration.[3] The simplified model is shown in Figure 3.1, with the dimensions given in Table 3.1. For the purposes of these estimates, an x-ray yield of 10^{12} calories and a γ-ray yield of 10^{23} MeV was assumed. The resulting flux time histories at the two experimental stations are described in Reference 1. At the far end of the pipe (inside), the peak x-ray fluence is $\sim$ 100 cal/cm^2 and the peak γ-ray flux is 2×10^{24} MeV/m^2/sec .

Table 3.1 Values of the parameters indicated in Figure 3.1 for the Husky Pup geometry.[3]

h_3:	183 meters
h_1:	298 meters
h_2:	243 meters
θ_1:	0.235°
θ_2:	0.354°
θ_3:	0.534
θ_4:	0.0656°

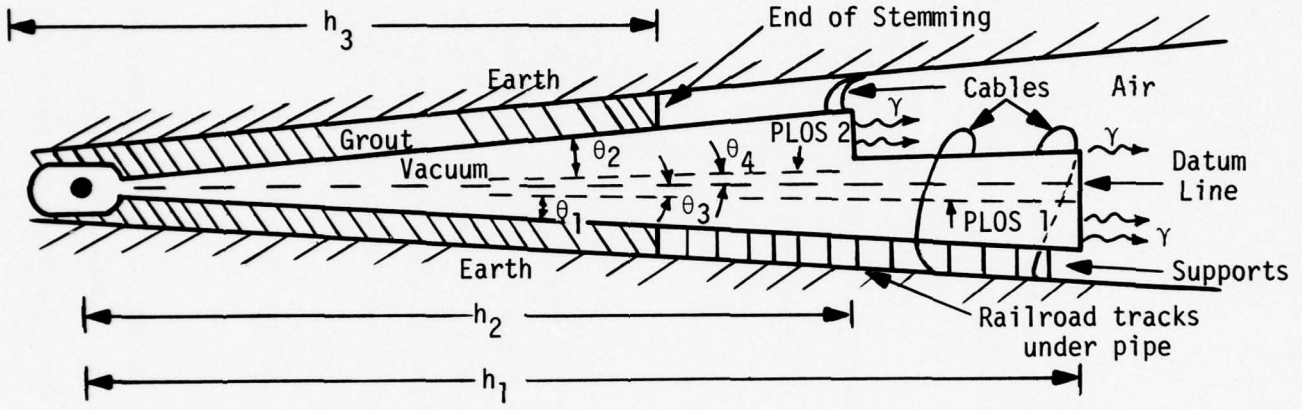

Figure 3.1 First order model of UGT geometry for use in the calculation of exterior pipe currents. Not drawn to scale. Values of the indicated parameters are given in Table 2.1 for Husky Pup.[3]

The ground around the pipe has been characterized by a conductivity of 1.5×10^{-2} mho/m and a relative dielectric constant of 20.

The four possible sources of noise that were investigated are:

1. Electromagnetic pulse (EMP) coupling into cables protruding from the pipe. These are shield currents due to the electric fields set up parallel to the tunnel beyond the end of the pipe. The electric field is generated by Compton electrons emitted from the pipe and those created in the air beyond the pipe. Unless the gammas are stopped in a thick shield, the field is found to have a peak value of 2×10^{5} V/m .

2. Systems Generated EMP (SGEMP) on ungrounded cassette within the pipe. This current replaces the electrons that were emitted from the cassette. The replacement currents due to x-rays and γ-radiation were evaluated separately.

3. Ringing modes set up in the line-of-sight (LOS) pipe. These modes are caused by the electric fields outside the pipe that are produced by the Compton electrons from the pipe and those formed in the surrounding air. The mode can be excited by gamma rays exiting at either experiment station or along the tapered length of the pipe. It can propagate along the transmission line formed between the pipe and tunnel wall, reflecting at the stemming and pipe end.

4. Currents induced in cables by direct photon and neutron interactions.

Sources of noise that were not investigated, because they were outside the scope of the present effort, include the coupling of electromagnetic fields propagating away from the pipe and main drift into cables buried in the earth.

3.1 EMP into Cables

Gamma rays exiting the vacuum pipe at the two stations create Compton currents in the air. These drive horizontal electric fields of the form shown in Reference 7 and illustrated in Figure 3.2. The field shown there is that which would exist in the absence of the pipe or ground.

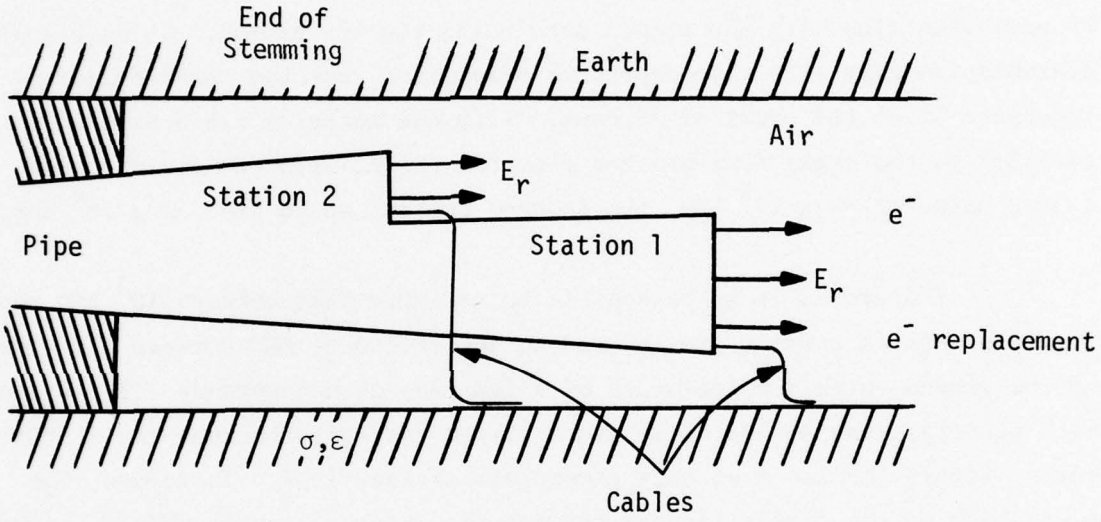

Figure 3.2. Sources of EMP excitation of cables.

It has a peak of $\sim 2 \times 10^5$ V/m. The presence of the various structures and the ground causes fields of other polarities to be generated and causes the horizontal field to be decreased in some places, such as the side of the pipe, and increased in others, such as at the station bulkheads. In addition, the air is conducting during the time that the field is present. Near the electric field peak, the conductivity is about 10^{-2} mho/m and the skin depth is on the order of 1 meter. The peak Compton current is 3000 amp/m^2 . (Reference 1)

The current running on a cable shield, before it leaves the main

drift and enters the ground, can be estimated in two ways. First, assume that all the current which is emitted from the pipe within a skin depth radius around the cable is returned as replacement current on the shield. Then, with a skin depth of one meter, the current is seen to be $\sim$ 9000 amps times the length of the irradiated cable along the tunnel.

The second estimate is made by modeling the cable shield as a transmission line with the return path being the air plasma. It is a lossy transmission line with time-dependent parameters, but the characteristic impedance is on the order of 10 ohms. With one meter of cable exposed parallel to the gamma flux and the electric field, with the field having a peak value of 2×10^5 V/m, the induced current would be $\sim 2 \times 10^4$ amp.

Therefore, it is reasonable to estimate that between 10^3 amp and 10^4 amp of shield current are induced on the shield by EMP between the pipe and the ground, with a pulse width of a few tens of nanoseconds. The fields which penetrate the shield will have a slower rise-time because the diffusion process favors the low frequency components of the field. Therefore, the pulse width of the fields induced between the inner and outer shield can be on the order of hundreds of nanoseconds.

This problem can be reduced by minimizing the length of cable along the tunnel exposed in the air, shielding the gamma ray flux behind the experiment stations, and using an outer shield around the cable bundle to decrease the coupling into signal wires.

3.2 SGEMP on Ungrounded Cassettes

Calculations were made for the purpose of estimating x-ray and gamma induced SGEMP currents on the shields of cables leading from ungrounded cassettes. The estimates described in Appendix A for the geometry illustrated in Figure 3.3 indicated that the x-ray induced currents were negligible, at least after steady state conditions have been established. These conditions are set up within a few tenths of a nanosecond. There are several factors which account for such small responses. First, under these high flux levels, the characteristic distances over which the electrons travel are only a few hundredths to tenths of a centimeter. Certain of the voltage-generating mechanisms cancel each other out under these conditions and there is very little, if any, charge transfer between cassette and ground. If the cassette was close enough to ground to allow charge transfer, the capacitance would have to be so large as to effectively short circuit the system. In any case, the plasma resistance would be low enough to act as a good short to ground.

Gamma-ray induced SGEMP is not ordinarily considered a serious charge-generating mechanism compared to the x-ray mechanism. However, under the conditions described above, when x-rays are ineffective, the gamma-ray mechanism can play a dominant role. High-energy electrons ($\sim$ 1 MeV) are emitted from the cassette and can travel large distances to the ground plane. A transfer current following the gamma flux time history with a peak of several thousand amps/m^2 is set up by the gammas. There is some question as to how well the x-ray induced plasma can short the cassette to ground, but if the gap is $\gtrsim$ 1 cm , the x-ray plasma should be confined well enough to be prevented from interfering.

As an example, a calculation was made in Appendix A in which the shield current was estimated for a cassette in the shape of a cylinder. The cylinder radius was 5 cm, as was its height. The cylinder was surrounded

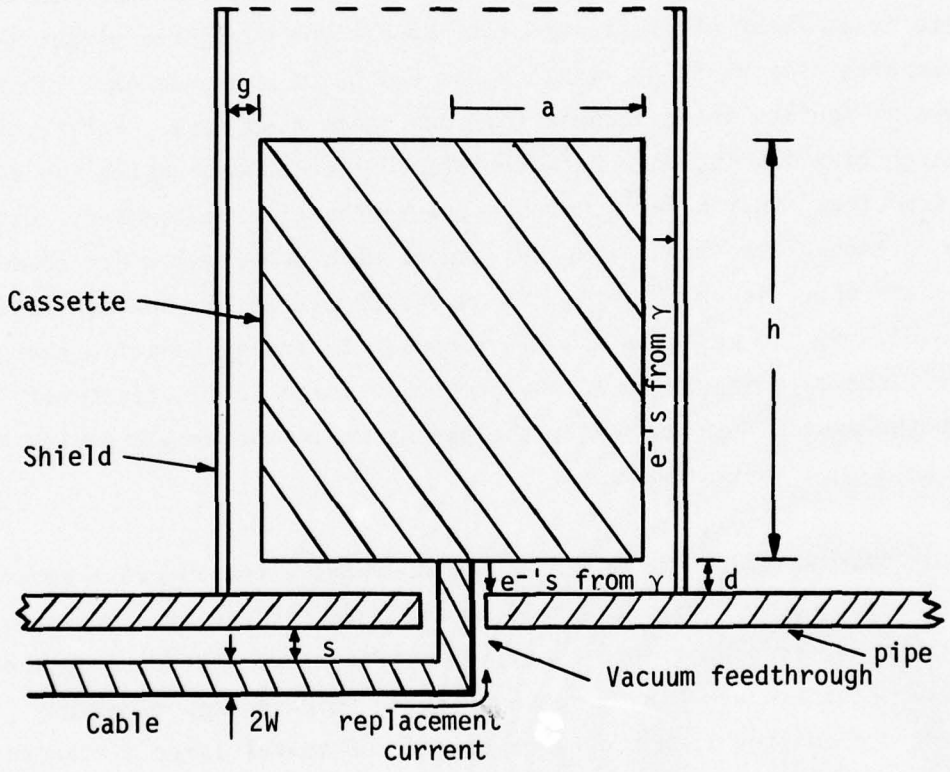

Figure 3.3 Schematic diagram of a representative shielded cassette with a floating ground.

by a grounded cylindrical shield. There was a 0.5 cm gap between the cassette and both the ground plane and the outer cylinder. Assuming a peak transfer current density of 1000 amp/m^2 , the cable shield current was about 10 amps and followed the gamma flux time history. The load impedance was taken to be 100 ohms. The load consists of the transmission line formed by the cable shield running a few centimeters above an infinite ground plane which represents the LOS pipe bulkhead.

The shield current will follow a time history somewhere between the gamma time history and its integral, depending upon the time constant defined by the cassette capacitance and the load resistance.

3.3 LOS Pipe Ringing

The EMP produced by gamma rays in the air can excite ringing modes on the LOS pipe. Radial electric fields propagating back and forth can couple into cables running radially away from it. This can be interpreted as a difference in ground potential between cable shields exiting from different points along the pipe. These radial electric fields will generally be less than the horizontal fields described above, being generated by gradients in the horizontal fields. Peak amplitudes are in the 10^4 - 10^5 V/m range. The time histories resemble the time derivative of the horizontal field. The exact form of these fields and the nature of the pipe ringing depends critically upon the placement of obstacles around the pipe and on the grounding of the pipe. (See Figure 3.4)

If the pipe were totally ungrounded, just a metal stub surrounded by a meter of air and an earth wall, waves would travel along it at about half the speed of light in free space and it would ring as a quarter wave stub with a frequency of $\sim$ 500 KHz. The pipe is assumed to be grounded at the end stemming point. The ringing would decay an e-fold in about 5 cycles.

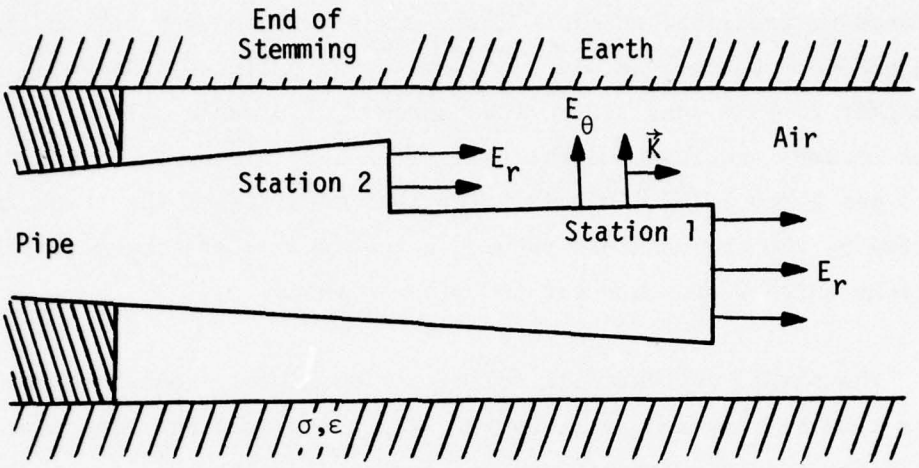

Figure 3.4. Sources of EMP excitation of LOS pipe.

If the pipe is ungrounded, but there are railroad tracks beneath it, and the tracks are not connected to the pipe by supports, a differential mode will be set up between the tracks and the pipe. These fields will ring relatively unattenuated at the speed of light in vacuum, producing many cycles of 1 MHz noise.

If the pipe is connected to the tracks by supports, and if this entire system can be considered as grounded to earth, the pipe will not ring at all. The system is overdamped.

More experimental effort should be exerted in this area if one is to define the importance of pipe ringing. In any case, grounding the pipe to the tracks will eliminate this noise source.

3.4 Cable Bundle Ringing

The ringing of cable shields in the common mode does not appear to be a problem because of the attenuation caused by the presence of the

finite conducting ground. Representative attenuation e-fold distances are 10 meters at 1 MHz and 100 meters at 100 kHz. (See Appendix B)

For cable shield ringing to be important, the differential mode between shields of different cables must be excited. In a bundle with cables which are not grounded together and, in addition, have different grounding configurations at the ends, the differential mode should not be hard to stimulate. For example, the gamma ray SGEMP signal from one ungrounded cassette will immediately set up a differential mode with the cables from grounded cassettes. The propagation of these modes is aided by the existence of a zipper shield, which prevents any dissipation by the earth. Since cable lengths on the order of a kilometer are involved for uphole cable runs, even the small gamma SGEMP shield current ($\sim$ 10 amp) can transfer to the interior of the coaxial cable. As examples, even if solid-shield cable is used, over a length of one kilometer, with a transfer impedance of 0.2 milliohm/m [7], a voltage of $\sim$ 2 volts can be generated in the coax; and with a length of 100 meters, .2 volts could be predicted. This can continue to occur for many cycles, and brings up the possibility that, if the phase velocity of waves inside the cable is different from that of the differential mode outside the cable, a beating of the two signals can occur. This would result in an oscillation of lower, but varying, frequency and a peak which occurs later in time than would be expected from EMP considerations alone.

In many experiments, the cable shields are tied together at an instrumentation alcove $\sim$ 10 - 30 m from the experiment. If a single-braid-shielded cable were used ($Z_T \sim$ 10 m ohm/m) [7], the same 10 A of shield current would produce $\sim$ 3 V of noise in a 30 m cable run.

Since the cable bundle in common mode with earth return makes a very lossy transmission line and the transmission lines formed by differential excitation of cable shields within a bundle are effective

propagators, it is important to avoid differential mode excitation between cable shields in a bundle. For the EMP drive, this can be achieved by overall EM shielding (i.e., zipper tube grounded at its terminus). For SGEMP excitation from a single test cassette, the differential mode excitation must be spoiled by grounding the shields together frequently enough so that the standing waves will be too high frequency to be of concern. If cables from the ungrounded cassette are to be colocated with cables from grounded cassettes, it is important to separate them with a zipper tube or other solid overall shield.

3.5 Radiation Induced Cable Currents

Radiation impinging on individual cables will induce replacement currents flowing between conductors. The effects are usually most severe in coaxial cables.

The gamma ray induced current per unit dose rate in solid insulator coax cables (e.g. RG 11, RG 58, RG 59, RG 213) approaches $\sim 10^{-13}$ C/rad per meter of irradiated cable after an initial charge release that may occur at a rate ten times greater for a dose of $\sim 10^{3}$ rad .[8] (Charge release $\sim 10^{-9}$ C/m) Semi-solid or foam dielectric cables may exhibit initial charge release at a rate of $\sim 10^{-10}$ C/rad - m, saturating at $\sim 10^{-12}$ C/rad - m.

The gamma dose to cables behind the experiment stations is likely to be less than the value required to saturate the cable response. The assumed radiation flux (see beginning of Section 3) may produce a current of up to 0.1 A per meter of irradiated solid-dielectric cable, or 10 A per meter of irradiated foam or semi-solid cable.

Neutrons also produce cable currents, both by direct interaction in the cable and by producing inelastic scattering and capture gammas in

surrounding materials. In most experiments, the neutron arrival is appreciably delayed from photon arrival by the energy-dependent time of flight

$$t(\text{sec}) \approx \left(L \frac{7 \times 10^{-8}}{\sqrt{E}} - 3 \times 10^{-9} \right)$$

where L is the distance from W. P. to the station in meters and E is the neutron energy in MeV.

Neutron-induced cable currents vary from initial values of $\sim 3 \times 10^{-19}$ C - cm^2/neutron - m to asymptotic values of $\sim 1 \times 10^{-21}$ C - cm^2/neutron - m in solid dielectric cables.[8] Foam cables may exhibit a signal larger by a factor of 30.

These signals can be minimized by massive shielding, use of solid-dielectric cables, at least in the radiation field, and selection (probably by irradiation tests on samples from a cable spool) of cables that do not exhibit anomalous charge release.

SECTION 4

4.0 EXPERIMENTAL DATA REVIEW

The experimental data was reviewed to find examples of zero-time ("gamma flash") noise for comparison with theoretical predictions, and to identify the best cabling techniques for fast data and for low-level slow data.

Several underground nuclear tests were extensively reviewed. These included Husky Pup, Dido Queen, Ming Blade, and Dining Car. Some of the work performed on Mighty Epic was also investigated. These tests were selected because of the availability of Project Officer's Reports, their relatively constant geometry, and their state-of-the-art experimental data systems.

Experimental records were examined for each of the following:

(a) physical layout of the test,

(b) transducer distance from the working point,

(c) all cable types,

(d) individual cable lengths,

(e) shielding, grounding and coupling at transducer, instrumentation, and all intermediate locations,

(f) cable routing,

(g) cross-talk measurements made prior to the test (if made and recorded),

(h) signal observed, and

(i) noise observed during the event.

In the majority of cases, the entire instrumentation system was not adequately described in the POR's. In the case of Ming Blade, additional information was obtained from the Prefielding Instrumentation Meeting Report and the Instrumentation Results Meeting Report.

Many of the data records presented in the POR's were those that would best represent the success of the measurements made by the experimenter. A large number of the raw data records were of poor quality, making interpretation difficult. Many of the records of good quality had been converted to units associated with the measurement (i.e., stress) necessitating that the noise be expressed in a ratio with the signal. Some of the records, unfortunately even those that recorded only noise, lacked units on either axis.

Wherever possible, reproduction of the raw data is presented. Where this could not be accomplished, the data was transcribed with care to preserve, undistorted, the data presented by the experimenter. General results for Ming Blade are listed in Table 4.1. Table 4.2 lists other experiments performed on Ming Blade. In Table 4.2, there is no hard data on the grounding used, however, the grounding scheme listed is one that is inferred based on the experimenter's grounding policies.

All instrumentation systems shown illustrate Ming Blade signal systems with recording accomplished in trailers on the mesa. All cables connecting these experiments to the mesa were approximately 3,500 feet long. They were fed through three gas blocks: one located at the tail drift, one at the Alcove Splice Rack, and one at the Mesa Splice Rack.[2] The cables are routed from the pipe to the experimenter's alcove to the

Table 4.1. Ming blade results.

GAGE	GOOD	?	BAD	GROUNDING SEE FIG. #	COMMENTS
Linear Velocity (LVT)	17	-	-	4.14	
LVT	18	20	2	4.16	
Fast Spectral	19	-	-	4.1	
Strain	21	-	-	4.19	A large number of gages not reported on
Calorimeter	36	-	-	4.22	
Thermocouple	22	-	4	4.24	1 gage not reported on, 1 with noise
Quartz	16	-	-	4.3	2 with noise
Carbon Pressure	11	-	7	4.6	9 not reported on
Quartz	-	-	-	4.26	2 not reported on

Table 4.2. Ming blade results.

GAGE	GOOD	?	BAD	GROUNDING INFERRED SEE FIG. #	COMMENTS
Displacement	7	6	5	4.14	
Momentum	9	-	-	4.16	
Compton Diode	1	1	-	4.1	
X-Ray Diode	11	-	2	4.1	
Strain	3	1	-	4.16	First 180 μsec of data invalid

bypass drift and then to the Alcove Splice Rack. They then went uphole to the Mesa Splice Rack where they were branched on electrically isolated metal trays to the experimenter's trailer.[2]

In the following data summary, we will present separately the response of fast channels (coax cables and oscilloscopes) and slow channels (twisted pairs and oscilloscopes or tape-recorders). In terms of the noise signals discussed in Section 3, the fast channels are able to record the noise in real time; the slow channels are effectively excited by an electrical impulse and respond in a manner determined by their own frequency response.

4.1 Fast Data Channels

Fast data channels (bandwidth > 20 MHz) are used for measuring the time-resolved radiation pulse and the response of test items that tend to follow, more or less, the radiation pulse. Examples of radiation diagnostics instruments are x-ray diodes (XRD), filter-fluorescers, PIN diodes, and scintillator-photodiode combinations. Examples of fast response test items are quartz, carbon stress gauges, and Radiation Induced Pulse (RIP) signals. Formerly, fast channels were used to measure the response of electronic materials and devices, but these experiments were effectively completed with Line-of-Sight-to-the-Surface UGT configurations.

Figure 4.1 represents the fast spectral signal system used on Ming Blade.[9f,10a] A floating ground scheme was employed with either RG 213 or RG 214 coax running from the transducer to the alcove. In the alcove, signal conditioning was accomplished with one channel delayed and fed into an unmatched tee (reducing the signal by 33 percent) and then sent to the trailer on foamflex (RG 331 or RG 333) to the mesa trailer. At the trailer, the signals were equalized and fed into a matched tee for a dual recording. The coax shield was tied to the trailer shell. This system had a bandwidth of at least 150 MHz.

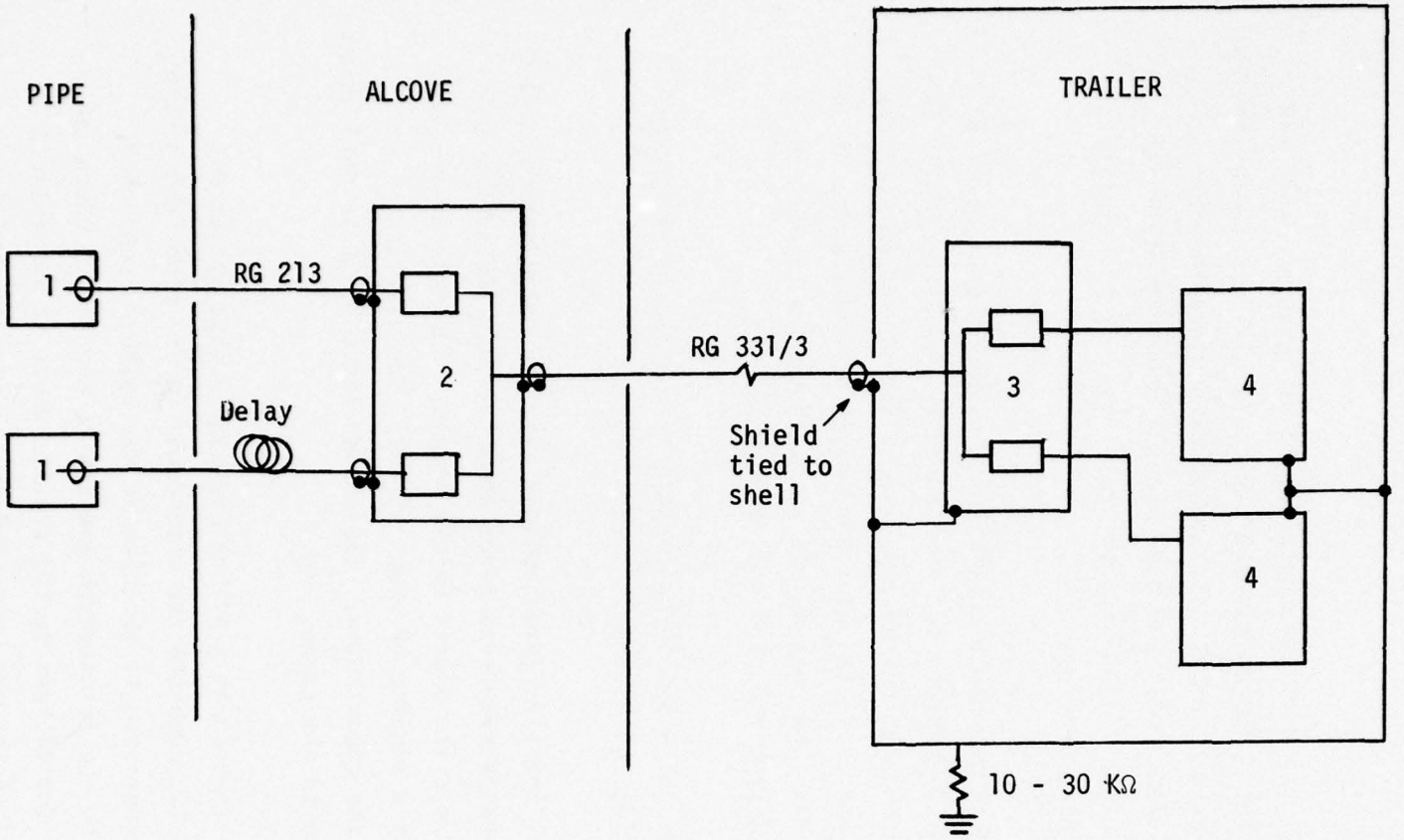

Figure 4.1. Fast spectral signal system.

Figure 4.2 is a digitized data record of an x-ray diode (XRD).[11] The bandwidth is 120 MHz. The multiplexed traces are similar. The initial negative pulse is a fiducial mark. The noise, if any, would occur at the same time as the XRD signal at ∿ +10 nsec, and is undetectable in the presence of the ∿ 200 V signal. The wiggles on the tail of the signal are due to imperfect matching, not noise.

Figure 4.3 represents a quartz gauge signal system utilized on Ming Blade.[9g,10c] RG 58 connects the transducer to the electrically isolated vacuum feedthrough port on the pipe. RG 214 coax transmitted the signal from the pipe portal to the alcove where it was spliced to RG 331 for the run to the mesa. The coax shield was tied to the trailer shell. The system is isolated from the pipe and from ground.

Figures 4.4 and 4.5 illustrate data from these quartz gauges.[12] It had a system bandwidth of 25 MHz.

The initial negative gamma spike drives the oscilloscope deflection off scale. The trace reappears after about .2 μsec indicating that the spike is very large with respect to the signal. The data trace prior to the signal exhibits a ringing of about 15 MHz. The signal arrives about 1.5 μsec after the gamma spike. The second large positive deflection is due to a reflection in the gauge.

Figure 4.6 represents a carbon pressure signal system for Ming Blade.[9c,10h] RG 223 connects the transducer to the pipe feedthrough. The cable shield was connected to the pipe at the bulkhead connector. RG 214 was connected to the feedthrough and ran to the alcove where it was spliced to RG 331 for the run to the trailer where it was spliced to RG 213. The shield of the coax was tied to the trailer shell.

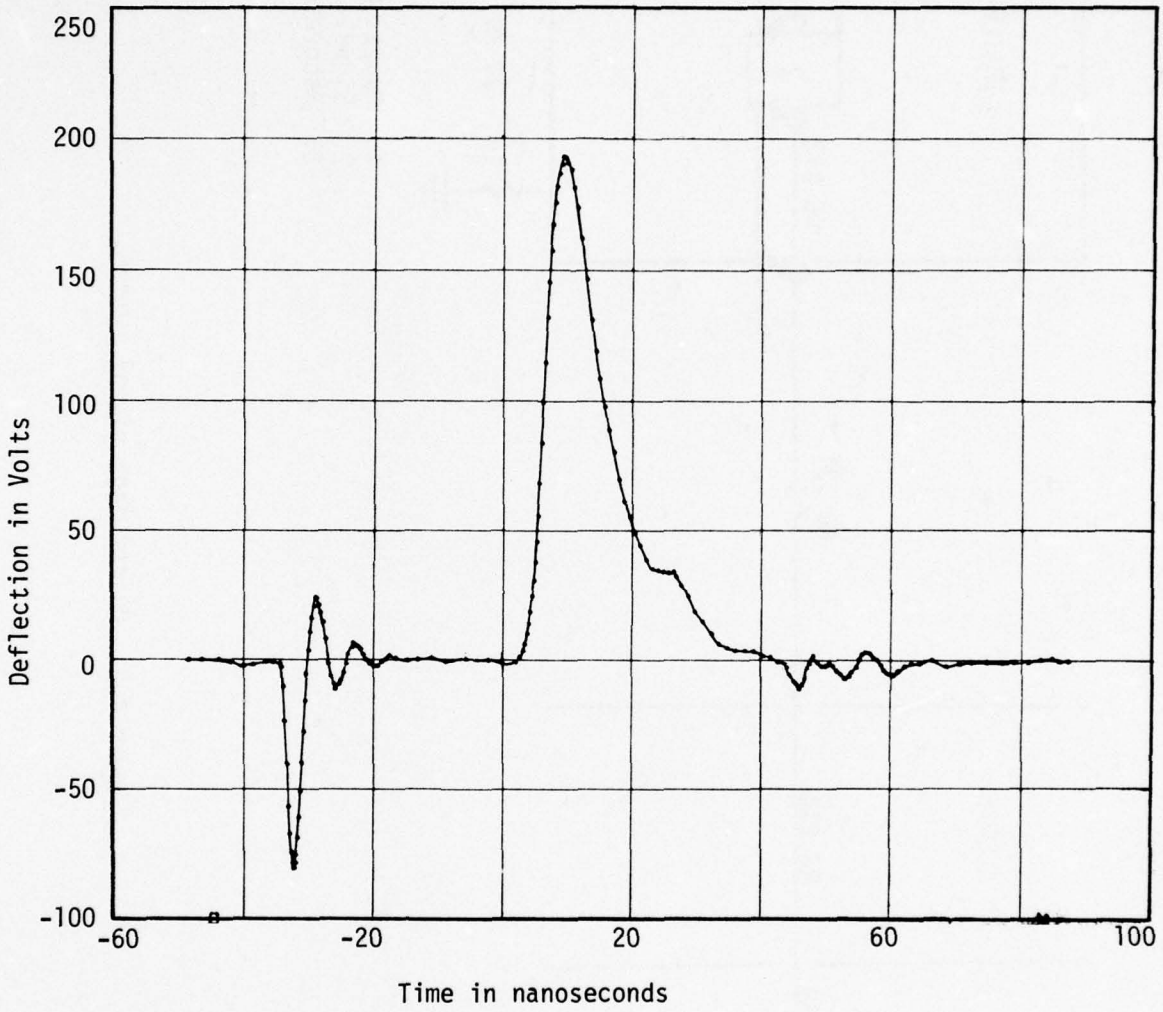

Figure 4.2. XRD digitized response.

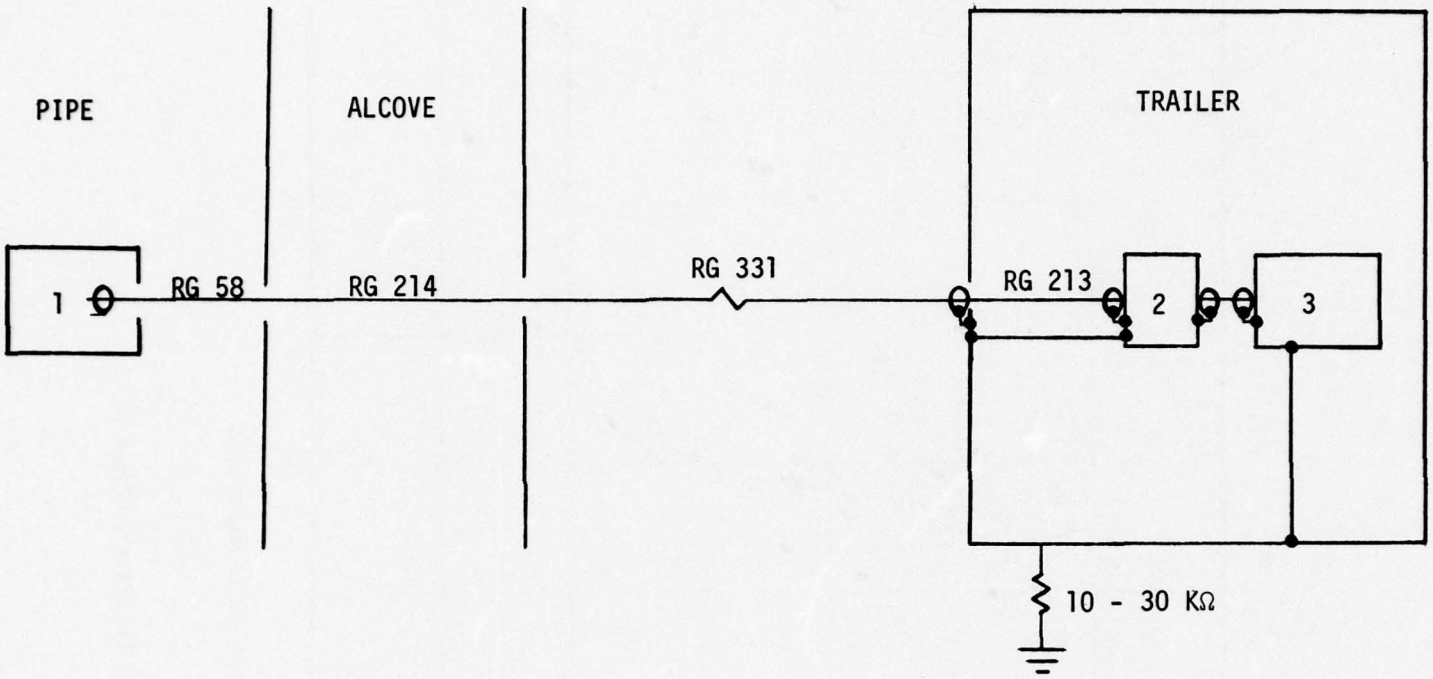

Figure 4.3. Quartz gage signal system.

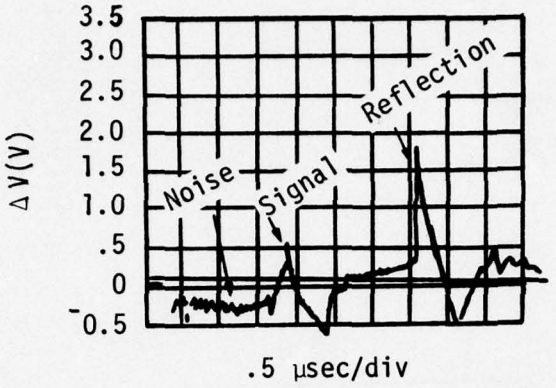

Figure 4.4. Quartz gauge response.

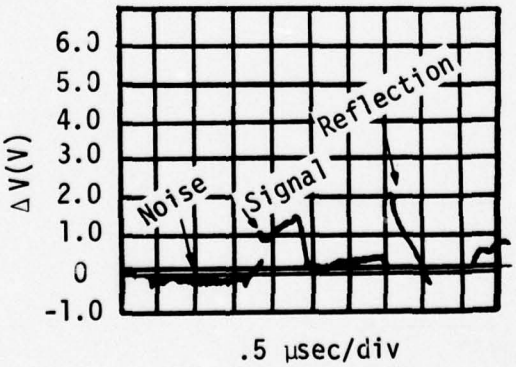

Figure 4.5. Quartz gauge response.

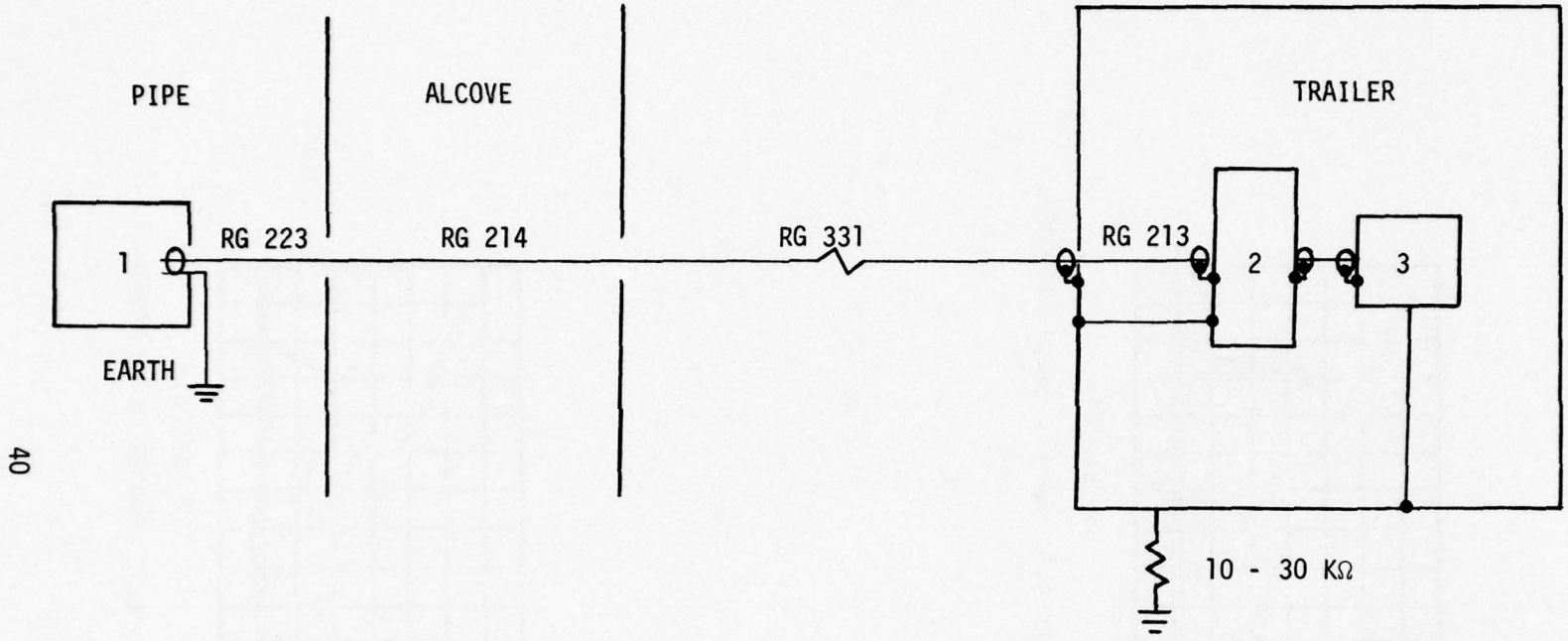

Figure 4.6. Carbon pressure signal system.

Figures 4.7 and 4.8 illustrate data obtained from this carbon gauge experiment.[12,13] The system bandwidth was 25 MHz.

There were 16 data records presented by the experimenter. The experiment was divided into four groups of four gauges each. Three of the gauges were multiplexed onto a single cable while the fourth was transmitted on a single cable. The first data channel in each of the multiplexed traces has a significant amount of apparent ringing noise after the initial noise spikes. The single data channel that was not multiplexed (not shown) does not contain this noise. The second and third data channels in the multiplexed line do not exhibit as much either.[12] It is quite possible that the shield current flowing along the input cable interacted with the multiplexer ahead of the first stress gauge data. The second and third channels were delayed with $\sim$ 400 and 800 meters of cables respectively.

Presumably these cables were coiled in the alcove with the multiplexer. In this case the shield currents would not be delayed but couple capacitively across from input to output shield arriving simultaneously with the short-cable noise signal. If the long cables had been stretched out and buried, the shield current would have been attenuated by lossy earth.

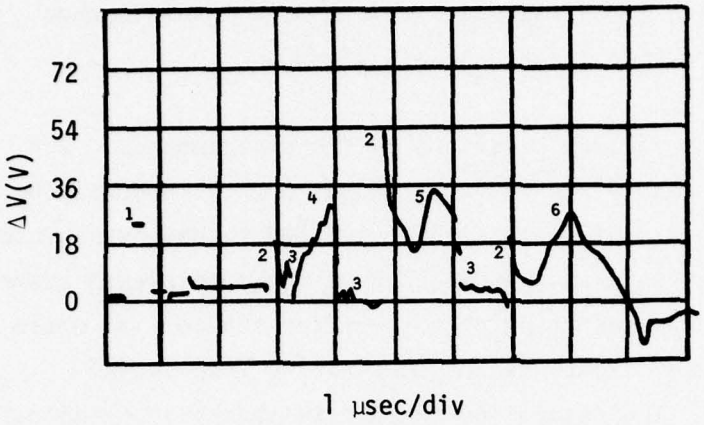

1. Calibration Pulse
2. Gamma Spike
3. Noise
4. 1st Gauge Response
5. 2nd Gauge Response
6. 3rd Gauge Response

Figure 4.7. Multiplexed carbon gauge response.

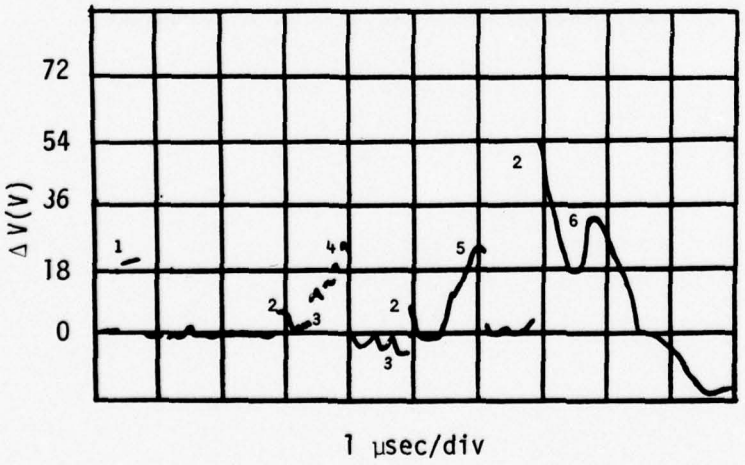

1. Calibration Pulse
2. Gamma Spike
3. Noise
4. 1st Gauge Response
5. 2nd Gauge Response
6. 3rd Gauge Response

Figure 4.8. Multiplexed carbon gauge response.

Figure 4.9 represents a RIP signal system.[9b,10d] The cable shield was insulated from the pipe; a zipper tube over twinax ran from the transducer to the J Box in the alcove. From the electrically isolated bulkhead connector, the zipper (and cables) were enclosed in an EMP pipe that was Earth grounded. The zipper tube was connected to the EMP pipe with two 27 Ω resistors, one at the bulkhead and one at the J Box. RG 333 coax was run from the J Box to the mesa trailer where its shield was tied to the trailer shell.

Figure 4.10 is a data trace from a RIP experiment designed to yield information on the EMP present.[9b] The floating ground system had a bandwidth of 167 MHz. The signal begins at about 55 nanoseconds. The, variation in the signal before 55 nanoseconds is <u>not</u> believed to be noise by the experimenter, and he indicated that the variations after 70 nanoseconds may be due to neutrons. If the neutrons were to have an energy of 14 MeV from the (d,t) reaction[6,14], the time of arrival (from Section 3.5) at SS978 [5,9b] would be on the order of 4×10^{-6} seconds. This indicates the neutrons themselves cannot physically cause these variations. If the variations are from gammas emitted from neutron-activated material near the W.P., it is not clear why the variations change sign. Hence, the variations are treated as noise in Table 4.3.

Figure 4.11 represents a Mighty Epic cable noise study.[15] An amplitude modulated 20 MHz carrier signal generated in ROSES was sent uphole on RG 331 to the trailer, where the two cable shields were terminated with a 10 Ω and ∿1 KΩ resistance to Earth ground, respectively. The signal passed through high-pass filters in the ROSES and in the trailer and was recorded on oscilloscopes. The signal was also branched at the trailer and recorded after passing through low-pass filters. Shield currents were measured with current probes at the termination point (see Figure 4.11, Item 5).

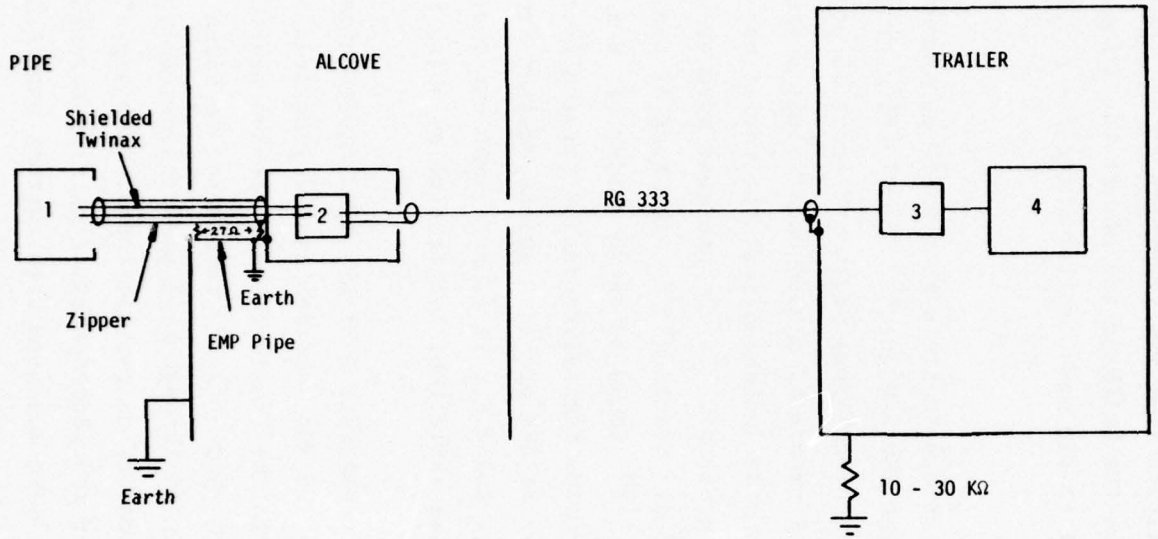

Figure 4.9. RIP signal system.

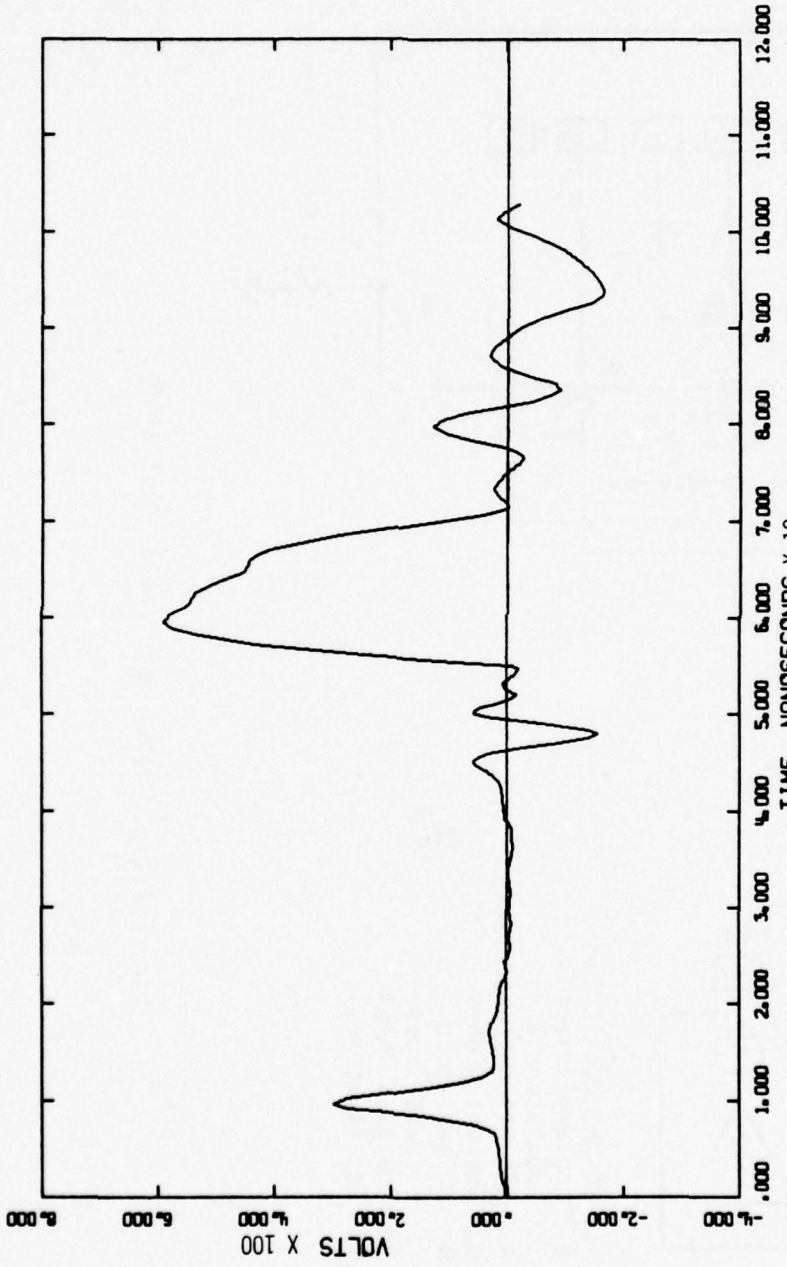

Figure 4.10. RIP response.

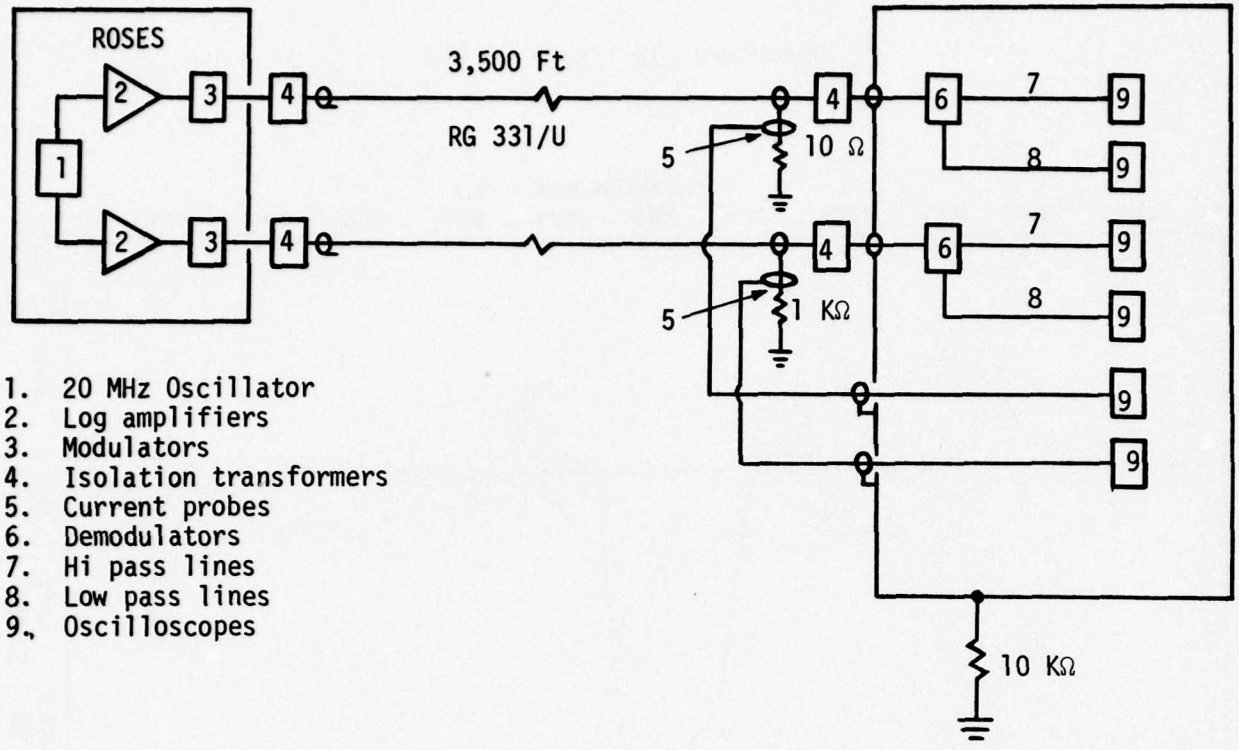

Figure 4.11. Mighty epic cable noise study.

Signals ($\sim$ 200 - 500 V and $\sim$ 100 kHz on the shields, $\sim$ 10 mV on the center conductors) were observed during signal dry runs generated from the simulated XF1DV. They decreased by a factor of $\sim$ 10 on the final dry run. During the nuclear test, the signals were much larger, as shown in Figures 4.12 and 4.13, amounting to > 2 kV ptp on the shield (> 200 A through 10 Ω, > 2 A through 10^3 Ω) and > 5 V ptp on the center conductor.

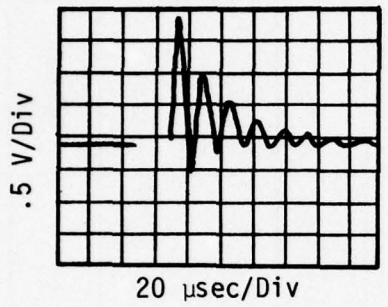

Figure 4.12. Cable noise signal.

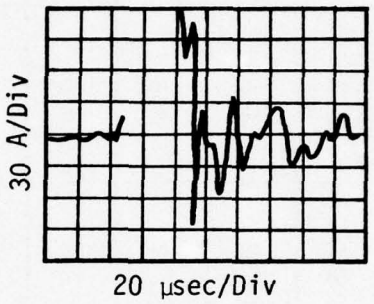

Figure 4.13. Cable noise signal.

This experiment clearly establishes the importance of shield currents in the uphole cable plant (presumably differential-mode excitation as discussed in Section 3.4). The magnitudes of the $\sim$ 100 kHz noise signals appear to be unusually large compared to other fast cables (e.g., quartz gauges). If 5 V at 100 kHz appeared in those channels, they would have pushed the traces to a maximum deflection or off scale entirely. The carbon gauge records (Figures 4.7 and 4.8) could possibly have a $\sim$ 5 V, 100 kHz background signal, but not much more. It is possible that this signal is enhanced by terminating the coax cable in isolation transformers since this leaves an open circuit termination for the shield current.

Table 4.3 summarizes the fast data channels.

Table 4.3. Ming blade results from available data records.

GAUGE	DURATION OF NOISE	NOISE	SIGNAL	GROUNDING/ BLOCK DIAGRAM	COMMENTS
Carbon Gauges	.1 μsec	8 V	16 V	4.6	
Carbon Gauges	-	8 V	12 V	4.6	1.5 V noise on signal
Carbon Gauges	.2 μsec	+ 4 V > - 6 V	17 V	4.6	
Carbon Gauges	.2 μsec	6 V	9.7 V	4.6	
Carbon Gauges	.4 μsec	18 V	11 V	4.6	
Carbon Gauges	.4 μsec	20 V	16 V	4.6	
Carbon Gauges	.4 μsec	2 V	9.7 V	4.6	
Carbon Gauges	.35 μsec	>> 20 V	11.6 V	4.6	(Bandwidth 25 MHz)
Carbon Gauges	.25 μsec	> 20 V	12 V	4.6	
Carbon Gauges	.25 μsec	17 V	12 V	4.6	
Carbon Gauges	.25 μsec	20 V	16 V	4.6	

Table 4.3 Ming blade results from available data records (cont).

GAUGE	DURATION OF NOISE	NOISE	SIGNAL	GROUNDING/ BLOCK DIAGRAM	COMMENTS
X-Ray Diode			420 V	4.1	(Bandwidth 120 MHz)
X-Ray Diode			410 V	4.1	
X-Ray Diode	20 nsec		190 V	4.1	
X-Ray Diode			140 V	4.1	
X-Ray Diode			450 V	4.1	
X-Ray Diode			115 V	4.1	
RIP	30 nsec	+ 100 V - 200 V	600 V	4.9	(Bandwidth 167 MHz) Noise starting during signal and continues for 30 nsec after signal when recording ends
Quartz	1500 nsec	.05 V	.2 V	4.3	(Bandwidth 25 MHz) zero spike > - 0.3 V
Quartz	1500 nsec	.025 V	.15 V	4.3	zero spike > - 0.3 V

4.2 Slow Channels

Slow data channels are typically wired with shielded twisted pair (STP) cables. They are used for integrated radiation measurements (e.g. calorimeters) and slow response measurements (e.g., wire strain gages, velocity gauges, displacement gauges). In some of the slowest channels (e.g., calorimeters), the significant signal levels can be in the millivolt range.

4.2.1 Relation of Noise-Frequency Response

The width of the radiation-induced electrical noise pulse is invariably smaller than the response time of the slow data channels. In this case, the amplitude of the observed noise is determined by the area under the noise pulse (amplitude times time) and the upper frequency band edge of the data channel. The time response of the noise pulse is determined exclusively by the data channel frequency response.

The noise pulse is approximated by two step functions (one up and one down) resulting in a pulse of amplitude K volts and width of T seconds. If we assume an idealized data channel that has a unity gain amplifier (filter) such that it has uniform transmission in the frequency range from zero to f_o and no transmission above this frequency, a first order approximation can be made to the data channel's response to the noise.[16,17]

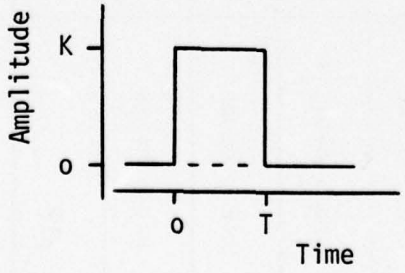

Rectangular Input Pulse

The Fourier transform is defined as

$$F(\omega) = \int_{-\infty}^{+\infty} e^{-j\omega t} \; f(t)\, dt$$

The inverse transform is

$$f(t) = \int_{-\infty}^{+\infty} e^{j\omega t} \; F(\omega)\, d\omega$$

$$F(\omega) = \int_{0}^{T} e^{-j\omega t} \; K\, dt = \frac{K}{j\omega}(1 - e^{-j\omega T})$$

The inverse transform is used to determine the output of a low-pass filter. It is

$$f(t) = \frac{1}{2\pi} \int_{-\omega_o}^{+\omega_o} e^{j\omega t} \left[\frac{K}{j\omega}(1 - e^{-j\omega T})\right] d\omega$$

$$= \frac{K}{2\pi} \int_{-\omega_o}^{+\omega_o} \left[\frac{e^{j\omega t} - e^{j\omega(t - T)}}{j\omega}\right] d\omega$$

which yields

$$f(t) = \frac{K}{\pi} \int_{0}^{\omega_o} \left[\frac{\sin\omega t}{\omega} - \frac{\sin\omega(t - T)}{\omega}\right] d\omega$$

$$= \frac{K}{\pi} \int_{\omega_o t - \omega T}^{\omega_o t} \frac{\sin x}{x}\, dx$$

Let $x = \omega_o t + y$

$$f(t) = \frac{K}{\pi} \int_{-\omega_o T}^{0} \frac{\sin(\omega t + y)}{\omega t + y}\, dy$$

$$= \int_{-\omega_o T}^{0} \frac{\sin \omega t \cos y + \cos \omega t \sin y}{\omega t + y}\, dy$$

for $|\omega_o T| = |y| << 1$

$$f(t) = \frac{K}{\pi}\ \omega_o T\ \frac{\sin \omega_o t}{\omega_o t} + \frac{\omega_o T^2}{2}\ \frac{\cos \omega_o t}{\omega_o t}$$

$$f(t) \approx \frac{K}{\pi}\ \omega_o T\ \frac{\sin \omega_o t}{\omega_o t}$$

The output is represented below

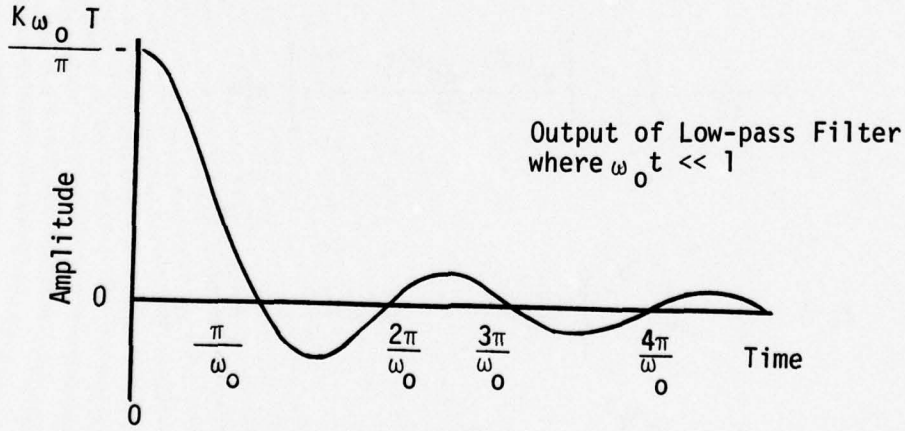

In summary, the impulse response of a data channel with upper cut off frequency, ω_o, has an amplitude proportional to the excitation impulse (kT) times ω_o and a time response determined by ω_o, independent of T.

4.2.2 Experimental Data

Figure 4.14 is representative of one linear velocity signal system used.[9b,10d] It also represents the TRIM signal system. The TRIM did not use zipper tube to the alcove. The cable used was twisted shielded pairs (TSP) with an overall shield. The cable was enclosed in a zipper tube from the transducer to the alcove where the zipper was tied to the overall shield of the TSP. The zipper tube was tied to the experiment shell, which was isolated from the pipe. The outer shield was terminated in its characteristic impedance ($\sim$ 10 Ω) at the outside of the instrumentation trailer. The individual shield pairs were terminated at the instrumentation in the trailer and bussed to the trailer shell. To minimize overall shield currents, the entire cable bundle was wound on a toroidal tape core of very high permeability to impede the flow of these currents. The tape core was in the alcove. A signal conditioning unit was located in the trailer. Diode clipper and divider networks were employed to reduce the gamma and noise spikes.

Figure 4.15 is data from a TRIM gage fielded in the configuration shown in Figure 4.14 without the zipper tube to the alcove.[13] The bandwidth was 20 KHz .

Figure 4.16 represents the second linear velocity signal system used on Ming Blade.[9g,10c] It is also the system used for this experimenter's strain measurements. The cabling was TSP with an overall shield. Signal conditioning was performed in both the alcove and the trailer. The TSP overall shield was tied to the floating trailer shell. The inner shield is tied to circuit ground at the signal conditioning units.

Figure 4.17 is a typical data trace for a linear velocity transducer (LVT).[9e] It was fielded with a bandwidth of 50 KHz.

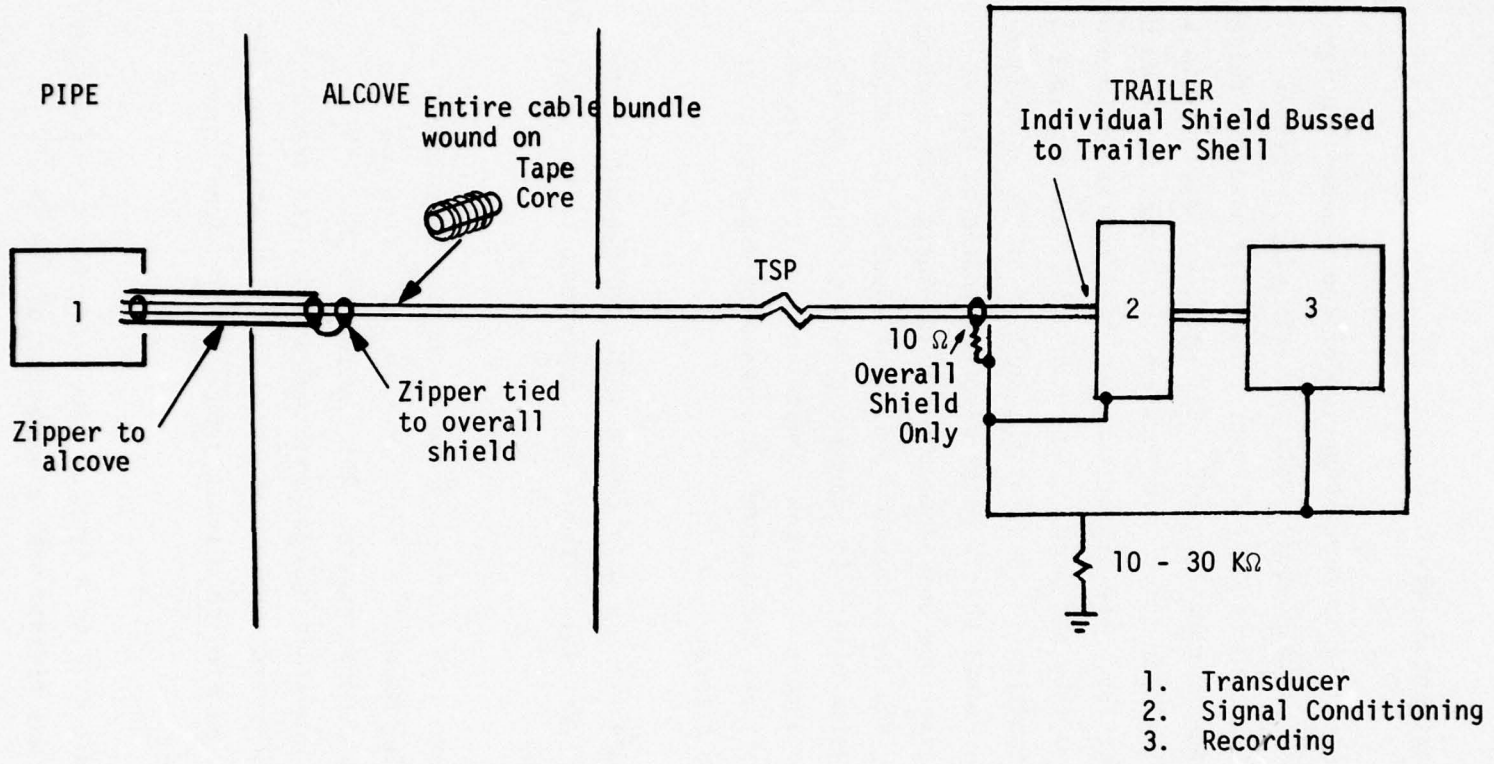

Figure 4.14. Linear velocity signal system. (Also representative of TRIM signal system that did not utilize zipper to the alcove.)

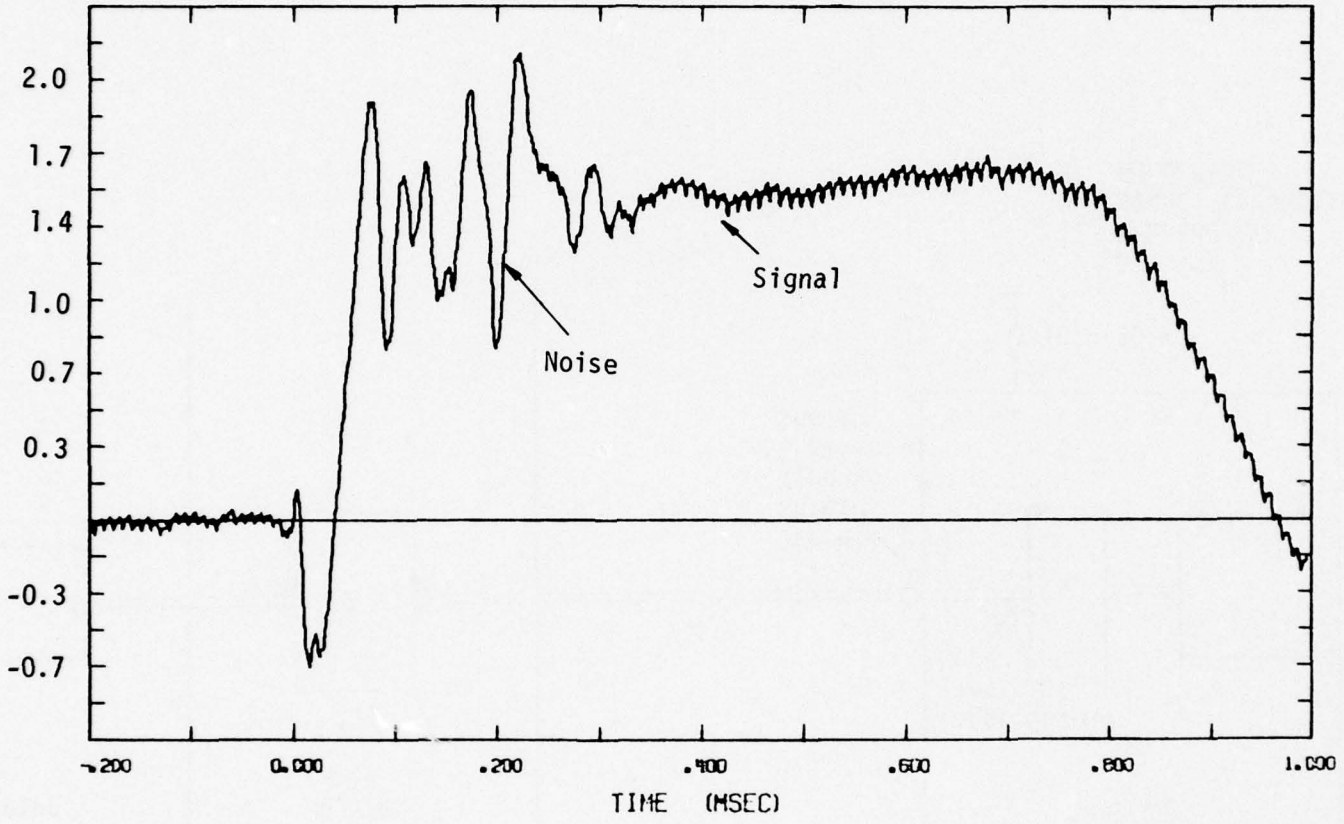

Figure 4.15. TRIM gauge response.

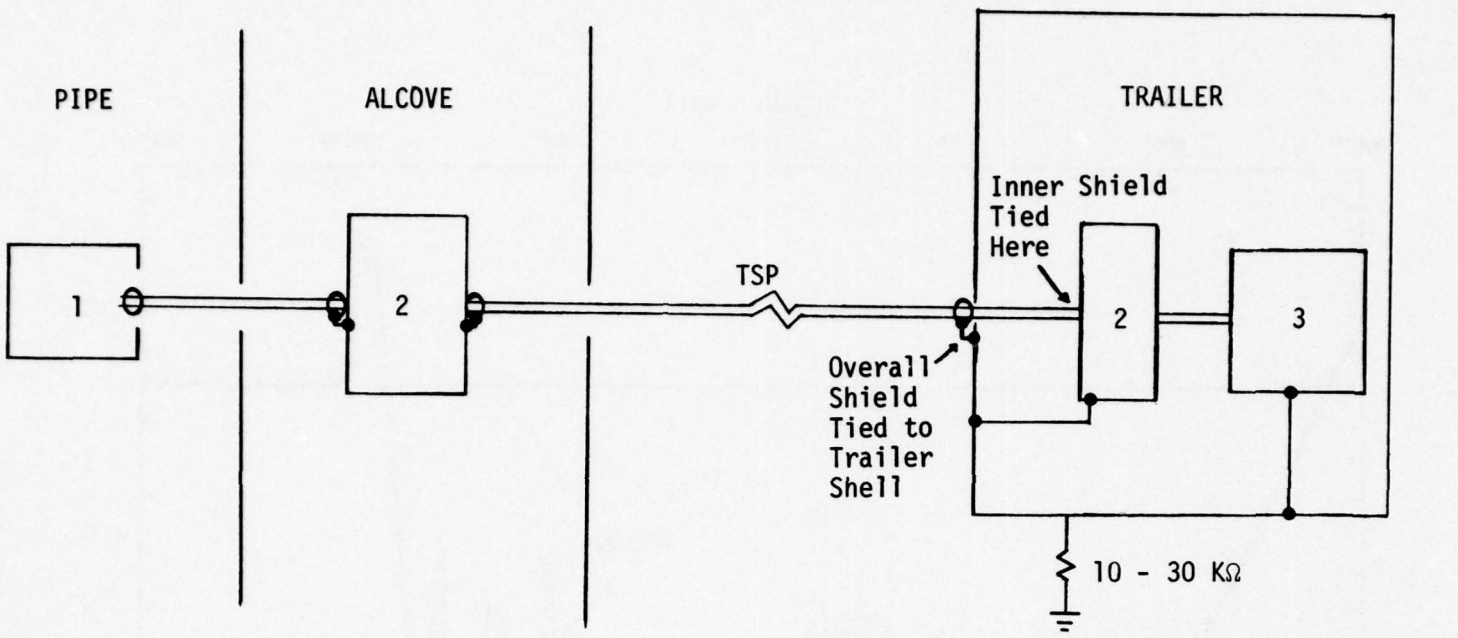

Figure 4.16. Strain/linear velocity signal system.

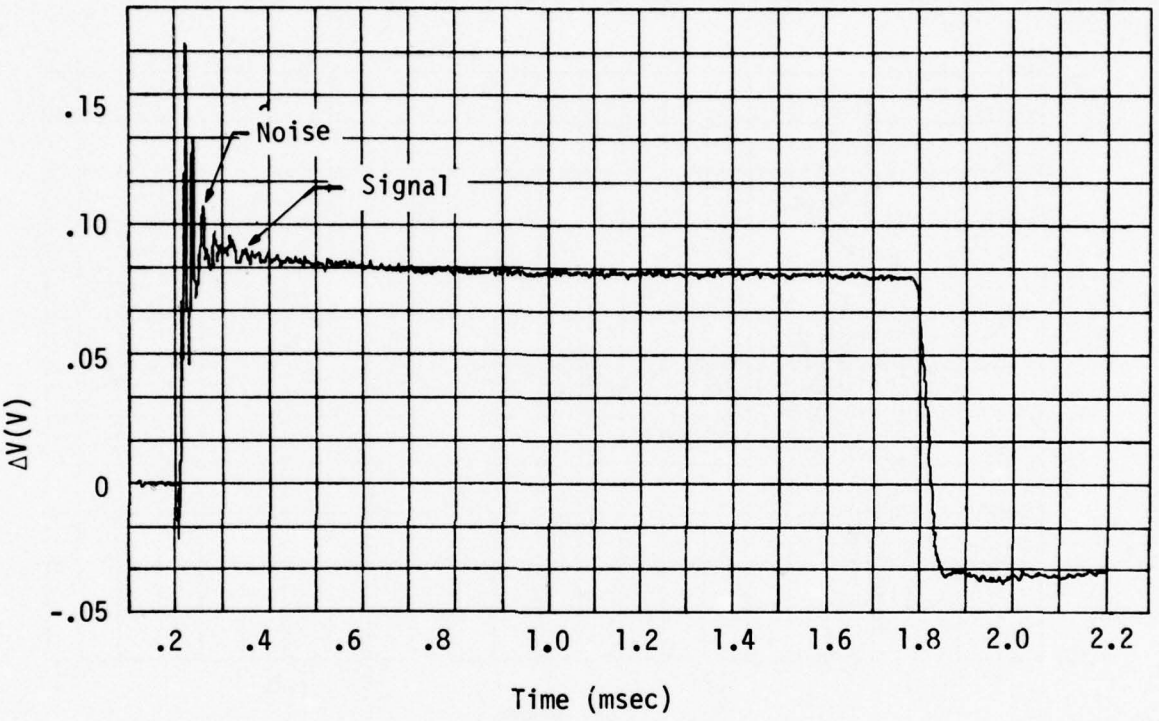

Figure 4.17. Linear velocity gauge response.

Figure 4.18 is representative of strain measurements made.[9e] The system had a bandwidth of 50 KHz . The data was filtered at 20 KHz . The experimenter indicates that the first 180 μsec of data records are noise responses and that typical recovery times are on the order of 50 - 200 μsec . The noise ringing is about 18 KHz.

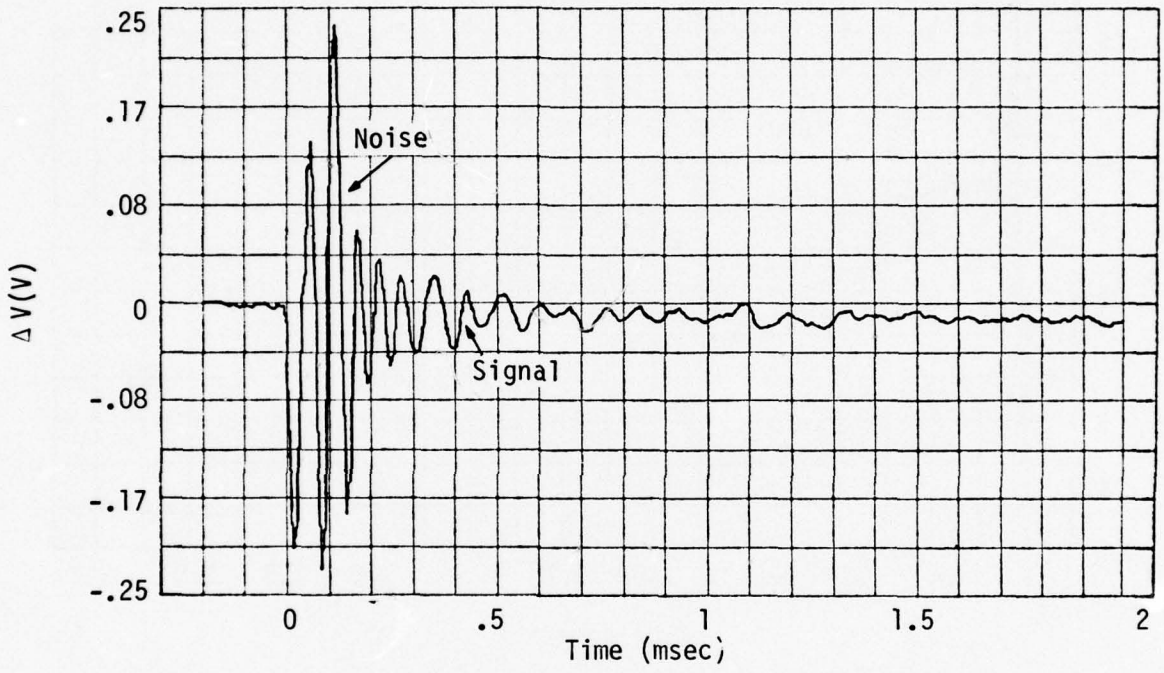

Figure 4.18. Strain gauge response.

Figure 4.19 represents another strain gauge signal system used on Ming Blade.[9b,10d] TSP with an overall shield (connected to the mesa trailer shell) was used to transmit the signals with a floating ground configuration. Zipper tubing enclosed the TSP from the transducer to the alcove, where it was tied to the TSP overall shield. Signal conditioners were employed in the alcove. Low-pass filters were used to attenuate noise above the data band. The signal was then amplified and passed through a diode clipper and divider network and recorded. The TSP shield were terminated in their characteristic impedance of 10 Ω .

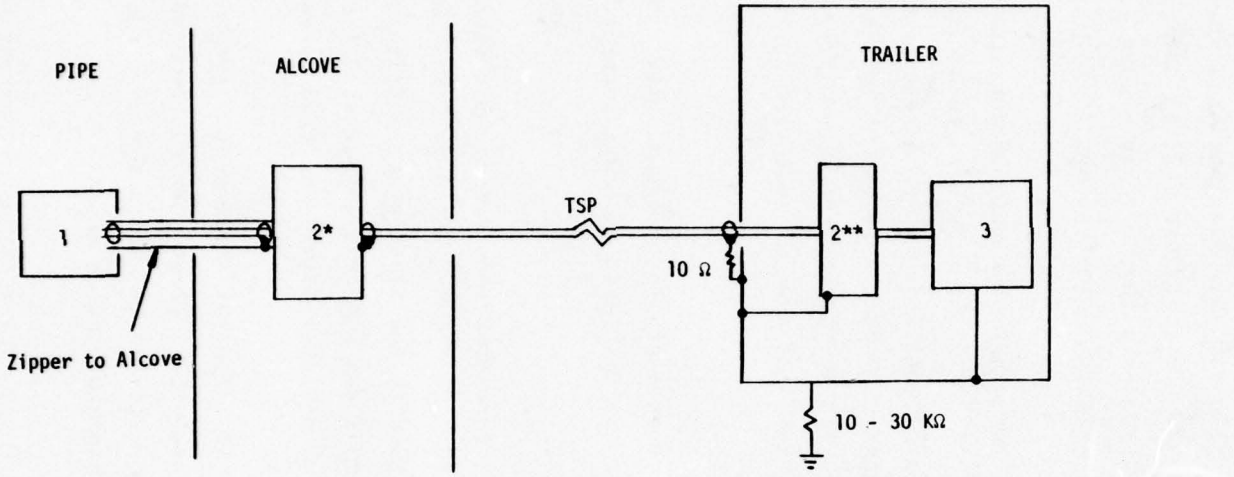

Figure 4.19. Strain gauge signal system.

Figures 4.20 and 4.21 are data obtained from this system.[18] The bandwidth is believed to be 20 KHz . Figure 4.21 is data from a background channel that measured only noise. The noise in Figure 4.20 appears to ring at about 30 KHz and in Figure 4.21 at about 18 KHz .

Figure 4.22 represents the calorimeter signal system employed on Ming Blade.[9e,9f,10a,10e,19] The floating ground (common trailer shell) system consisting of a differential-amplifier line-driver package located in the alcove sent a signal of about 3 volts on TSP with an overall shield to the mesa trailer. Within the trailer were differential line receivers and recorders. The shields of the TSP were tied to the trailer shell.

Figure 4.23 represents three calorimeter data channels.[13,19] The bandwidth was believed to be 20 KHz with the data recorded on an apparent bandwidth of about 10 Hz .

Figure 4.24 represents the thermocouple signal configu - ation used on Ming Blade.[9b,9c,9h,10d,10f,10h] The signal was transmitted on TSP with the overall shield tied to the floating ground (common trailer shell). In the trailer, the signal was fed to a low-level differential amplifier and then recorded. The individual shield was tied to amplifier.

Figure 4.25 is a typical thermocouple response.[9g] The resolution is limited by the oscilloscope trace. We can conclude that the noise pulse recovered in << 100 msec, as it should for a 5 kHz channel. The system to that point had a bandwidth of 5 kHz.

Figure 4.26 represents a frequency carrier test block diagram.[9g,10c] The cable types used are listed on the diagram. The dummy gauges used and a minimum of 8 ft of cable were arranged in the beam, in

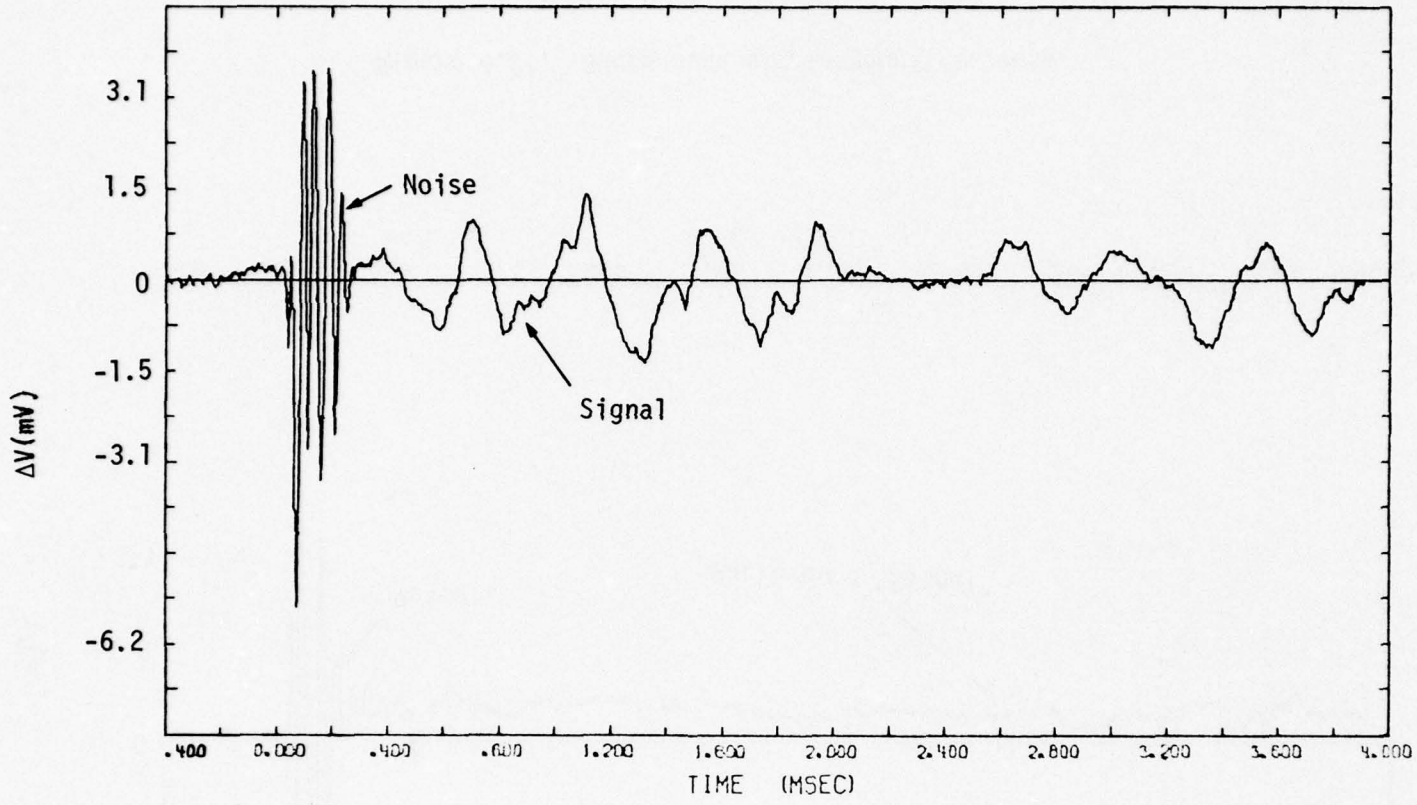

Figure 4.20. Strain gauge response.

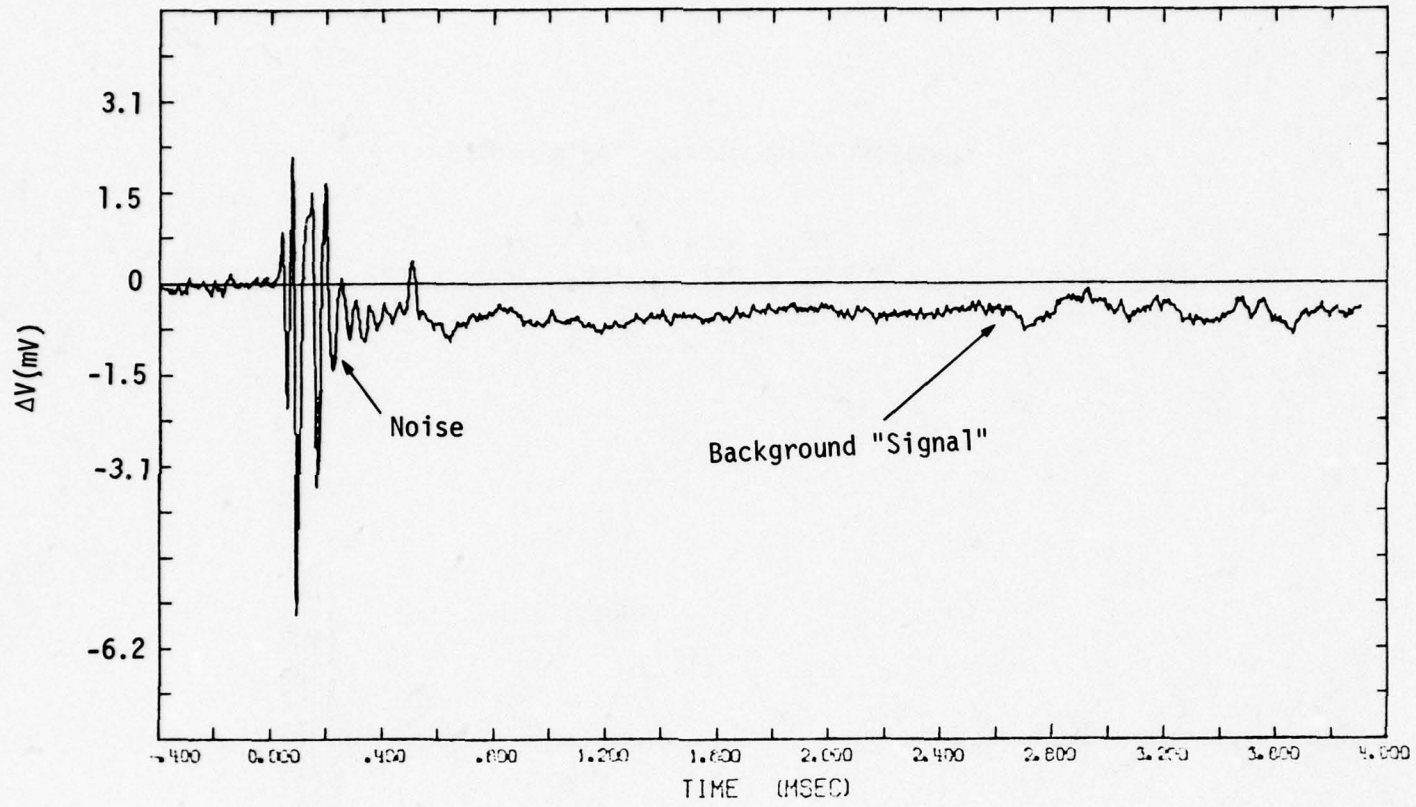

Figure 4.21. Background strain gauge response.

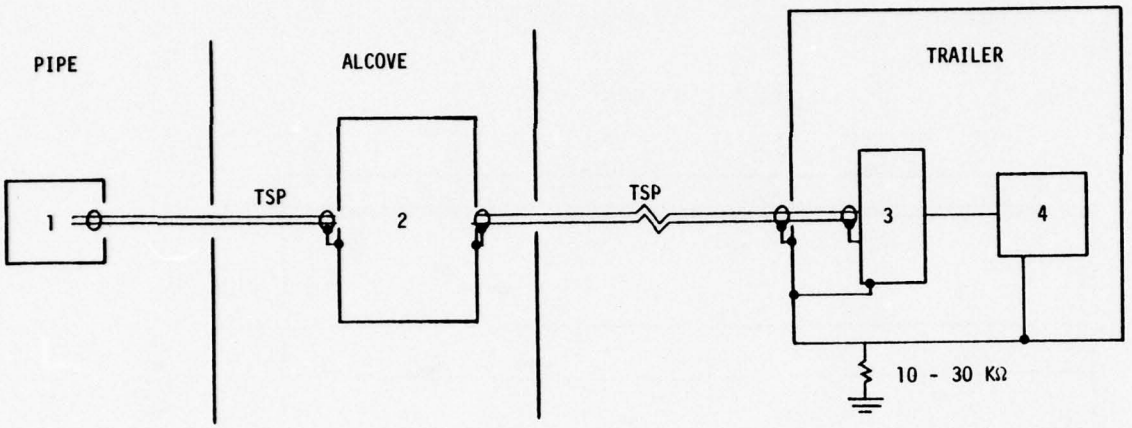

Figure 4.22. Calorimeter signal system.

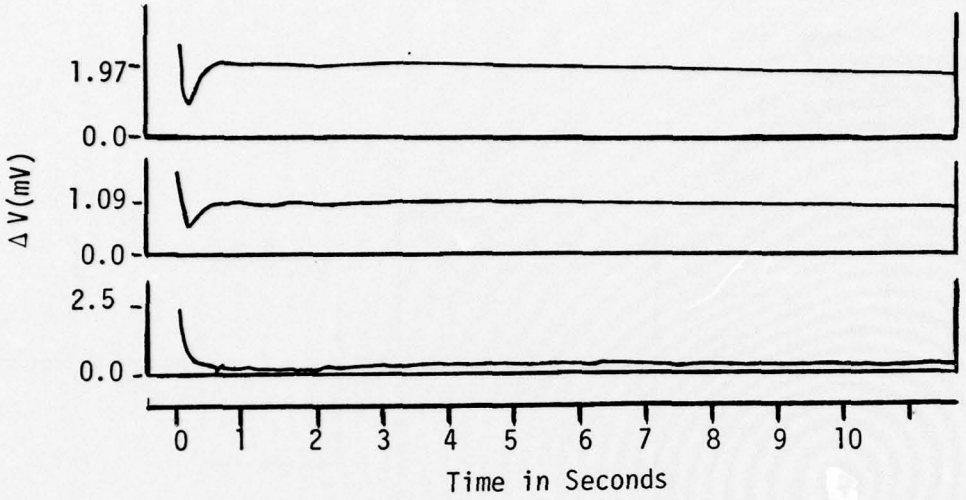

Figure 4.23. Calorimeter records. The trace at the bottom is a background channel.

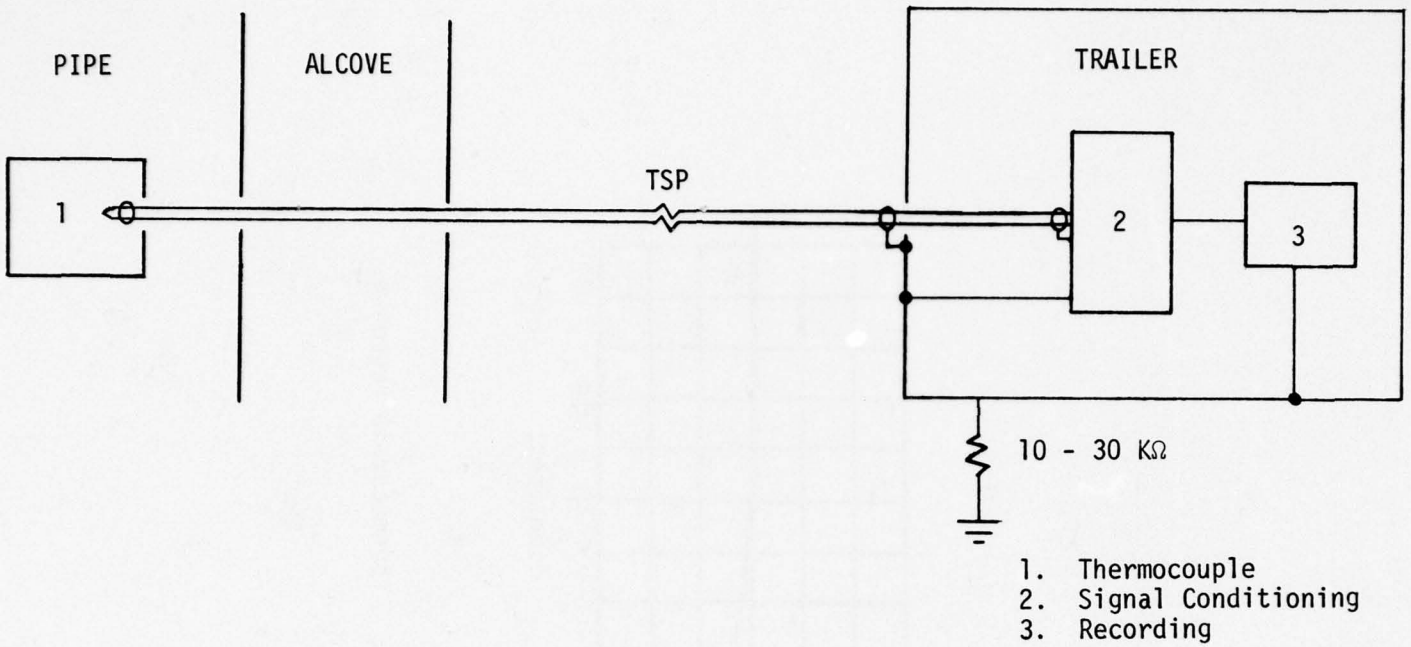

Figure 4.24. Thermocouple signal system.

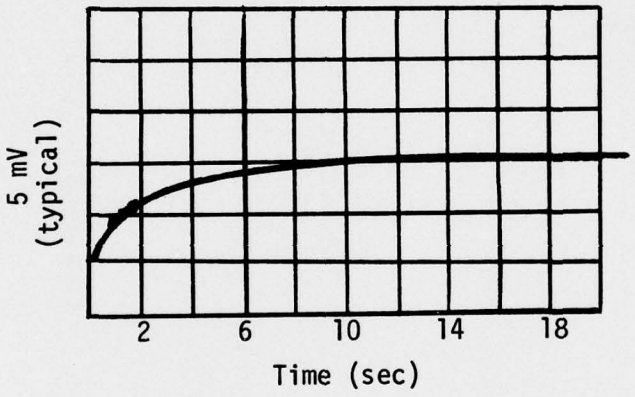

Figure 4.25. Thermocouple response.

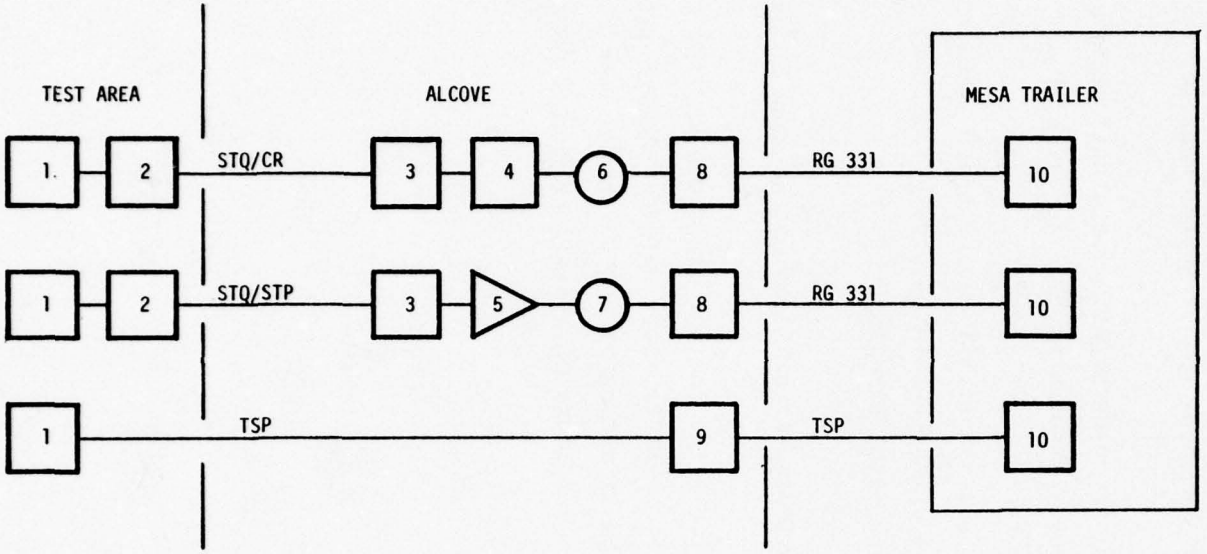

1. Dummy Gage
2. Source Coupler
3. Translator Coupler
4. 10 MHz Carrier (A.M.)
5. D.C. Differential Amplifier
6. 50 KHz F.M. Multiplex
7. PCM Encoder
8. External Cable Isolation
9. J Box
10. Recorders

Figure 4.26. Carrier test block diagram.

such a way as to avoid exposure variation at SS 825. Single point ground of the outer shield was at the alcove. The "signals" were placed on a Carrier (A.M.) then multiplexed and sent uphole to the mesa for recording.

Figure 4.27 represents part of the data obtained on Ming Blade for a carrier frequency experiment.[9e] The "signal" was 4.5 mV D. C. The data is interesting from two standpoints. First and obvious is that the 10 MHz carrier data was essentially noise free. The second is that the noise on the "standard bridge" exhibits some of the same signature observed on the stress, LVT, and TRIM gauges.

Table 4.4 summarizes the data on the slow channels.

Table 4.5 lists the nominal bandwidth and the observed noise frequency for some of the low-level, slow-response gauges. In general they agree reasonably well, with exception of the LVT gauge. We will use the observed noise frequency as a measure of overall channel bandwidth.

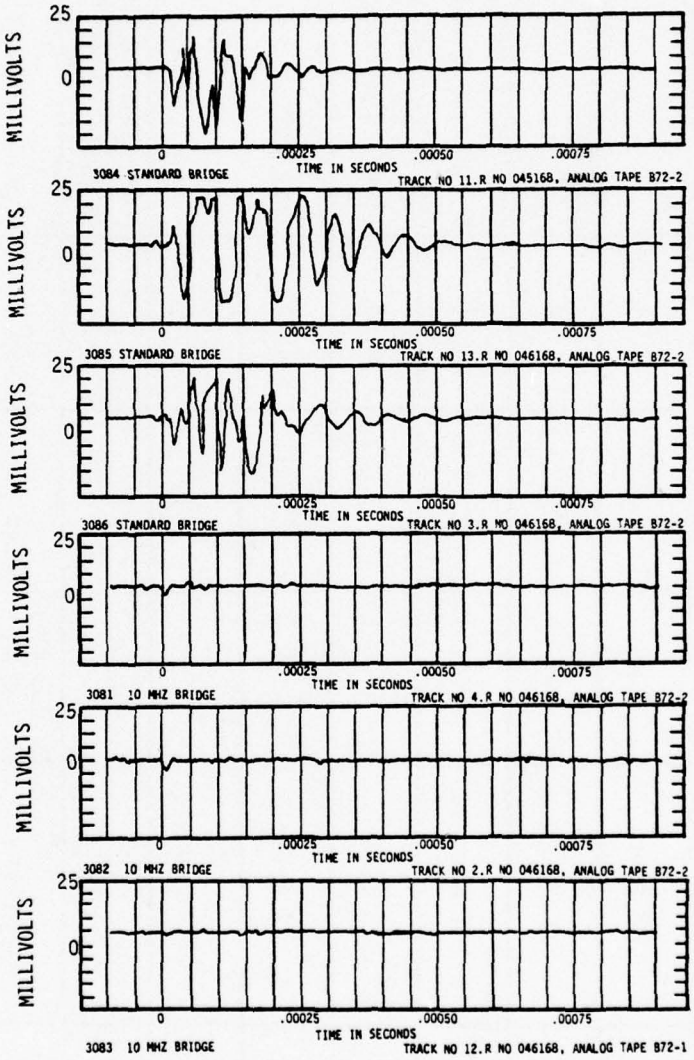

Figure 4.27. Data obtained from frequency carrier experiments.

Table 4.4. Ming blade results from available data records.

GAUGE	DURATION OF NOISE	NOISE	SIGNAL	GROUNDING/ BLOCK DIAGRAM	COMMENTS
TRIM	.03 msec	-0.74	+ 1.36 V	4.14	(Bandwidth 100 KHz) Attributed some noise to tape core used for shield current reduction. The experimenter no longer uses the tape core.
TRIM	-	-	+ 0.0425 V	4.14	
TRIM	.03 msec	± 3 V	+ 2.25 V	4.14	
TRIM	.075 msec	- 1.36 V	+ 1.0 V	4.14	
TRIM	.3 msec	+ 0.34 V - 0.17 V	+ 0.38 V	4.14	
TRIM	-	-	± 6 V	4.14	
STRAIN	150 μsec	± 230 mV	- 83 mV	4.16	(Bandwidth 50 kHz) Recorded at 20 kHz signal rings to -14 mV
STRAIN	150 μsec	+ 208 mV - 220 mV	125 mV	4.16	signal rings to 17 mV
STRAIN	150 μsec	+ 142 mV - 167 mV	104 mV	4.16	signal rings to 21 mV
STRAIN	300 μsec	+ 3.7 mV - 5.8 mV	± 1.5 mV	4.14	(Bandwidth 20 kHz)

Table 4.4. Ming blade results from available data records (cont'd).

GAUGE	DURATION OF NOISE	NOISE	SIGNAL	GROUNDING/ BLOCK DIAGRAM	COMMENTS
THERMOCOUPLE			6 mV	4.24	(Playback Bandwidth 10 - 100 Hz)
THERMOCOUPLE			5 mV	4.24	(Bandwidth 5 KHz)
CALORIMETER		-		4.22	filtered spectrum
CALORIMETER		> 6 mV	3.1 mV	4.22	(Bandwidth > 20 kHz)
CALORIMETER					
CALORIMETER		> 10 mV	7.8 mV	4.22	filtered spectrum
LVT	30 μsec	-0.02 V	.08 V	4.6	
LVT	80 μsec	-0.1 V	.15 V	4.6	
LVT	125 μsec	+0.18 V -0.1 V	1 V	4.16	(Bandwidth 50 KHz)
LVT	125 μsec	+0.1 V -0.05 V	1.2 V	4.16	

Figure 4.4. Ming blade results from available data records (cont'd).

GAUGE	DURATION OF NOISE	NOISE	SIGNAL	GROUNDING/ BLOCK DIAGRAM	COMMENTS
CALORIMETER		.5 mV	-	4.22	beryllium, background
CALORIMETER		3 mV	1.97 mV	4.22	beryllium
CALORIMETER		1.5 mV	1.09 mV	4.22	beryllium
CALORIMETER		1 mV	1.77 mV	4.22	beryllium
CALORIMETER		1 mV	2.77 mV	4.22	beryllium
CALORIMETER		.75 mV	1.84 mV	4.22	beryllium
CALORIMETER		.9 mV	1.84 mV	4.22	beryllium
CALORIMETER		1 mV	-	4.22	beryllium, background
CALORIMETER		.7 mV	-	4.22	beryllium, background

Table 4.5. Comparison of bandwidth with observed noise ringing frequency.

GAUGE	BANDWIDTH	OBSERVED RINGING
Strain	20 KHz	17 KHz
Strain	20 KHz	17 KHz
Strain	20 KHz	30 KHz
Strain, Dummy	20 KHz	18 KHz
TRIM	20 KHz	28 KHz
LVT	50 KHz	5 KHz
Dummy Bridge	50 KHz	15 KHz
Dummy Bridge	50 KHz	15 KHz
Dummy Bridge	50 KHz	20 KHz

SECTION 5

5.0 DISCUSSION, CONCLUSIONS, RECOMMENDATIONS

A summary of noise data in the fast channels is presented in Table 5.1. The RIP signal is different from the others, probably due to a special interaction of radiation with the sensor (capacitor) or the front section of the cable. The other signals are all consistent with a noise pulse of $\sim$ 20 V that recovers in $\lesssim$ 0.1 μsec. Even though the cabling practice on these channels is very similar, there is no controlled experiment to compare an experiment grounded to the pipe with one that is floating, thus we cannot conclude which is best. We may try to infer that if the gamma pulse signal on the floating quartz gauges had been as large as on the grounded carbon gauges, it would not have recovered as quickly as it did.

Unfortunately, the reported data on cable routing and alcove configuration do not allow us to make a detailed comparison with the theory presented in Section 3, however the magnitude is consistent with the estimates given in that section. The recovery time clearly indicates that the noise is generated near the sensor (including the cable to the alcove), rather than in the uphole cable run. Either the direct gamma-induced cable current or the EMP/SGEMP driven differential mode drive of the cable bundle to the alcove could be the dominant source. The data shows no evidence of pipe ringing.

A summary of noise data in the slow channels is presented in Table 5.2. The fact that the amplitude and ringing of the noise is determined by

Table 5.1. Noise in fast channels.

	Δ V	Recovery Time
XRD	< 50 V	< .03 μsec
QUARTZ	> .2 V	∿ 0.1 μsec
CARBON	∿ 20 V 5 - 50 V	∿ 0.1 μsec ∿ 0.1 μsec
RIP	- 100 V	2 nsec

Table 5.2. Noise is slow channels.

	Δ V	Ringing Frequency
TRIM	1 V	28 kHz
LVT	.2 V	5 kHz
Strain I II	.2 V 3 mV	20 kHz 20 kHz
Calorimeter	2 mV	10 Hz
Frequency Carrier Test	20 mV	20 kHz

the frequency response of the data channel is consistent with the data. The observed amplitude of ~ 0.5 V in ~ 20 kHz channels indicates an excitation of $\sim 10^{-5}$ Vsec , which is only slightly larger than the 20 V x 0.1 μsec observed in the fast channels.

It is apparent that a large variation in noise level can be achieved by different cabling practices (e.g., compare the two strain gauge channels). It is tempting to ascribe the lower noise in the second strain gauge channel to the use of zipper tube between the sensor and alcove. If all other parameters were the same, we could be confident of this conclusion. As it stands, we must derive most of our confidence in that conclusion from theoretical considerations.

The theoretical calculations described in Section 3 could be compared to the experimental results if we had a detailed description of the cable geometry. Unfortunately, this information is not generally given in the reports. Instead we must rely on using typical values of lengths and transfer impedances to compare the calculations and experimental results.

The calculations revealed that $\sim 10^3$-10^4A of shield current could be produced by EMP coupling into grounded cable shields exposed to the gamma flux beyond the experiment bulkhead. An ungrounded cassette could produce $\sim$ 10-10^2A along its cable shields, depending on the irradiated area. The common-mode shield currents will not ring for a cable buried in earth. Typical attenuation distances will be $\sim$10m. The differential mode shield currents within a cable bundle can propagate over very long distances. Finally, the radiation induced cable currents will vary from $\sim$1A/m for solid-dielectric cables to $\sim$10A/m for semisolid or foam dielectric cables.

If we use a shield current of 10^3A, a transfer impedance of mOhm/m^7, and a 10m attenuation length we calculate a signal of V in coax cables exposed to the tunnel EMP. This is reasonably consistent with the $\sim$20V fast spikes

seen on some data channels (see Table 5.1) and the $\sim 10^{-5}$ Vsec excitation of slow channels. The gamma induced cable current for a 3m irradiated length of solid dielectric cable will produce ~15V across a 50 ohm load. This is also in the same regime as the observed values. Whether one or both of these mechanisms is responsible for the signal in a given channel depends on the detailed geometry, which has not been reported.

We conclude that the following grounding and cabling practices are preferred.

1. Whether the sensors are grounded to the pipe or not, the cables from a given experiment should be enclosed in a conducting shield (zipper tube or pipe) until the cable run escapes from the radiation field and the electric field induced in the tunnel air and wall. This shield should be earth grounded at its end. The cable shields should be shorted together at this point, and more frequently as determined by the upper frequency response of the channel.

2. The uphole cables should have their outer shields shorted together at the gas seal bulkhead , alcove splice rack and mesa splice rack.

3. The transfer impedance for low-noise experiments should be minimized by using solid-shield cables and conducting foil bridges over connectors. The extra cost of solid-shield cables to be incurred only when low noise and high-frequency response are both needed.

4. Electrically pulsing the transmission line between cable shields and enclosing shield (e.g., zipper) is an effective means of quality control on the transfer impedance.

5. The direct photon-induced cable currents should be minimized by using radiation shielding and solid-dielectric cables in the irradiated region.

We recommend that an experiment be performed on a forthcoming UGT to demonstrate teh efficacy of these methods in reducing noise in all signal channels. The grounding of the shields of the uphole cables would affect all experiments on the event, but considering the degree of capacitive and inductive interaction that already exists between these cables, frequent grounding can only improve noise conditions. The front-end practices can be checked on any experiments, preferably ones that include fast ($\gtrsim$ 50 MHz) and slow ($\sim$20 kHz) channels and preferably ones that include both experiments that are grounded to the pipe and floating.

REFERENCES

1. Messier, M. A., UGT Noise Characterization Memo 6: Supplemental Estimates of Gamma Induced EMP, October 1976 (unpublished).

2. Hussar Sword Series (U) Ming Blade Event (U) Test Execution Report (U), POR #6856 (unpublished).

3. Hussar Sword Series (U) Husky Pup Event (U) Test Execution Report (U), POR #6920 (unpublished).

4. Hussar Sword Series (U) Dining Car Event (U) Test Execution Report (U), POR #6885 (unpublished)

5. Miller, R. I., et al., Minute Gun Series (U) Ming Blade Event (U) Output Diagnostics (U), POR #6865, 14 August 1975 (unpublished).

6. Hussar Sword Series (U) Ming Blade Event (U) Measurement of Radiation - Induced Temperature In An Energy Coupling Experiment (U), POR #6859 (unpublished)

7. Perala, R. A. and T. F. Ezell, Engineering Design Guidelines For EMP Hardening of Naval Missiles and Airplanes, December 1973.

8. van Lint, V. A. J., "Radiation - Induced Currents in Coaxial Cables", IEEE Trans. Nucl. Sci., Vol. NS-17, No. 6, p. 210, December 1970

9. Thayer, H. J., ed., Minutes of Ming Blade Instrumentation Results Meeting, Defense Nuclear Agency, 2 May 1975.

a. Enclosure 3
b. Enclosure 5
c. Enclosure 6
d. Enclosure 7
e. Enclosure 8
f. Enclosure 9
g. Enclosure 10
h. Enclosure 13

10. Thayer, H. J., ed., Minutes of Ming Blade Prefielding Instrumentation Meeting, Defense Nuclear Agency, 10 July 1974.

a. Enclosure 3
b. Enclosure 4
c. Enclosure 5
d. Enclosure 6
e. Enclosure 7
f. Enclosure 9
g. Enclosure 11
h. Enclosure 12

11. Sites, K. R., Science Applications, Inc., Private Correspondence, 19 October 1976.

12. Durham, Harry J., Hussar Sword Series (U) Ming Blade Event (U) Air Force Weapons Laboratory Experiments (U), POR #6862, 30 July 1975 (unpublished).

13. Czotwell, Major G. P. Jr. and B. H. Ellis, Jr., Hussar Sword Series (U) Ming Blade Event (U) Preliminary Results Report (U), POR #6857, 22 May 1975 (unpublished).

14. Stahl, R. H., et al., Hussar Sword Series (U) Ming Blade Event (U) Measurement of Close - In EMP (U), POR #6863, 15 August 1975 (unpublished)

15. Sites, K. R., Mighty Epic Cable Noise Study, Science Applications, Inc., 2 August 1976.

16. Ku, Y. H., Transient Circuit Analysis, Boston Technical Publishers, 1965.

17. Goldman, S., Frequency Analysis, Modulation and Noise, McGraw-Hill Publishers, 1948.

18. Cole, E., Kaman Sciences Corporation, Private Correspondence, 1 November 1976.

19. Passell, T. O., et al., Hussar Sword Series (U) Ming Blade Event (U) Diegnostic Measurements (U), POR #6866, 14 August 1975 (unpublished)

20. Thayer, H. J., ed., Minutes of Ming Blade Instrumentation Results Meeting, Defense Nuclear Agency, 2 May 1975.

21. Thayer, H. J., ed., Minutes of Ming Blade Prefielding Instrumentation Meeting, Defense Nuclear Agency, 10 July 1974.

APPENDIX A

UGT NOISE CHARACTERIZATION

Physical Models

APPENDIX A

INTRODUCTION

This appendix describes the physical models, approximations, and calculations used to produce the estimates used in the preceding report.

We begin by modeling the line-of-sight (LOS) pipe and use this to estimate x-ray and gamma intensities at the experimental stations. In Section 2, estimates of Compton current and air conductivity are made. The quantities are needed to estimate the electric field generated outside the pipe. Section 3 discusses the voltages generated in ungrounded cassettes by SGEMP effects. Sections 4 and 5 address the questions of current propagation along the LOS pipe and cable shields. Finally, Section 6 shows how electric field induced currents are estimated for cables exiting the experimental station bulkheads. More realistic estimates are made in Reference 1 of the main report.

A.1. FLUX CALCULATIONS

In this section we make estimates of the x-ray and gamma ray fluxes at the two stations of the simplified LOS pipe model described in UGT Noise Memo #1. A diagram of this representative model is shown in Figure 1; dimensions are given in Table 1. These are based on the Husky Pup configuration. X-ray fluxes will be computed inside the pipe; gamma ray fluxes outside the pipe bulkheads.

Later, the x-ray flux levels will be needed to estimate photocurrents emitted from cassettes at the two stations. The gamma ray flux will be needed to estimate Compton drivers and air conductivity in the air space between the pipe and earth.

For the purpose of making crude estimates, we will assume x-ray and γ-ray yields of 10^{12} calories and 10^{23} MeV, respectively. The resulting geometrically attenuated fluences are shown in Table 2.

The model pipe contains an attenuator which reduces the x-ray fluence incident on station 1. Gamma intensities are not significantly affected. The attenuator, shown schematically in Figure 2 (holes are not drawn to scale) is in the form of a perforated plate. The holes are partially obstructed by steel wires strung vertically behind them. Half of the attenuator allows 40% of the x-radiation to pass, while the other half allows 25%. Two different environments must then be considered at station 1. We will therefore refer to station 1A (high dose) and 1B (low dose) when discussing x-ray environments. The attenuated x-ray fluences are given in Table 3.

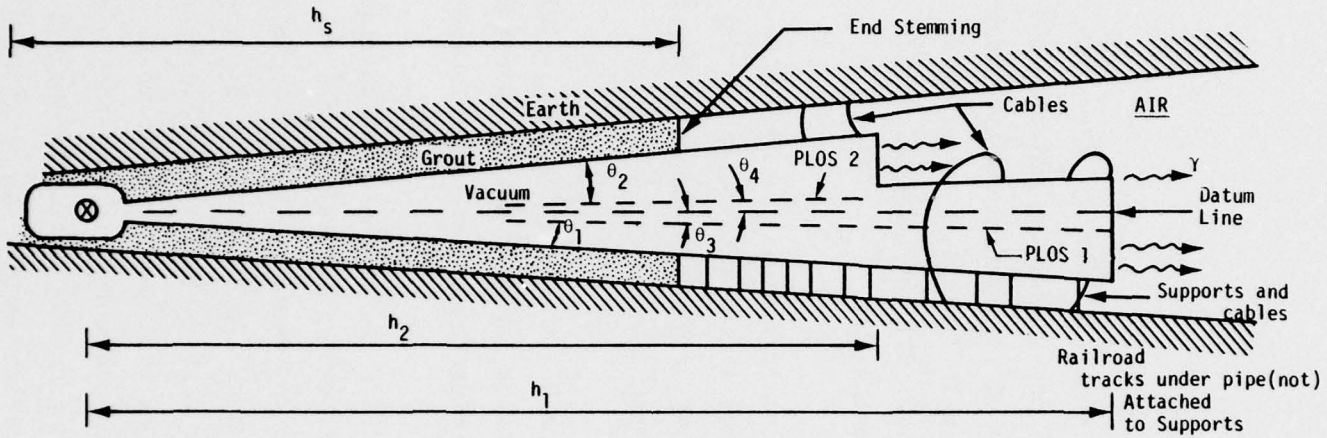

Figure A.1. First order model of UGT geometry for use in the calculation of exterior pipe currents. Not to scale. Values of the indicated parameters are given in Table 1 for Husky Pup.

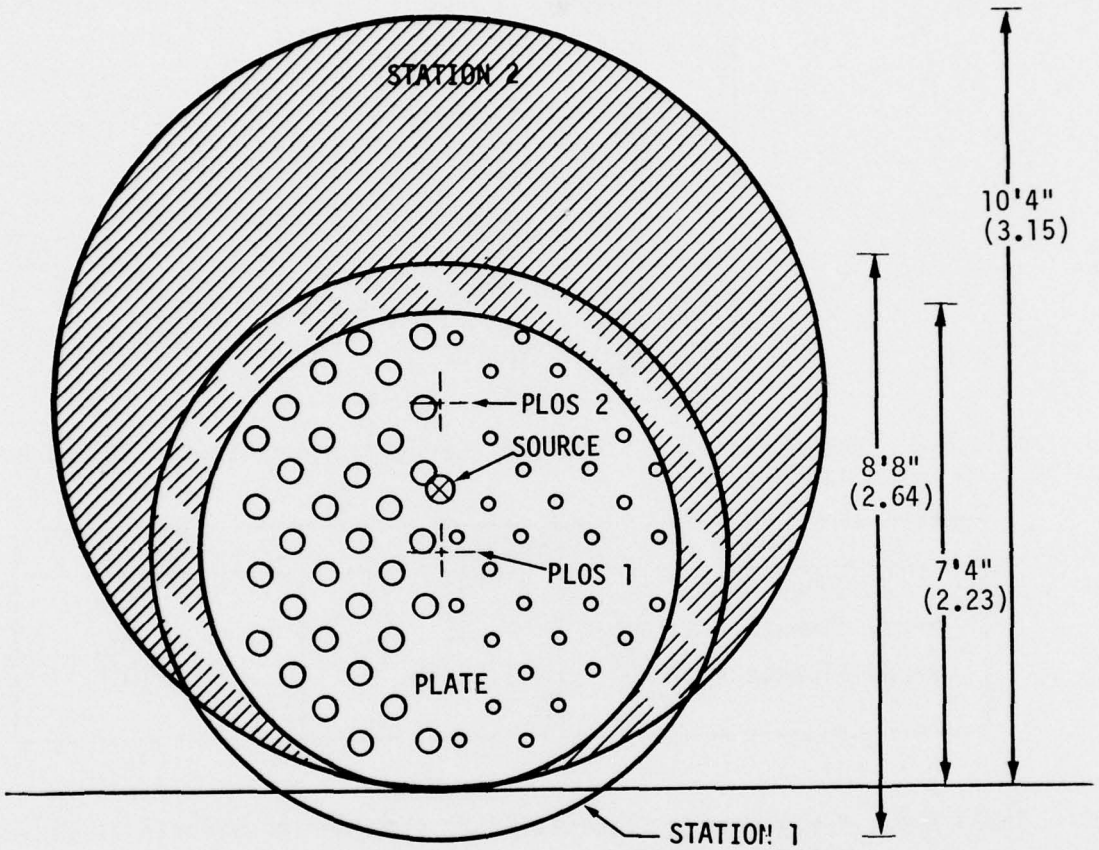

Figure A.2. Location of stations 1 and 2 and scattering plate as seen from end of pipe. Note positions of pipe lines of sight (PLOS) and radiation source. The source diameter (entrance of pipe) and plate holes are not drawn to scale. Dimensions in parentheses are in meters.

Table A.1. Values of the parameters indicated in Figure 2 for the Husky Pup geometry.

h_s:	183 meters
h_1:	298 meters
h_2:	243 meters
θ_1:	0.235°
θ_2:	0.354°
θ_3:	0.0534°
θ_4:	0.0656°

Table A.2. Geometrically attenuated energy fluences at two LOS pipe stations.

	Station 2	Station 1
Distance (m)	243	298
x-ray fluence (cal/cm^2)	135	90
γ-ray fluence (MeV/m^2)	1.35×10^{17}	9×10^{16}

Table A.3. X-ray energy fluences after considering effects of sieve attenuator.

Location	Fluence (cal/cm^2)
Station 2	135
Station 1A	36
Station 1B	23

To estimate the x-ray flux as a function of time, we assume the triangular time waveform described by

$$f(t) = \begin{cases} f_{pk} \dfrac{t}{t_1} & 0 \le t < t_1 \\ f_{pk} \dfrac{t_2 - t}{t_2 - t_1}, & t_1 < t \le t_2 \\ 0, & t > t_2 \end{cases} \tag{1}$$

The area (fluence) is

$$F = \frac{f_{pk}}{2} t_2 \tag{2}$$

Choosing t_1 = 3 ns and t_2 = 6 ns, the peak fluxes at the two stations are found to be the values given in Table 4.

Table A.4. Peak x-ray fluxes.

Location	Peak Flux (cal/cm^2/ns)
Station 2	45
Station 1A	12
Station 1B	8

The gamma ray flux is described by the time waveform

$$f(t) = \frac{F_\gamma \, f_0 \, e^{\alpha t}}{1 + \frac{\alpha}{\beta} e^{(\alpha+\beta)(t-t_0)}} \tag{3}$$

where

$$f_0 = \frac{1}{\pi} (\alpha+\beta) e^{-\alpha t_0} \sin\left(\frac{\pi\alpha}{\alpha+\beta}\right)$$

normalizes the function to unit area. F_γ is the gamma fluence. Since the waveform extends back to $t = -\infty$, t_0 must be chosen to give a value of $f(t)$ at $t = 0$ which is small compared to the peak flux, $f(t_0)$. If R is the ratio of these fluxes, i.e.,

$$R \equiv \frac{f(0)}{f(t_0)} = \frac{f(0)}{f_{pk}} \tag{4}$$

the peak time is determined by

$$t_0 \simeq t_1 + t_2 \tag{5}$$

where

$$t_1 = -\frac{1}{\alpha} \ln\left(\frac{R}{1+\alpha/\beta}\right)$$

$$t_2 = \frac{1}{\alpha+\beta} \ln\left[1 + \frac{\alpha}{\beta}\left(\frac{R}{1+\alpha/\beta}\right)^{\frac{\alpha+\beta}{\alpha}}\right]$$

As before, f_{pk} is the peak flux. As an example we choose $\alpha = 2\times10^8$ sec^{-1}, $\beta = 1\times10^8$ sec^{-1}, and $R = 10^{-3}$, the peak of time is found to be 4.0×10^{-8}. The peak fluxes are given in Table 5.

Table A.5. Peak gamma fluxes inside the LOS pipe.

Location	Peak flux ($MeV/m^2/sec$)
Station 2	1.9×10^{24}
Station 1	1.2×10^{24}

The gamma rays are attenuated an additional 50% in passing through the steel bulkheads. The peak fluxes entering the air are given in Table 6.

Table A.6. Peak gamma fluxes entering the air.

Location	Peak flux (MeV/m^2/sec)
Station 2	9.3×10^{23}
Station 1	6.2×10^{23}

A.2. COMPTON CURRENT AND AIR CONDUCTIVITY ESTIMATES

The Compton currents and ionization rates in the air around the pipe can be estimated from the gamma flux. The currents estimated in this way will be larger than one should really expect because the effect of the electric field on electron motion is neglected. In this case, the error is around a factor of 2.

Outside of calculating EMP, the air conductivity estimates are useful in determining how long the air remains conducting enough to affect the ringing of the LOS pipe, excited by the EMP. For all practical purposes, the excitation is an impulse, so that it's exact form is not critical for that part of the problem.

The current, in our "prescribed" current approximation is given by

$$J(t) = ef(t) \frac{R_{mf}}{E_\gamma R_\gamma} \text{ (amp/m}^2\text{)} \qquad (6)$$

where

e = electron charge

R_{mf} = mean electron range

R_γ = mean gamma range

E_γ = γ-ray energy

$f(t)$ = gamma flux

The quantity $\left(\frac{R_{mf}}{E_\gamma R_\gamma}\right)$ is a slowly varying function of E_γ. For 2 MeV photons, it has the value 0.007 (MeV^{-1}).

The ionization rate is approximately

$$S(t) = \frac{\mu_a \rho}{3.4\times10^{-5}} f(t) \quad \left(\frac{\text{ion-pairs}}{m^3\text{-sec}}\right) \tag{7}$$

where

ρ = material mass density

μ_a = Compton absorption coefficient

The quantity $\left(\frac{\mu_a \rho}{3.4\times10^{-5}}\right)$ is a slowly varying function of E_γ, with the value 95 $\left(\frac{\text{pairs}}{\text{MeV-m}}\right)$ for E_γ = 2 MeV.

Table 7 shows the peak currents and ionization rates developed, along with the total number of electron-ion pairs.

Table A.7. Peak Compton current, ionization rate, and total number of electron-ion pairs generated.

	Station 1	Station 2
Current (amp/m^2	1.7 10^3	1.1 10^3
Ionization Rate (pairs/m^3/sec)	1.4 10^{26}	9.6 10^{25}
Total Ionization (pairs/m^3)	6.4 10^{18}	4.3 10^{18}

We will now proceed to estimate the conductivity that develops around the pipe. Our main objective will be to estimate the late time conductivity to see whether it persists long enough to affect the LOS pipe ringing. Towards this end, we will not solve the full three-species air chemistry equation set, normally solved in EMP calculations. Instead, we will perform two separate computations of electron and ion conductivity, assuming in the first case that electron-ion pairs form instantaneously and that attachment is the dominant loss mechanism. This estimate will show that electrons are lost quite rapidly in the time frame of interest. The second computation will assume that the original electrons attached instantaneously and that the ion loss mechanism is ion-ion recombination. This process continues for a substantial period of time and, despite the low mobility of ions relative to electrons, the ion conductivity cannot be assumed to be negligible for times of interest. Of course, the question of negligibility depends on other factors, e.g., the ground conductivity and air gap size, which affect the damping rate of the pipe signal.

Beginning with the electron conductivity calculations, the electron density is governed by the equation

$$\frac{dN}{dt} = - \beta N \tag{8}$$

where N is the density and β is the electron attachment rate (to oxygen). The solution is

$$N(t) = N_0 \exp(-\beta t) \tag{9}$$

where N_0 is the initial density.

AD-A050 772 MISSION RESEARCH CORP LA JOLLA CA F/G 9/1
UGT NOISE MINIMIZATION TECHNIQUES.(U)
NOV 76 J B SMYTH, V A VAN LINT, M A MESSLER DNA001-76-C-0280
UNCLASSIFIED MRC/SD-R-7 DNA-4306F NL

2 OF 2
AD
A050772

END
DATE
FILMED
4-78
DDC

The conductivity is given by

$$\sigma(t) = e\mu N(t) \tag{10}$$

where μ is the electron mobility and e is the electron charge. We will use values of the mobility corresponding to zero electric field. This will give an overestimate, but the electric field should have decayed to relatively small values by the times of interest, so that the field dependence would not be important anyway. Then, for sea level air, the attachment rate and mobility are given respectively by:

$$\beta = 10^7 \ (6.1 + 1.8 \ P) \qquad (\text{sec}^{-1}) \tag{11}$$

$$\mu = \frac{6.4}{\sqrt{1 + (11.0 \ P^{0.8}_{0})^2}} \ (\text{m}^2/\text{V-sec}) \tag{12}$$

where P is the percentage water vapor content.

The air in an UGT environment can be expected to have a relatively high water vapor content. This lowers the conductivity in two ways: the mobility is decreased and the attachment rate is increased over what could be expected in dry air. By using the zero water vapor values ($P = 0$), we will obtain an upper limit.

Using the total ionization at station 2 (Table 7) as the initial value of electron density (N_0), we obtain the curve shown in Figure 3 (the part labled "electron dominated"). We will discuss this curve after computing the ionic conductivity.

We now assume that all electrons attach instantaneously and that the number of ion pairs given in Table 7 denotes the number of positive air

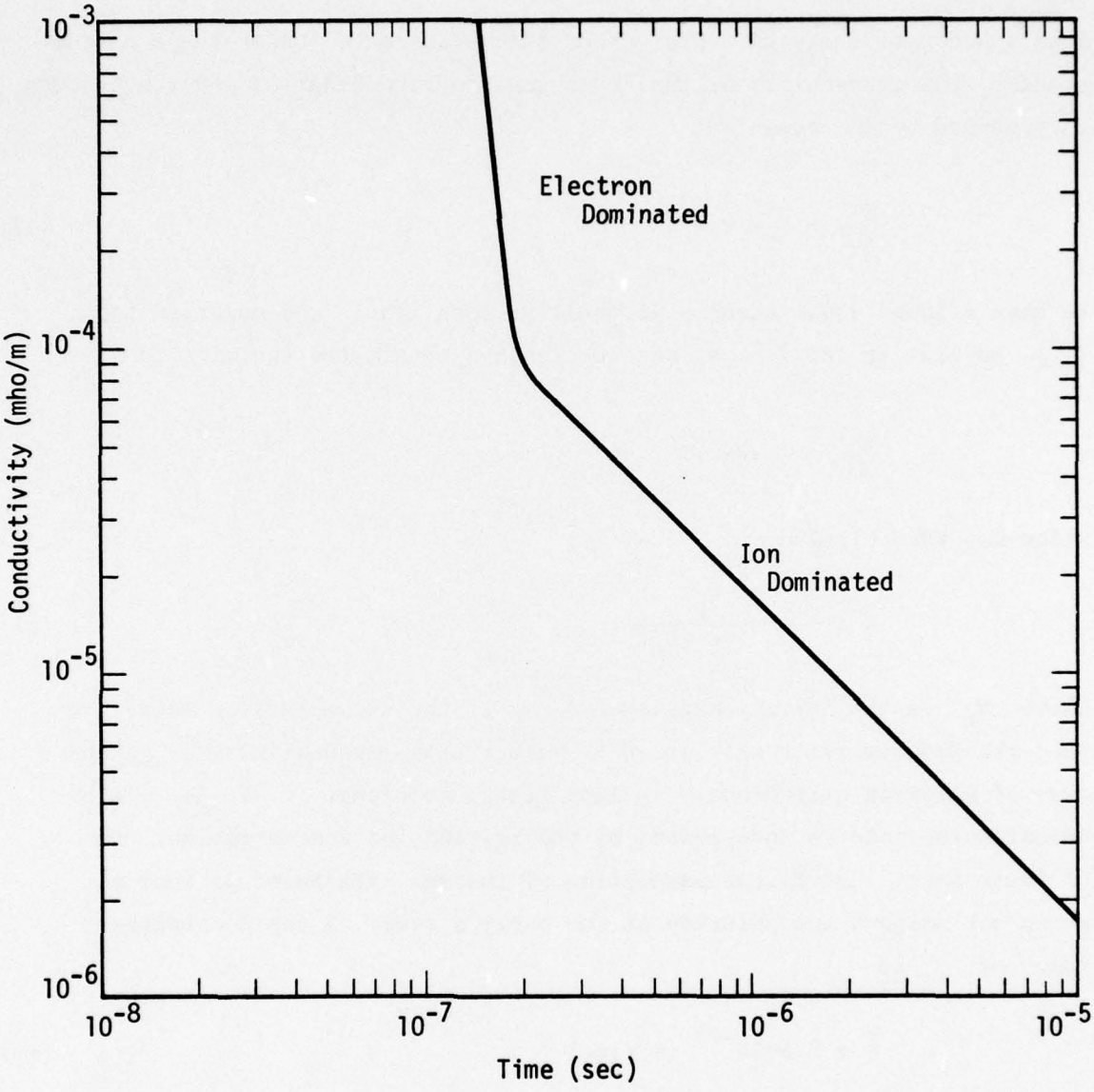

Figure A.3. Approximate conductivity time history at station 2.

ions and negative oxygen ions, rather than electrons. Under these circumstances, the charge loss mechanism is ion-ion recombination and the process is governed by the equation

$$\frac{dN^+}{dt} = \frac{dN^-}{dt} = - \gamma N^+ N^- \tag{13}$$

We have assumed equal numbers of positive ions (N^+) and negative ions (N^-) so that we can look at one species and obtain the equation

$$\frac{dN^-}{dt} = - \gamma (N^-)^2 \tag{14}$$

which has the solution

$$N^-(t) = \frac{N_0}{1 + \gamma N_0 t} \tag{15}$$

where N_0 is the initial density and γ is the recombination rate. Note that the density falls only as t^{-1}, rather than exponentially as in the case of electron attachment. At late times, such that $t >> \frac{1}{\gamma N_0}$, the deionization rate is independent of the initial ion concentration. Both of these facts justify our assumption of instant attachment so long as we do not believe the solution at too early a time. A representative value of γ is

$$\gamma = 2.3 \times 10^{-12} \ (m^3/sec) \tag{16}$$

The ionic conductivity is calculated in the same way as electron conductivity (assuming singly ionized molecules) using an ion mobility of

$$\mu_i = 2.5 \times 10^{-4} \ (m^2\text{-sec/V}) \tag{17}$$

The result is the curve labeled "ion dominated" in Figure 3. Because the deionization rate is eventually independent of initial concentration, the conductivity will be the same at both stations.

In order to interpret the conductivity curve of Figure 3 in terms of something useful we must determine some characteristic times. If signals traveled at the speed of light in free space along the pipe, it would travel the unburied length (55 meters) in about 0.2 μsec. If the pipe ring as a quarter wave stub, it would have a period of 0.8 μsec (~ 1 MHz frequency). In actuality, the phase velocities along the pipe will be less than the free space light velocity, so the period will be longer. This is due to the finite conductivity of the earth around the pipe.

One measure of the effectiveness of the air conductivity in affecting the pipe ringing is to compare the relaxation time implied by it with the characteristic times of the ringing. In Figure 4 we show the relaxation time, t_r, as a function of time. The times shown are those in which ion-ion recombination dominates. The relaxation time is given by

$$t_r = \frac{\varepsilon_0}{\sigma} \tag{18}$$

where σ is the conductivity and ε_0 is the permittivity of free space (8.854×10^{-12} farad/m).

From Figure 4 we see that even at 1 μsec, the relaxation time is 0.5 μsec. This is comparable to the times at which interesting events are occurring and this fact makes the conductivity significant. It would have to be included in a computation of the pipe ringing.

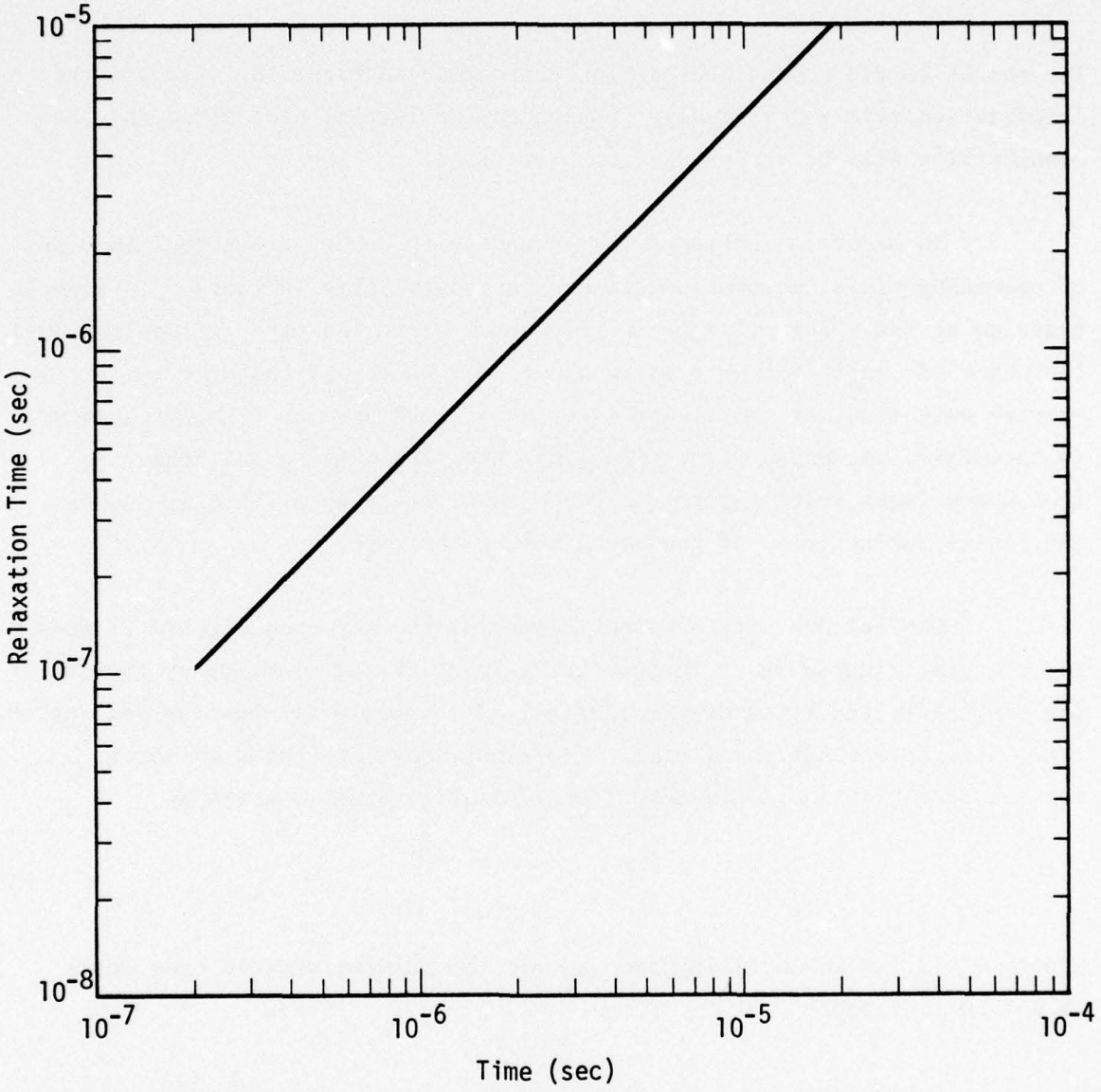

Figure A.4. Relaxation time of plasma as a function of time

A.3. CIRCUIT ANALYSIS OF CASSETTE RESPONSE

Experimental cassettes are exposed to photon radiation at various stations along the pipe. They are commonly mounted on a metal bulkhead, which is essentially normal to the photon wavefront. Most cassette cable shields are grounded to the bulkhead. Therefore, no noise escapes from the interior of the pipe. Some cassettes float above ground, however, and currents can propagate out on the shield. It is this problem that will be of concern here.

Using a quasi-static approximation[1], a circuit model representing the response of the cassette to the x-ray/gamma flux can be developed. This circuit is shown in Figure 5(a). The analysis will be aided in part by reducing the circuit to the Thevenin equivalent shown in Figure 5(b). In the reduction process, the capacitance to the ground plane, C_T, and the plasma resistance, $R_T(t)$, have been lumped with the load resistance, R_L, into a load impedance, Z_L. The current through R_L is the desired quantity.

By definition, we have

$$\frac{1}{C_\infty} = \frac{1}{C_1(t)} + \frac{1}{C_2(t)} + \frac{1}{C_3(t)} \tag{19}$$

where C_∞ is the constant, the capacitance to infinity of the cassette minus that between the base of the cassette and the gound plane directly beneath it (C_T). In the case where the cassette is adjacent to grounded cassettes, these will be considered part of the ground plane and the capacitance between the sides of the ungrounded cassette and the sides of the grounded

---

[1] Messier, M.A., "Stub Antenna Response: Analytical Model Development and Preliminary Predictions:, Mighty Epic Pretest Predictions, Memo #5, Mission Research Corporation, Santa Barbara, CA, March 1976.

cassettes will be included in C_T. $C_1(t)$ represents the capacitance of the layer across which charge is transferred when it is emitted from the cassette, but is not transferred directly to the ground plane. Similarly, $C_3(t)$ represents the capacitance of the layer across which charge is transferred when it is emitted from the ground plane, but does not reach the cassette.

The open circuit voltage driver, in the time domain, is then

$$V(t) = \int_0^t \left[\frac{i_b}{C_1(t)} + \frac{i_g}{C_2(t)} + \frac{i_T}{C_3(t)} \right] dt \tag{20}$$

Here, i_b is the current emitted into space from the cassette, i_g is that emitted from the ground plane, and i_T is the net current transferred directly between cassette and ground plane.

The current into Z_L is, in the frequency domain

$$I_L = \frac{\frac{1}{s}\left[\frac{i_b}{C_1(s)} + \frac{i_g}{C_3(s)} + \frac{i_T}{C_\infty} \right]}{Z_L + \frac{1}{sC_\infty}} \tag{21}$$

The plasma sheath capacitances, C_1 and C_3, appear only as ratios with the currents that move across them. Under the flux conditions discussed earlier, the characteristic sheath thickness are on the order of 10^{-4} meter, i.e., much less than the dimensions of a realistically sized cassette. Both the currents and capacitances will be proportional to emission surface area throughout their time history. The time history of the cassette current will be proportional to that of the ground plane time history. The areas then cancel in the driver terms i_b/C_1 and i_g/C_3, so that we can utilize current density and capacitance per unit length directly; there is no need to estimate an effective area. More importantly,

since i_b and i_g have opposite polarity, they will cancel each other as long as phase differences between the two drivers can be ignored. This is true even if different materials are involved.

The driver currents i_b and i_g, which are the net spatial currents, are proportional to the square root of the electron yield, Y. The sheath thickness, D_v, which enters the capacitance calculation, is inversely proportional (for practical purposes) to the square root of Y. Therefore, C_1 and C_3 are proportional to $\sqrt{Y}$ and this cancels the $Y^{-1/2}$ dependence of i_g and i_b. These two driver terms cancel, even though the ground plane and cassette are constructed from different materials, except for phase differences. This analysis assumes steady state conditions have developed. The time for steady state conditions to develop is about 0.1 ns or faster, for the fluxes under consideration.

With i_b and i_g effectively removed from consideration as drivers, the direct transfer current, i_T, and the leakage resistance, $R_T(t)$, becomes the prime factors controlling the load current. The direct transfer current, i_T, is computed from the emission current density, rather than the net current density as is the case with i_b and i_g. The resulting circuit representation is shown in Figure 6. Here, C_{TOT} has been defined as the total capacitance, i.e.,

$$C_{TOT} = C_\infty + C_T \tag{22}$$

The differential equation describing the load current (I_L) is

$$\frac{dI_L}{dt} + \frac{I_L}{\tau(t)} = K\, i_T(t) \tag{23}$$

where

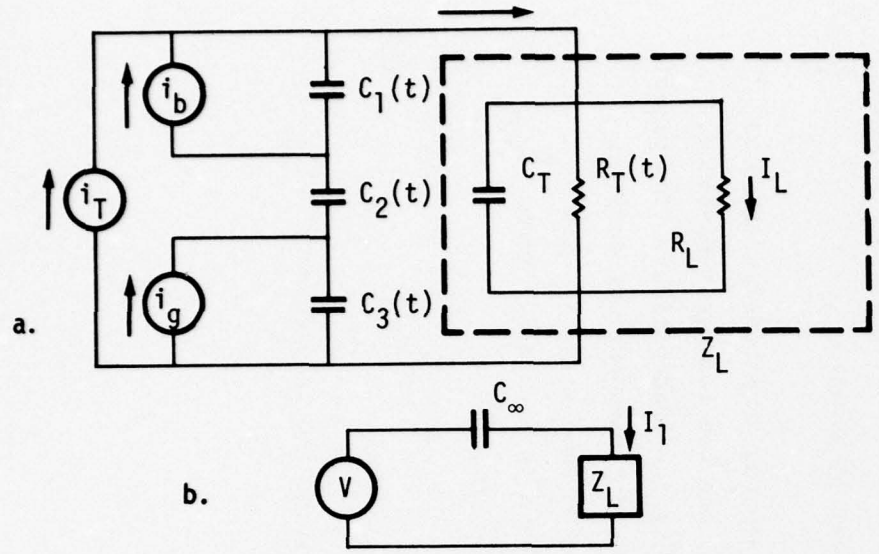

a. Current driver form (time domain)

b. Voltage driver form (frequency domain). Note definition of Z_L and I_1 above.

$$\frac{1}{C_\infty} = \frac{1}{C_1(s)} + \frac{1}{C_2(s)} + \frac{1}{C_3(s)}$$

$$V(s) = \frac{i_b}{s(C_1(s))} + \frac{i_g}{s(C_3(s))} + \frac{i_T}{sC_\infty}$$

Figure A.5. Two forms of the equivalent circuit representing the SGEMP response of a cassette. The voltage driver form is shown as a frequency domain representation for simplicity.

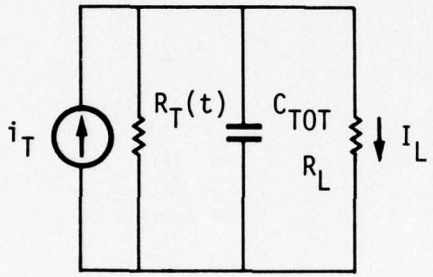

Figure A.6. Simplified equivalent circuit resulting from the elimination of two current drivers, i_g and i_b, from consideration.

$$\tau(t) = \frac{R_L C_{TOT}}{1 + \frac{R_L}{R_T(t)}}$$

$$K = \frac{1}{R_L C_{TOT}}$$

In integral form, the current is given by

$$I_L(t) = K \int_0^t i_T(t') \exp\left[-\int_{t'}^t \frac{dt''}{\tau(t'')}\right] dt' \tag{24}$$

The resistance term has a linear approximation valid for the electrons with energy large compared to the potential barrier which they must cross in going from the ground plane to the cassette or the reverse. This approximation (developed in UGT Noise Memo #2) is

$$R_T = \frac{\sqrt{2 \frac{m}{e} \mathcal{E}_{ev}}}{eNA} \tag{25}$$

where

$\mathcal{E}_{ev}$ = characteristic initial electron energy (eV)

e = electron charge (1.60×10^{-19} coul)

m = electron mass (9.11×10^{-31} kg)

N = electron density (elec/m^3)

A = area across which charge is transferred (m^2)

The driver, i_T, being proportional to the emission current, follows the x-ray flux time history. It is given by

$$i_T = eY\dot{\phi}A \text{ (amps)} \tag{26}$$

where

e = electron charge (1.602×10^{19} coul)

Y = electron yield (electrons/cal)

$\dot{\phi}$ = x-ray flux ($cal/m^2/sec$)

A = effective area across which charge is transferred (m^2)

In Figures 7 and 8 we show the normalized direct transfer current (i_T/A) and the Debye length, ℓ_D. The Debye length is needed to compute A. Figure 7 also shows the electron density. These are computed for Station 2, the high flux station (see Table 4). The current and electron density scale with flux and ℓ_D scales inversely as the square root of flux. In this way, the quantities at stations 1A and 1B can also be computed. These quantities were computed for a representative blackbody x-ray spectrum and emission material and are meant only to be representative.

One can see from Figure 8 that the characteristic distances involved in the electron motion are so small compared to any cassette dimensions, including gaps between grounded and ungrounded parts of the cassette system, that it would be unrealistic to expect any accurate predictions from an analytical model. The response will be highly dependent on the exact cassette configuration. However, we can make some general observations on the time waveforms that can be expected and on the upper limits of the signal magnitudes. These predictions involve multiplying some very large current and electron densities by very small areas, resulting in a number whose order of magnitude is even questionable.

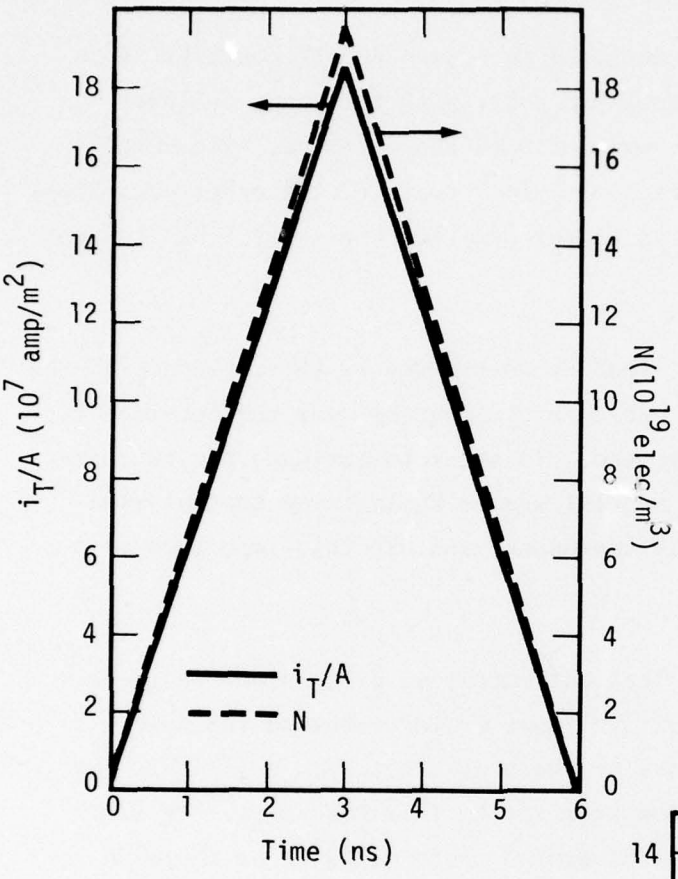

Figure A.7. Normalized direct transfer current and electron density vs time for cassette at Station 2.

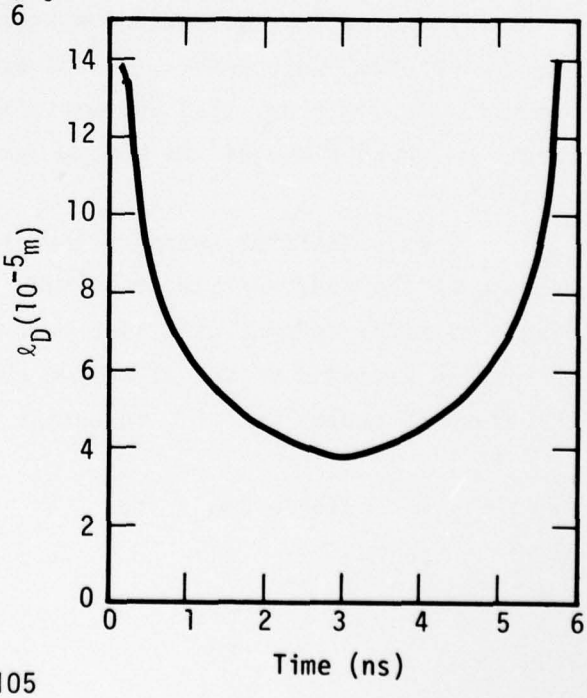

Figure A.8. Debye length vs time for cassette at Station 2.

Consider the cassette depicted in Figure 9. It consists of an outer cylinder grounded to the bulkhead wall, with the inner cylinder representing the instrumentation which floats above ground. The outer cylinder protects the instrumentation against contact with other cassettes, provides electromagnetic shielding and/or modifies the x-ray flux incident on the instrumentation.

The equivalent circuit load is determined by the impedance of the transmission line formed by the cable shield running over the outside of the LOS pipe and then into the ground. In order to estimate the currents being injected onto the shield, we will assume an infinite transmission line, estimate its characteristic impedance, and use this impedance as a resistive circuit load.

In order to make numerical estimates, we will assume that electrons are emitted from the top of the inner cylinder toward the outer shield. It is not clear that many of these will actually cross this gap because its size must be large compared to ℓ_D (see Figure 8). We will assume that they do, however, for otherwise there would be no response to compute. In addition, this current will be opposed by electrons emitted from the ground plane at the bottom back toward the cassette.

We will first estimate the plasma resistance, to see how it compares with the load resistance (which is on the order of 100 ohms). The direct transfer current will also be estimated. Both of these computations require an estimate of the effective charge transfer area. We will use the cassette radius and ℓ_D to obtain this, i.e.,

$$A(t) = 2\pi a\, \ell_D(t) \tag{27}$$

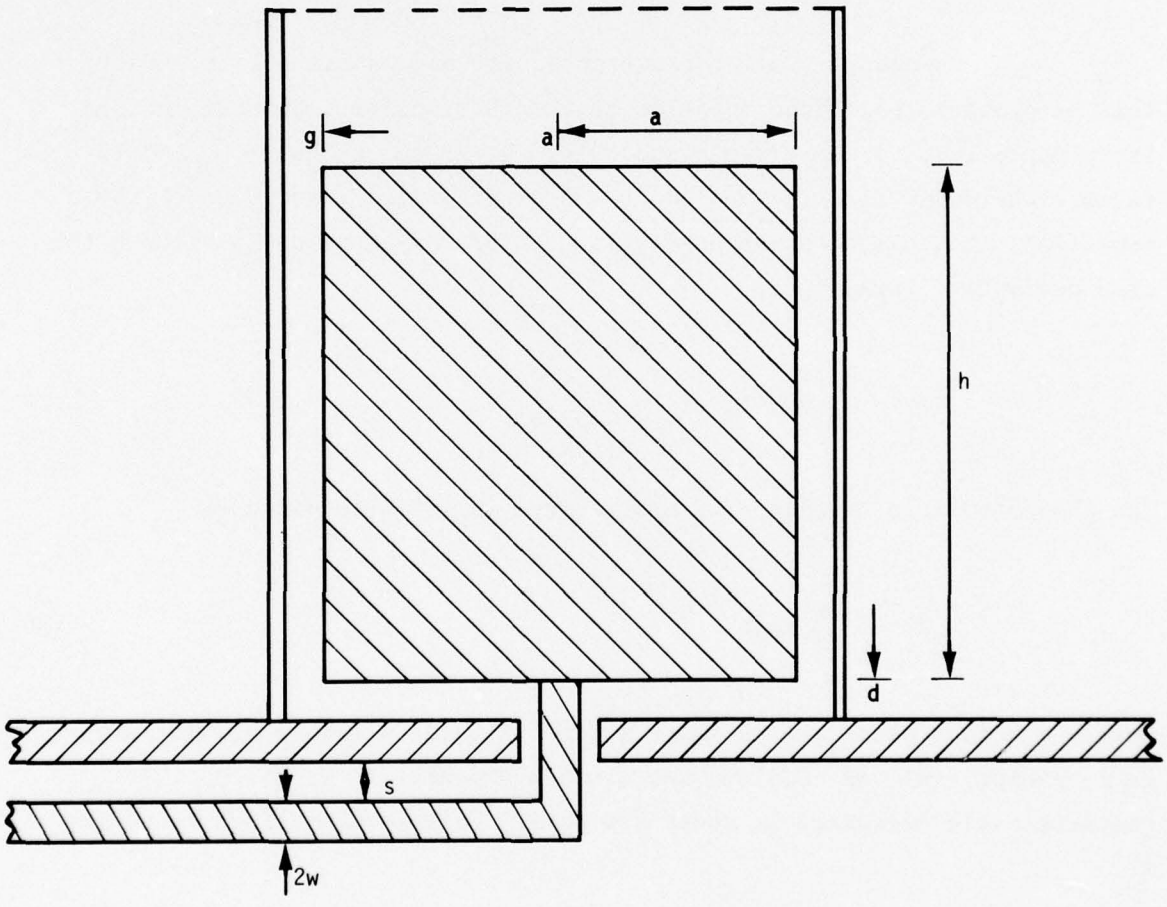

Figure A.9. Schematic diagram of a representative shielded cassette.

The current and resistance are shown in Figures 10 and 11 respectively. The resistance is clearly much less than any reasonable load resistance. Even if it is 100 times too small an estimate, it is still much less. The load is therefore effectively short circuited. The decay constant of Equation 23 is then

$$\tau(t) \simeq R_T(t)\ C_{TOT} \tag{28}$$

A reasonably small gap distance (g and d) is 0.2 cm. Even this is probably too large to allow charge to transfer. However, using it to approximate a capacitance and using h = 5 cm, we have $C_{TOT} \simeq 10^{-10}$ farad. The decay time is then on the order of 5×10^{-12} sec. Under these conditions, the cassette response will be given by Equation 23 without the time derivative term, i.e.,

$$I_L = \frac{R_T(t)}{R_L}\ i_T(t) \tag{29}$$

The characteristic impedance of a wire over an infinite plane is

$$Z_c = \frac{\eta}{2\pi} \cosh^{-1} \frac{s}{w} \tag{30}$$

where $\eta = 120\pi$ ohms and s and w are defined in Figure 9. Assuming a cable radius (w) of 0.5 cm and a cable height (s) of 5 cm, the characteristic impedance is about 200 ohms. This is the value we use for R_L.

The time variation of $R_T(t)$ cancels that of $i_T(t)$, i.e., $R_T i_T$ = constant. Using the above resistance, we have

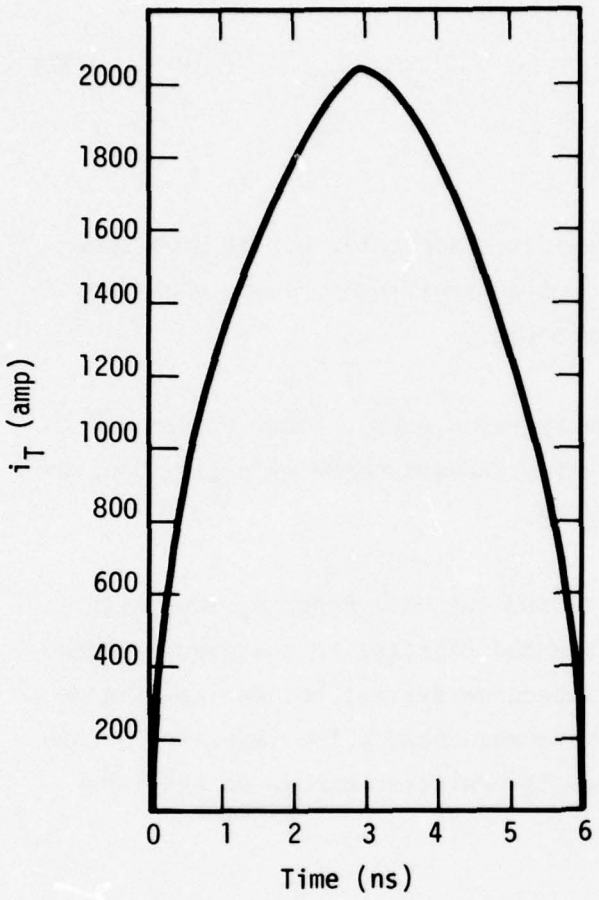

Figure A.10. Direct transfer current computed for the cassette depicted in Figure 9.

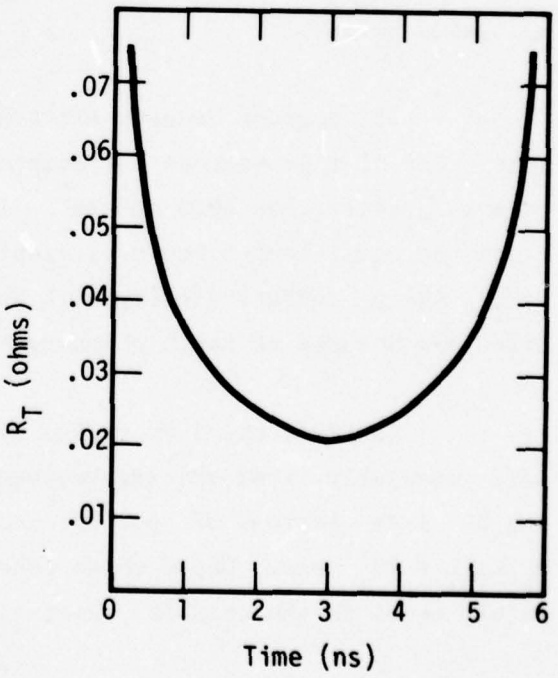

Figure A.11. Plasma resistance computed for the cassette depicted in Figure 9.

$$I_L(t) = 0.22 \text{ (amp)} \tag{31}$$

The voltage across the load is 44 volts.

This computation cannot be considered accurate, but it does show the difficulty one has in trying to predict a significant response on the shields of ungrounded cassettes within the pipe.

An SGEMP can also be generated by gamma rays. Under the conditions which exist here, i.e., when the x-ray induced SGEMP is negligible, the the gamma ray mechanism gains in importance.

Gamma rays can easily penetrate the cassette knocking some high energy electrons ($\sim$ 1 MeV and below) from the cassette to the ground plane. These electrons constitute a very high impedance driver, but the resistance of the plasma cloud generated by the x-rays may cause a low impedance return path. Therefore, it is important to know the relative timing of the x-ray and gamma pulses.

The current density emitted from the cassette will be of the same order of magnitude as the Compton current generated in the air. The peak is greater than 1000 amps/m^2. If we ignore the x-ray plasma's resistance the equivalent circuit is simply the parallel RC formed by R_L and C_{TOT}. All of current density will be transferred across any reasonable sized gap because of the high energies involved.

Consider the 5 cm radius cylinder described above, but with a more reasonably sized spacing between cylinder and ground. Let that spacing be 1 cm instead of 0.2 cm and C_{TOT} becomes 5×10^{-10} Farad, so that $R_L\ C_{TOT} = 10^{-7}$ sec. Under these conditions, the load current is approximately equal to the emission current, or $I_L > 8$ amp.

One factor that has been ignored is the response of the cassette to EMP fields generated within the pipe. This response may become more important in view of the small SGEMP response.

A.4. LOS PIPE RINGING

Gamma rays exiting through the LOS pipe at station bulkheads will induce electric fields which can excite ringing modes in the pipe. Figure 12 shows where these fields are generated. The electric fields are essentially radial. The gamma range in air is about 200m. Thus, the entire top side of the pipe beyond station 2 is surrounded by gamma flux and a parallel (radial) electric field, which is shorted out by the metal surface. The shorting of the radial E-field produces gradients which generate a normal (theta) electric field. The latter propagates along the pipe at the speed of light with the gamma wavefront. The coherent addition of new fields to the propagating field generates a sharp pulse, such as is generated by a surface nuclear burst.

A similar mechanism does not exist to enable currents outside station 1 to generate a coherent signal which propagates back along the pipe. However, the field will excite pipe modes and it will induce a high frequency (compared to pipe oscillation frequencies) signal in cables exiting the bulkhead and hence, parallel to the field lines. The field can exist large distances down the tunnel, because of the long mean free path of the gamma rays. The radial fields will couple with cables running parallel to the tunnel, if they are not protected by a sufficient amount of earth. Since it is apparently the practice to run cables from the pipe into the ground and then along a parallel drift, this method of coupling should not be important, except in the immediate vicinity of the pipe.

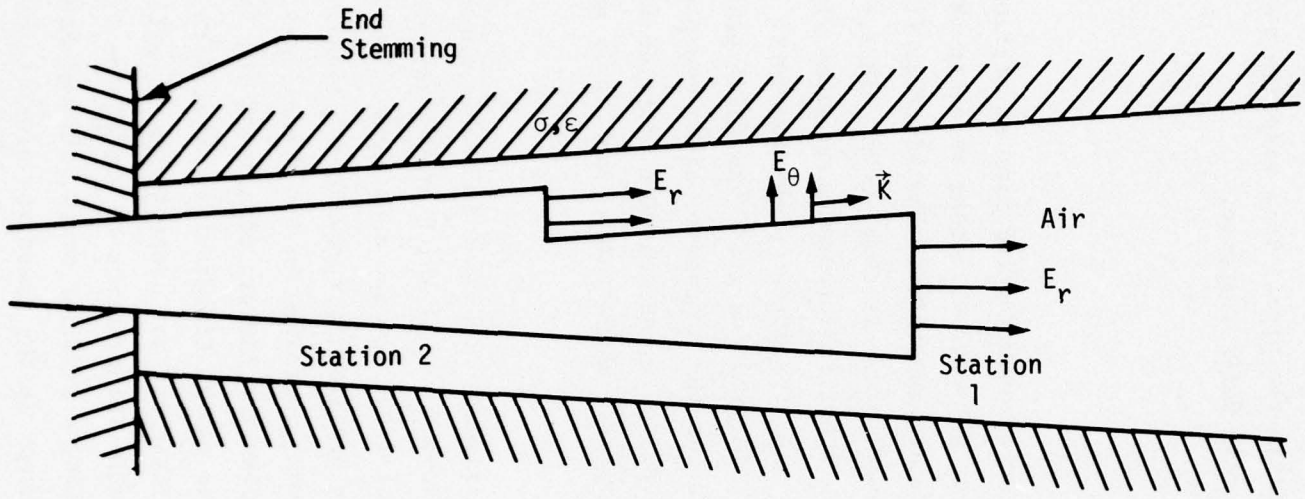

Figure A.12. Sources of EMP excitation of LOS pipe.

When the coherent pulse originating at station 2 reaches the end of the pipe, it will be partially reflected. The reflection will be highly frequency dependent. The pipe is terminated in a tunnel which behaves as a waveguide. If it were perfectly conducting, it would have a sharp cutoff frequency, ω_c, given by (for the TM modes)

$$\omega_c = \frac{c}{a} p_{n\ell} \tag{32}$$

where

$c = 3\times10^8$ m/sec

a = cylinder radius

$p_{n\ell} = \ell^{th}$ root of $J_n(\chi) = 0$

$J_n(\chi) = n^{th}$ order Bessel function

The lowest mode cutoff frequency is given by $p_{01} = 2.405$. Given a tunnel radius of about 3 meters, the cutoff frequency is on the order of 240 MH_z. The finite conductivity of the walls will lower ω_c, but for all practical purposes, one can say that the significant EMP spectrum is below the waveguide cutoff frequency. If the pipe were not partially shorted to ground by cables which are grounded to it, it could be considered a lossy transmission line terminated by a capacitor. The impedance looking into the waveguide is

$$Z_{TM} = \eta\left[1 - \left(\frac{\omega_c}{\omega}\right)^2\right]^{1/2} \tag{33}$$

For $\omega << \omega_c$,

$$Z_{TM} \simeq - j \frac{\eta\omega_c}{\omega} \tag{34}$$

where $\eta = 120\pi$ ohms and where the negative sign is chosen to make the impedance that of a positive capacitor with the value

$$C_{TM} = \frac{1}{\eta \omega_c} \tag{35}$$

The presence of cables and supporting struts places inductances in parallel with this capacitor and with each other. They are also distributed along the length of the pipe and are therefore in parallel with the transmission line distributed admittance. At low frequencies, these projections become short circuits, with their effectiveness depending on how well they are grounded.

Some types of measurements show noise which takes the form of a slowly decaying oscillation with a frequency in the 20 kH_z to 1 MH_z range. One possible source of these oscillations is the pipe ringing mentioned above. Another is the ringing of cable shield currents. Here we will show that it is unlikely that pipe ringing is the source of this noise as long as the differential mode between the pipe and the railroad tracks beneath it have been eliminated by shorting the pipe to the tracks. From the information available, it appears that the practice of welding and bolting the pipe supports to the tracks might suffice as an effective short circuit at the frequencies of interest. There is also a grounding of the entire system, for welding safety purposes, which should suffice to dampen the common mode oscillation more than it would otherwise be.

Consider first the case of an iron pipe with a 1.4 meter radius surrounded by a 1 meter air gap between it and the earth. The earth is characterized by a conductivity (σ) of 1.5×10^{-2} mho/m and a relative dielectric constant (ε_r) of 20. This represents the ungrounded LOS pipe with zero air conductivity. Van Blaricum has computed the propagation constants for this configuration using transmission line theory (see Appendix B). The real and imaginary parts of the propagation constant, Γ, are shown in Figures 13 and 14. Note that these vary almost linearly with

ω indicating a nearly constant phase velocity. For his studies, Van Blaricum defined the propagation constant, Γ, such that a wave propagating in the $+Z$ direction varies as $e^{-\Gamma Z}$. The attenuation with distance is then given by the real part of Γ.

In free space, with signals traveling at the velocity $c = 3\times10^8$ m/sec, the 55m long exposed pipe would ring at a frequency of nearly 1 MH_z, if the stemming is treated as perfectly conducting and the pipe behaves as a quarter wave stub. The lossy cavity will reduce the phase velocity so that it rings with a lower frequency.

As already mentioned, the phase velocity (v) is essentially constant. With the finite conductivity wall, the phase velocity is complex, giving rise to a complex Γ. The real part of v gives the velocity at which a wave travels along the pipe. The real part of v, i.e., v_r, is given from the propagation constant by

$$v_r = \omega \frac{\Gamma_i}{|\Gamma|^2} \tag{36}$$

From Figures 13 and 14 we find that v is essentially real and has the value $v_r/c \simeq 0.52$, i.e., half the velocity of light in free space. Since the resonant frequency in free space was ~ 1 MH_z, the insulated pipe frequency is ~ 500 kH_z.

When the pipe is shorted to ground, the system becomes overdamped and does not support any oscillations. This is indicated by the propagation constant of Figures 15 and 16. Here we see that the real and imaginary parts are equal and vary as $\sqrt{\omega}$, characteristic of the behavior of a wave propagating in a good conductor.

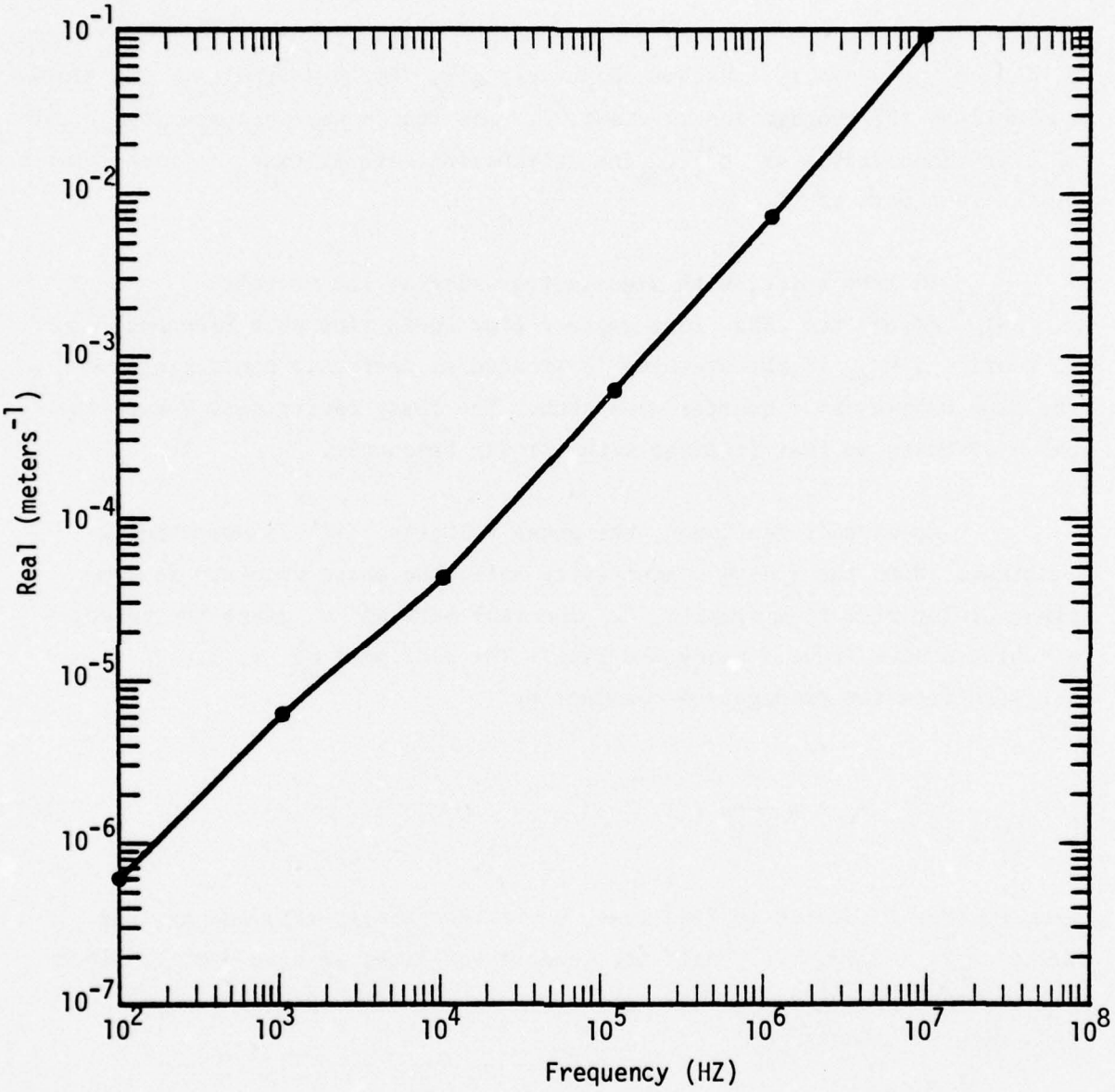

Figure A.13. Real part of propagation constant for 1.41 meter radius iron pipe with 1 meter air insulation buried in earth.

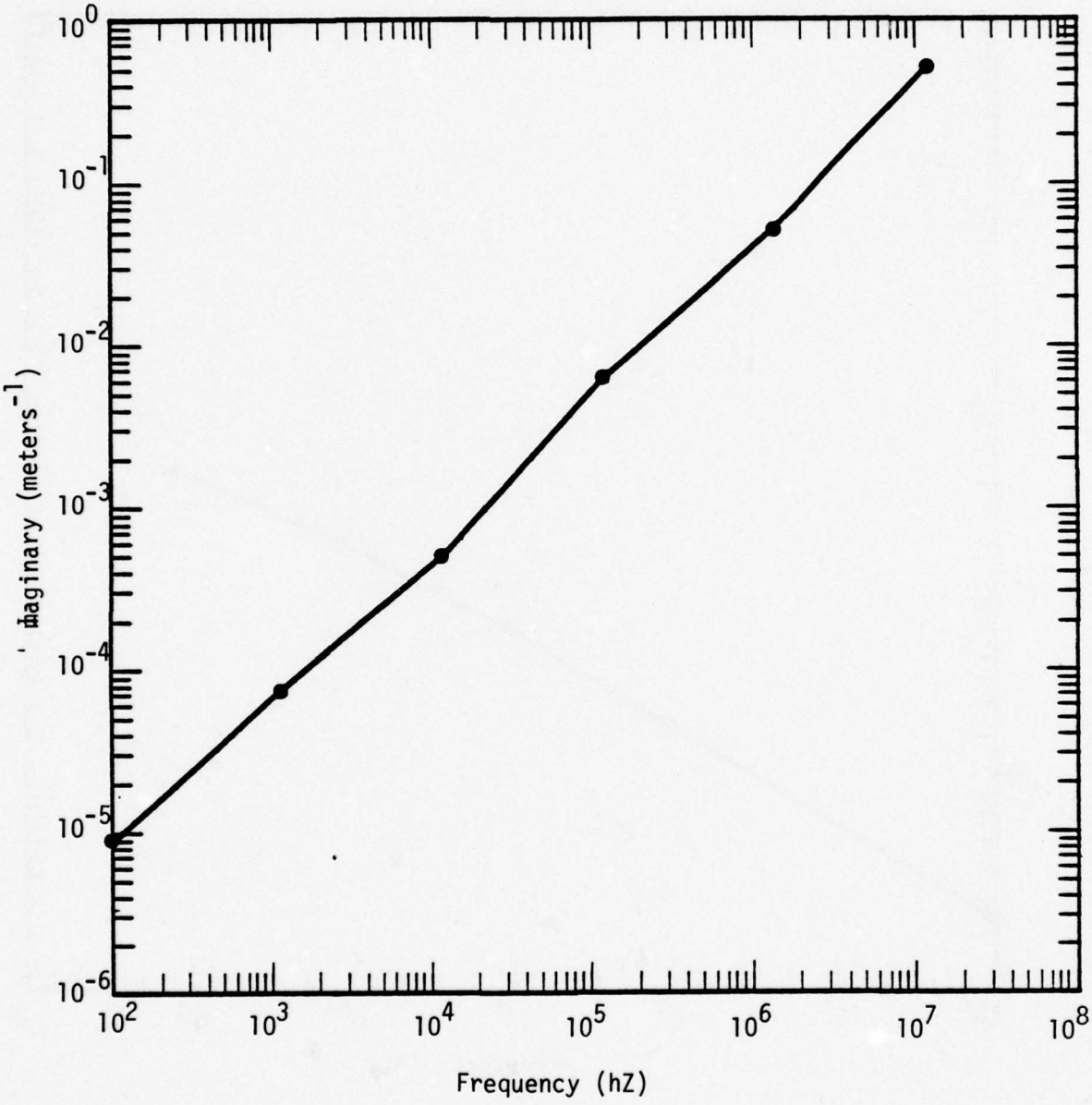

Figure A.14. Imaginary part of propagation constant for 1.41 meter radius iron pipe with 1 meter air insulation buried in earth.

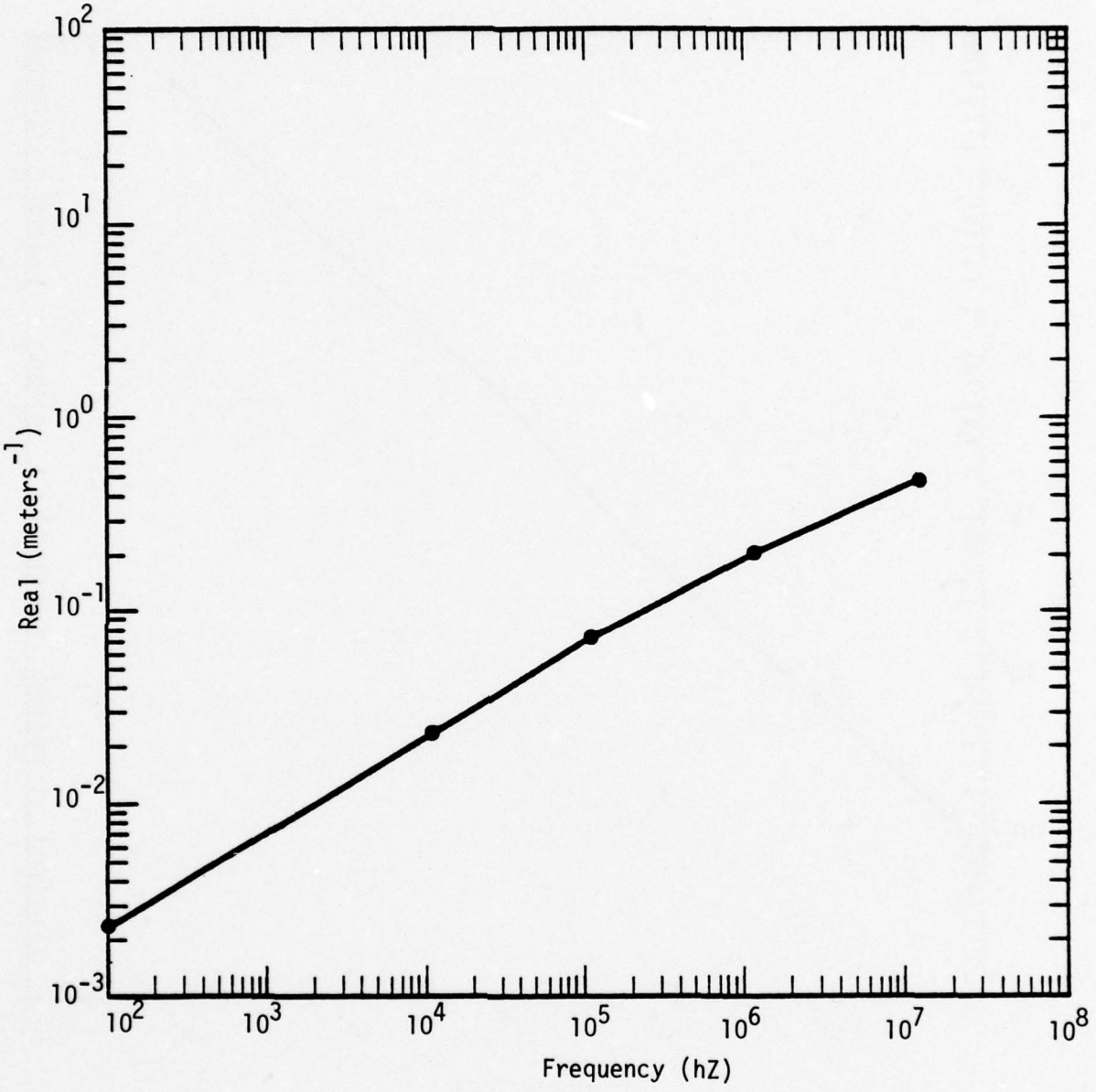

Figure A.15. Real part of propagation constant for 1.41 meter radius pipe made of iron buried in earth.

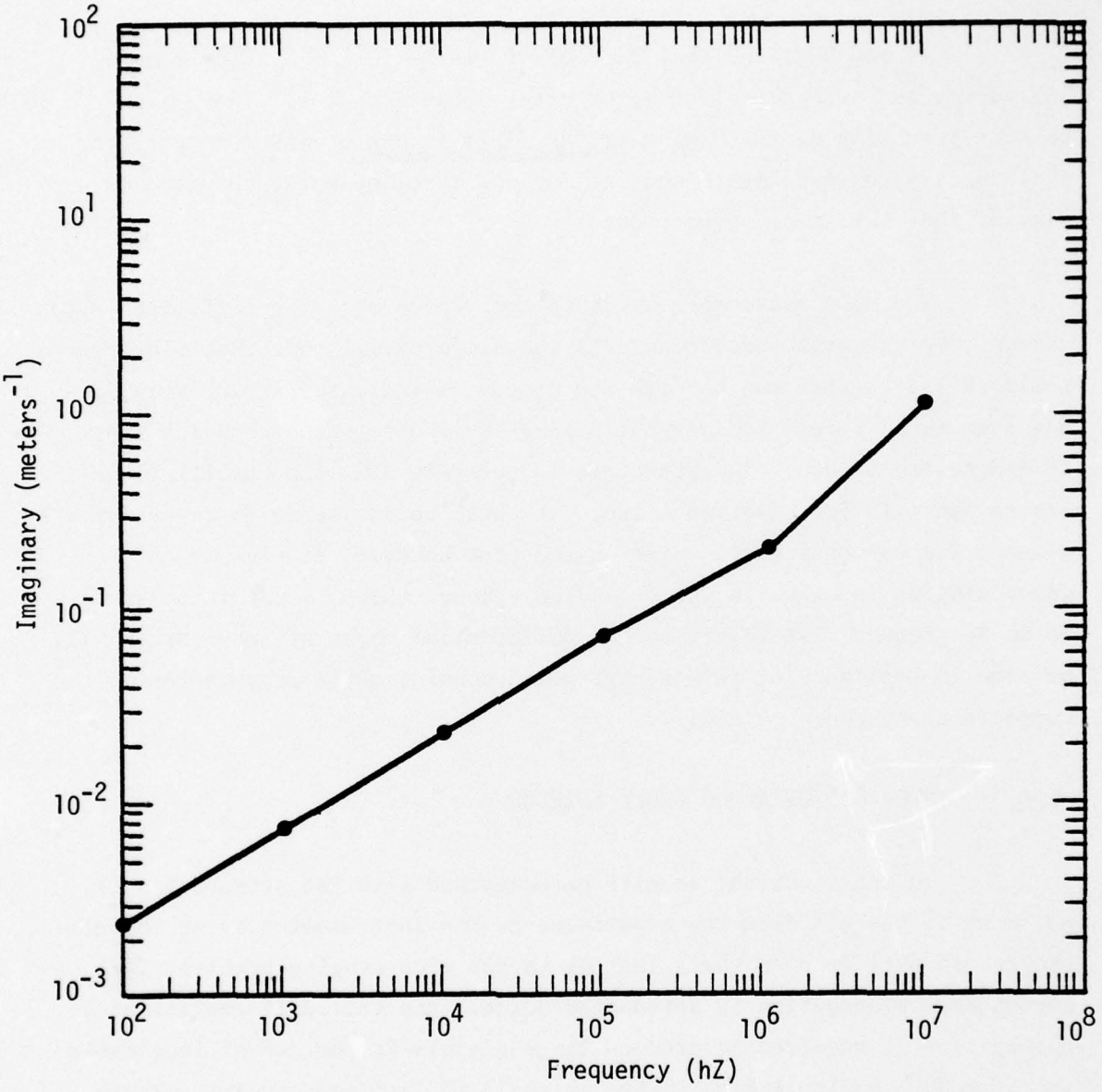

Figure A.16. Imaginary part of propagation constant for 1.41 meter radius pipe made of iron buried in earth.

At 500 kH_z, the real part of Γ is 1×10^{-3} m^{-1}. The ringing will decay an e-fold in 1000 m, or after about 5 cycles. Thus, even without grounding or scattering of the field by cables and supports, the field decays too quickly to account for the types of noise observed on many of the "late time" experiments.

The most reasonable way that the pipe could ring sufficiently to account for the measured data is via the differential mode involving the railroad tracks that run beneath the pipe. As indicated above, this does not seem to be likely because the pipe is welded to supports which are welded to the tracks. Therefore, it is unlikely that pipe oscillations are responsible for observed noise. It would be advisable to experimentally measure the currents which exist on the pipe however, in view of the uncertainties involved in the grounding scheme, which is not intended to be an RF ground. The importance of differential modes of propagation will be seen in Section 5 of this report which considers the propagation of currents along cable shields.

A.5. PROPAGATION ALONG CABLE SHIELDS

In this section, we will be concerned with the attenuation of noise as it travels from the experiment to the instrumentation or to splice racks. It will be seen that, just as in the pipe ringing problem, that common mode propagation is attenuated quickly and that differential mode propagation is required to produce large signals at the end of long cables or to produce cable ringing noise, which is to last many cycles. There are two obvious ways to introduce differential modes. The first, as suggested by Sites[2] is the differential mode between cables within the same bundle. This is possible because of the different grounding schemes

---

[2] Sites, K.R., "Mighty Epic Cable Noise Study" Technical Report LV-103, Science Applications, Inc., Las Vegas, August 1976.

employed by various experimenters. It is probably enhanced by the introduction of a zipper shield which prevents any interaction of the differential mode fields with the conducting ground. The second possible differential mode involves the interaction of the cable bundle as a whole with a nearby railroad track or a second cable bundle.

Consider a single cable bundle lying over earth ($\sigma = 1.5\times10^{-2}$ mho/m and $\varepsilon_r = 20$, as before). Van Blaricum has computed the propagation constant for a 0.075 m radius cable with a 0.002 m thick dielectric coating ($\varepsilon_r = 2.75$). The results are shown in Figures 17 and 18. The calculations were made using the theory described in Appendix B.

From Figure 17 we see that the e-fold decay distance varies between 100 m and 10 m for frequencies between 100 kH_z and 1 MH_z. It goes without further discussion that such attenuation rates precludes the possibility of noise reaching instrumentation within these frequency limits. The attenuation decreases quickly below 100 kH_z, however. At 10 kH_z, the e-fold distance is about 2500 m. A representative distance from the experiment to a trailer on the mesa is 1000 m - 1500 m.

Computations performed by Van Blaricum indicate that the introduction of a railroad track at a distance of a meter or more does not improve the propagation qualities of the system. Therefore, high frequency noise cannot be propagated by that mode.

The most likely candidate for noise propagation mode of the year is the differential mode between bundled cables with different grounding schemes. Noise is injected near the pipe either by early time EMP coupling or TREES effects. Currents traveling on inner cables are protected from the dissipative effects of the ground by the cables around them. If a zipper shield is used, it protects even the outer cable shields. In this

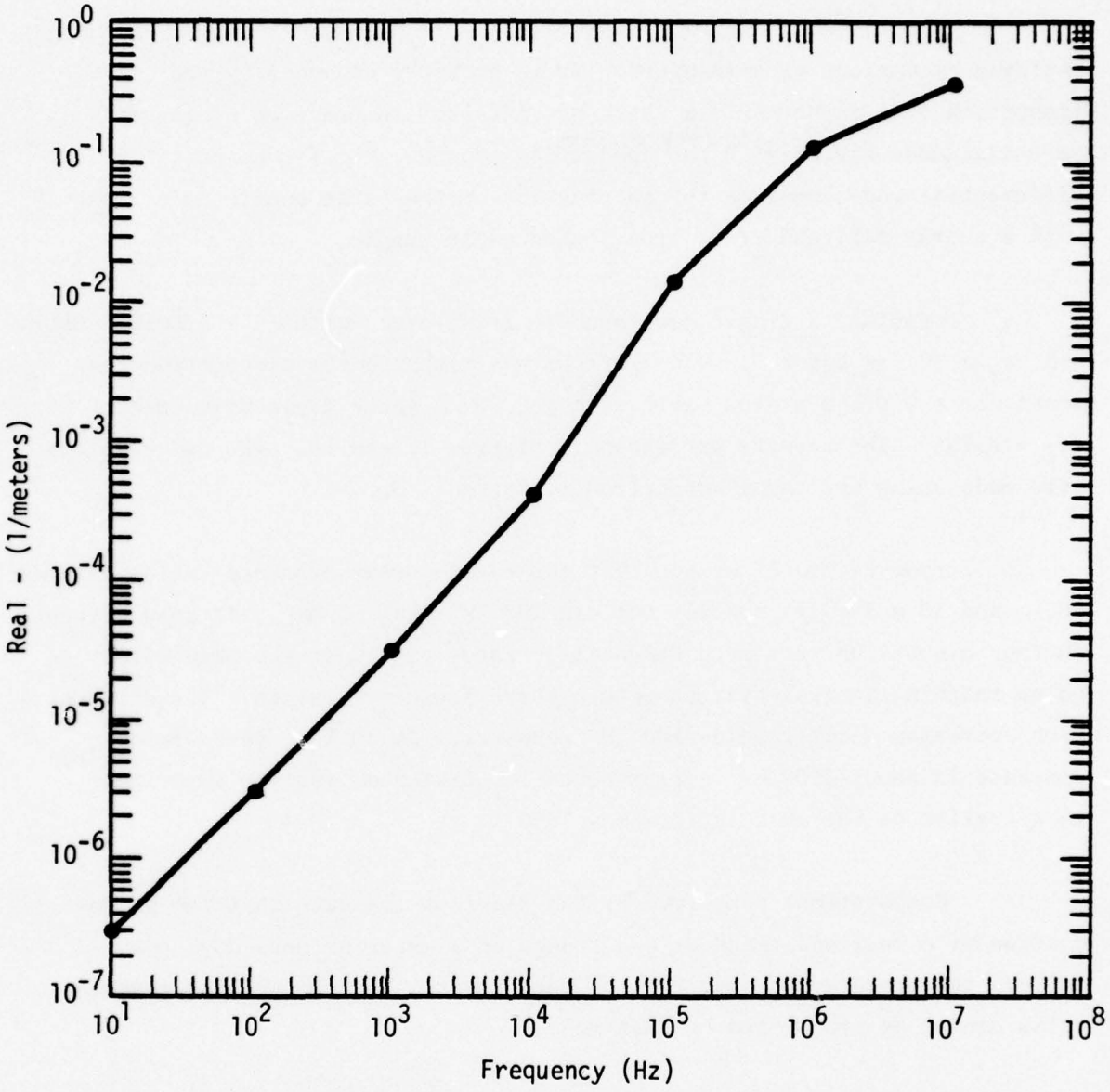

Figure A.17. Real part of propagation constant, Γ, for coated copper cable lying on earth.

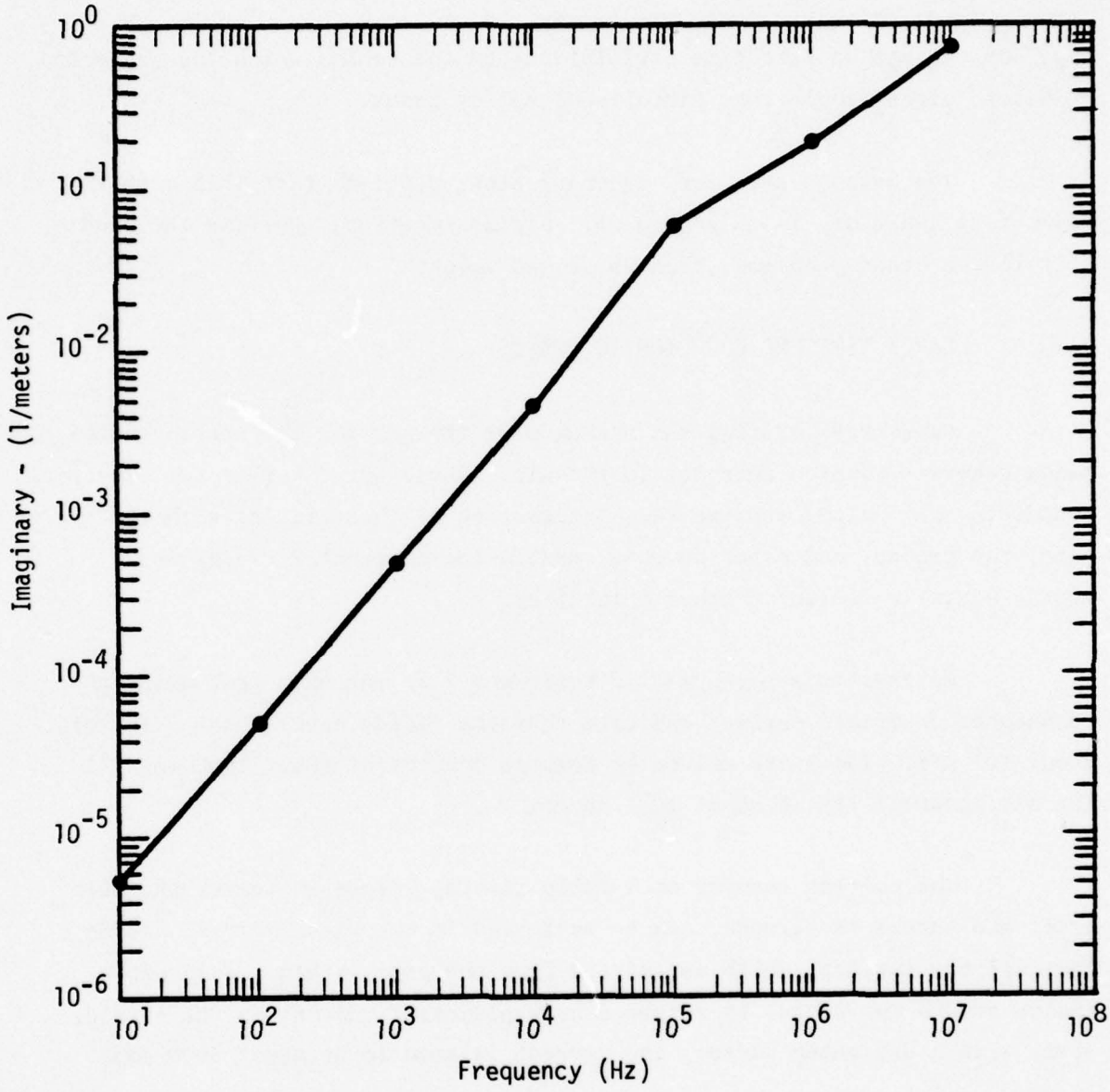

Figure A.18. Imaginary part of propagation constant, Γ, for coated copper cable lying on earth.

way, one can set up late time oscillations on the cables which, as suggested by Sites, might couple into circuits at splice boxes.

The obvious solution, ignoring other problems that this author may not be aware of, is to ground all shields together. Burying the bundle will reduce other problems, such as ground loops.

A.6. EARLY TIME EMP COUPLING TO CABLES

Gamma rays exiting the vacuum pipe through the two station bulkheads generate Compton currents in the air. These drive horizontal electric fields in the ionized atmosphere. Interaction of these fields with the pipe, the ground, and other objects, modify the horizontal fields and create electric fields of other polarities.

Calculations performed in Reference 1 of the main text using the techniques described earlier indicate that the fields have a peak value of about 10^5 V/m. These are driven by Compton current of about 1000 amp/m^2. The air conductivity is about 10^{-2} mho/m.

The current running on a cable shield, before it leaves the main drift and enters the ground, can be estimated in two ways. First, assume that all the current, which is emitted from the pipe within a skin depth radius around the cable, is returned as replacement current on the shield. Then, with a one meter radius, the current is seen to be about 3000 amps.

The second estimate is made by modeling the cable shield as a transmission line with the return path being the air plasma. It is a lossy transmission line with time dependent parameters, but the characteristic impedance is on the order of 10 ohms. With one meter of cable exposed parallel to the field, and a peak electric field of 1×10^5 V/m, the induced current would be 1×10^4 amp.

Therefore, it is reasonable to estimate that between 10^3 amp and 10^4 amp of shield current are induced on the shield by EMP between the pipe and the ground. The pulse width is a few tens of nanoseconds. The fields which penetrate the shield will have a slower rise-time because the diffusion process favors the low frequency components of the fields. Therefore, the pulse width of the fields induced between the inner and outer shield can be on the order of hundreds of nanoseconds. The use of an outer shield around the cable bundle is indicated as a means of reducing this problem.

APPENDIX B

UGT NOISE CHARACTERIZATION

Determination of the Propagation Constants for Various Cable Configurations: The Theory

APPENDIX B

INTRODUCTION

In the underground test tunnels the transmission cables can take on many different configurations. They can be buried, lying on the surface, bare, insulated, or in close proximity to other cables or conducting systems. For the purpose of noise characterization it is necessary to know the values of the propagation constants on these various transmission systems.

This Appendix presents a unified method from which the approximate propagation constants for the following transmission systems can be obtained:

1. Bare wire buried in infinite earth.
2. Bare wire lying on air-earth interface.
3. Dielectrically coated wire buried in infinite earth.
4. Dielectrically coated wire lying on air-earth interface.
5. Two wires, either bare or coated, buried in earth.
6. Two wires, either bare or coated, lying on air-earth interface.

Of particular interest in the underground tunnel is the last configuration, #6, because in the tunnel there is a dielectrically coated cable lying on the ground in the presence of a conducting railroad track. Likewise, models #1 and #3 can be used to determine the transmission properties of the pipe in the tunnel.

The approximating procedures to be presented here have, for several of the above configurations, been derived elsewhere in the literature. However, because of the approximations made and in order to present one unified development, all of the necessary derivations will be shown. The appropriate references will be made as the development proceeds.

B.1. THE BARE CYLINDRICAL WIRE IN EARTH

The derivations of the propagation constants for all of the cable configurations listed in the introduction are based on that of the bare wire in earth. Hence, the propagation constant for the bare wire will be derived in rigorous detail starting with the necessary Maxwell's equations. The details of this derivation can also be found in Reference 1.

The appropriate Maxwell's equations are

$$\nabla \times \overline{B} = \mu\epsilon \frac{\partial \overline{E}}{\partial t} + \mu\sigma\overline{E} \tag{1}$$

$$\nabla \times \overline{E} = - \frac{\partial \overline{B}}{\partial t} \tag{2}$$

Assuming that only the dominant TM mode is present, then, in cylindrical coordinates, only the E_z, E_r, and B_θ field components can exist. If the vector fields are expressed as

$$\overline{E} = (E_z\hat{z} + E_r\hat{r})\ F \tag{3}$$

$$\overline{B} = B_\theta\hat{\theta}F \tag{4}$$

$$F = e^{j(hz-\omega t)} \tag{5}$$

then Equations 1 and 2 can be rewritten

$$j\omega B_\theta = jhE_r - \frac{\partial E_z}{\partial r} \tag{6a}$$

$$- jhB_\theta = (- j\omega\epsilon\mu + \mu\sigma)\ E_r \tag{6b}$$

$$\frac{1}{r}\left[\frac{\partial (rB_\theta)}{\partial r}\right] = (- j\omega\epsilon\mu + \mu\sigma)\ E_z \tag{6c}$$

Equation 6b can be rewritten

$$E_r = \frac{- jhB_\theta}{- j\omega\varepsilon\mu + \mu\sigma} \tag{7}$$

so that combining Equation 7 and 6a gives

$$\frac{-j\omega\lambda_i^2 B_\theta}{k_i^2} = \frac{\partial E_z}{\partial r} \tag{8}$$

where

$$k_i^2 = \varepsilon_i\mu_i \omega^2 + j\sigma_i\mu_i\omega \tag{9}$$

$$\lambda_i^2 = k_i^2 - h^2 \tag{10}$$

and the subscript i indicates which medium the fields are being expressed in. In this paper medium 1 is the conductor, medium 2 is earth, and medium 3 will be the dielectric insulating sheath, see Figure 1a and b. Putting Equation 8 into equation 7 gives

$$E_r = \frac{jh}{\lambda_i^2} \frac{\partial E_r}{\partial r} \tag{11}$$

Substituting Equation 8 in Equation 6c results in

$$\frac{1}{r} \frac{\partial}{\partial r} \frac{r\partial}{\partial r} E_z + \lambda_i^2 E_z = 0 \tag{12}$$

which is just Bessel's equation with $p = 0$.

The appropriate solutions to Equation 12 in the two regions (medium 1 and 2) can be written down for E_z, then Equation 8 and 11 can be used to express E_r and B_θ. The resulting field components are:

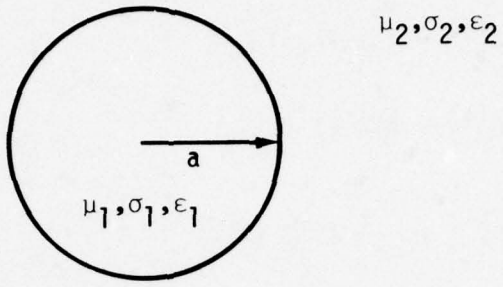

a. Bare cable

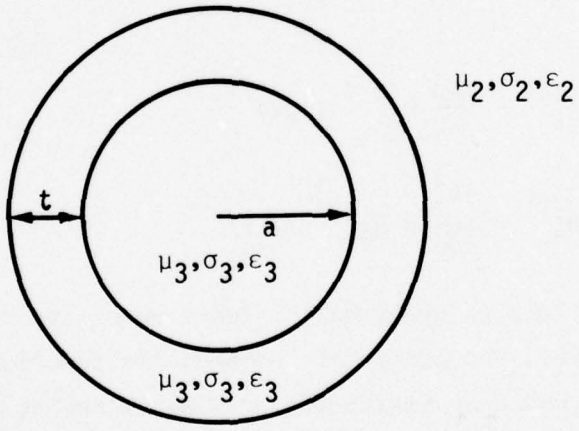

b. Insulated cable

Figure B.1. Buried cable configurations.

Medium 1 - In the Wire, $r < a$

$$E_z^{(1)} = A\, J_0(\lambda_1 r) \tag{13a}$$

$$E_r^{(1)} = \frac{jhA}{\lambda_1}\, j_0'\, (\lambda_1 r) \tag{13b}$$

$$B_\theta^{(1)} = \frac{jk_1^2}{\omega\lambda_1} A\, J_0'\, (\lambda_1 r) \tag{13c}$$

with

$$J_0'\, (\lambda_1 r) = \frac{dJ_0(\lambda_1 r)}{d(\lambda_1 r)} \tag{14}$$

and where $J_0(\lambda_1 r)$ is Bessel's function of zero order.

Medium 2 - the Earth, $r > a$

$$E_z^{(2)} = BH_0^{(1)}\, (\lambda_2 r) \tag{15a}$$

$$E_r^{(2)} = \frac{jhB}{\lambda_2} H_0^{(1)'}\, (\lambda_2 r) \tag{15b}$$

$$B_\theta^{(2)} = \frac{jk_2^2}{\omega\lambda_2} B\, H_0^{(1)'}\, (\lambda_2 r) \tag{15c}$$

where $H_0^{(1)}$ is the zero order Hankel function of the first kind and $H_0^{(1)'}$ is its derivative. The choice of the Bessel's function in medium 1 insured that the fields would be finite for $r < a$. Likewise the choice of Hankel functions in region 2 insures that the fields go to zero as r goes to infinity.

The constants A and B appearing in Equation 13 and 15 are solved by applying the boundary conditions at $r = a$. The boundary conditions

are that the tangential E and H components are continuous across the boundary, r = a. Since $\mu_1 = \mu_2 = \mu_0$ then:

$$E_z^{(2)} = E_z^{(1)} \quad , \quad r = a \tag{16a}$$

$$B_\theta^{(2)} = B_\theta^{(1)} \quad , \quad r = a \tag{16b}$$

hence

$$AJ_0(\lambda_1 a) = BH_0^{(1)}(\lambda_2 a) \tag{17a}$$

and

$$\frac{jk_1^2 AJ_0(\lambda_1 a)}{\omega\lambda_1} = \frac{jk_2^2}{\omega_2} BH_0'(\lambda_2 a) \tag{17b}$$

If A and B are solved from Equation 17 a and 17b then the expression

$$\frac{k_2^2 \lambda_1}{k_1^2 \lambda_2} \frac{H_1^{(1)}(\lambda_2 a)}{H_0^{(1)}(\lambda_2 a)} = \frac{J_1(\lambda_1 a)}{J_0(\lambda_1 a)} \tag{18}$$

results, where

$$J_1(z) = - J_0'(z) \tag{19a}$$

$$H_1^{(1)}(z) = - H_0^{(1)\prime}(z) \tag{19b}$$

The propagation constant of the bare wire in earth, h, can be solved as a function of frequency by using the transcendental Equation 18. Obviously the solving of Equation 18 is not a trivial procedure so the following approximate procedure[1,2] is usually followed in order to simplify the calculational effort.

Since the inner conductor's conductivity σ_1 is not infinite but is usually very high, then it can be argued that h differs only slightly from k_2. Thus

$$\lambda_2 = \sqrt{k_2^2 - h^2}$$

is a small quantity. Using the small argument expressions for the Hankel[3] functions

$$H_0^{(1)}(\lambda_2 a) \approx \frac{2j}{\pi} \ln\left(\frac{\gamma\lambda_2 a}{2j}\right) \tag{20}$$

$$H_1^{(1)}(\lambda_2 a) \approx \frac{-2j}{\pi\lambda_2 a} \tag{21}$$

where $\lambda = 1.781072$ gives for small $\lambda_2 a$

$$\frac{H_1^{(1)}(\lambda_2 a)}{H_0^{(1)}(\lambda_2 a)} \approx \frac{-1}{\lambda_2 a \ln\left(\frac{\gamma\lambda_2 a}{2j}\right)} \tag{22}$$

Since $|k_1| >> k_2$ and $k_2 \approx h$ then $\lambda_1 >> 1$ and the asymptotic expansion for J_0 and J_1 can be used. Stratton[4] shows that if the asymptotic expansion for J_0 and J_1 are used, then

$$\frac{J_1(\lambda_1 a)}{J_0(\lambda_1 a)} \to + j \tag{23}$$

Thus, Equation 18 can now be written

$$\frac{k_2^2\lambda_1}{k_1^2\lambda_2} \frac{(-1)}{\lambda_2 a \ln\left(\frac{\gamma\lambda_2 a}{2j}\right)} = j \tag{24}$$

Since it was assumed that $k_1 << h$ then $\lambda_1 \approx k_1$ and Equation 24 becomes

$$(\lambda_2 a)^2 \ln\left(\frac{\gamma \lambda 2^a}{2j}\right) = j \frac{k_2^2}{k_1} \cdot a \tag{25}$$

Equation 25 can now be solved for λ_2 by the iteration method of Sommerfeld[4]. Let

$$\xi = \left(\frac{\gamma \lambda_2 a}{2j}\right)^2 \tag{26}$$

then Equation 25 becomes

$$\xi \ln \xi = \frac{-\gamma_j^2 k_2^2 a}{2k_1} = \eta \tag{27}$$

The value of η is known from the parameters of the system. The value of $\ln\xi$ is slowly varying compared to ξ itself, hence we can write

$$\xi_{n+1} \ln \xi_n = \eta \tag{28}$$

which gives the iterative procedure for determining ξ. It will be shown in a later section that a good starting value for ξ_0 is

$$\xi_0 = \left(\frac{a}{a+\delta_2}\right)^2 \tag{29a}$$

where

$$\delta_2 = \sqrt{\frac{2}{\omega \mu_0 \sigma_2}} \tag{29b}$$

If the starting ξ_0 of Equation 29a is used it is found that ξ converges to one percent after only two to four iterations for realistic and typical wire and earth parameters. Once the final ξ is found, then

$$\lambda_2 = \frac{2j\sqrt{\xi}}{\gamma_a} \tag{30a}$$

and

$$h = \sqrt{k_2^2 - \lambda_2^2} \tag{30b}$$

B.2. TRANSMISSION LINE MODEL FOR THE BARE WIRE IN EARTH

In order to extend the bare wire formulation to that of a coated wire and in order to determine the distributed parameters it is necessary to formulate a transmission line model for the bare wire. The model development will follow that of Reference 1 and will incorporate the modification of Reference 2.

The transmission line model to be used is shown in Figure 2. The total longitudinal impedance per unit length, Z_b, is the series sum of the skin impedance, Z_s, of the conductor and the longitudinal inductive impedance, Z_L. The transverse admittance Y_b is determined from the transverse impedance Z_t.

The transverse impedance Z_t is defined as

$$Z_t = \frac{V_r}{I_r} \tag{31}$$

where the radial voltage V_r is

$$V_r = \int_a^\infty E_r d_r \tag{32}$$

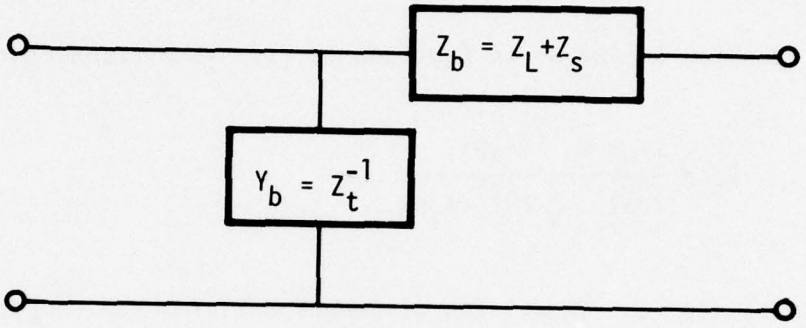

Figure B.2. Transmission line model.

and I_r is the radial current. The radial current I_r is defined as

$$I_r(a) = -\frac{dI_z}{dz} = -jhI_z(a) \tag{33}$$

The current I_z is related to the B_θ field as

$$I_z = \frac{2\pi a}{\mu_0} B_\theta(a) \tag{34a}$$

$$= -\frac{2\pi a\ jk_2^2\ BH_1^{(1)}(\lambda_2 a)}{\mu_0 \omega\ \lambda_2} \tag{34b}$$

hence

$$I_r = -\frac{2\pi a\ k_2^2\ hBH_1^{(1)}(\lambda_2 a)}{\mu_0 \omega\ \lambda_2} \tag{35}$$

Upon performing the integral in Equation 32 using Equation 15b for E_r one obtains

$$V_r = - \frac{jhB\ H_0^{(1)}(\lambda_2 a)}{\lambda_2^2} \tag{36}$$

Now, using Equation 36 and 35 in Equation 31 gives the transverse impedance

$$Z_t = \frac{j\mu_0\omega\ H_0^{(1)}(\lambda_2 a)}{2\pi a\lambda_2\ k_2^2\ H_1^{(1)}(\lambda_2 a)} \tag{37}$$

Using the small argument expression of Equation 21 for the Hankel functions gives

$$Z_t = - \frac{j\mu_0\omega}{2\pi k_2^2} \ln\left(\frac{\gamma\lambda_2 a}{2j}\right)$$

and if k_2^2 is expressed as in Equation 9, then

$$Z_t = - \frac{1}{2\pi(\sigma_2 - j\omega\varepsilon_2)} \ln\left(\frac{\gamma\lambda_2 a}{2j}\right) \tag{38}$$

The longitudinal inductive impedance is defined as

$$Z_L = - j\omega L \tag{39}$$

where L is the inductance and the minus sign appears because of the definition of F in Equation 5. The inductance is defined as

$$L = \frac{\phi}{I_z} \tag{40}$$

where the flux is

$$\phi = \int_a^\infty B_\theta \, d_r \tag{41a}$$

$$\phi = - \frac{jk_2^2 \, BH_0^{(1)}(\lambda_2 a)}{\omega \lambda_2^2} \tag{41b}$$

Hence,

$$L = - \frac{\mu_0 H_0^{(1)}(\lambda_2 a)}{2\pi a \, \lambda_2 H_1^{(1)}(\lambda_2 a)} \tag{42}$$

or again, for small arguments

$$L = - \frac{\mu_0}{2\pi} \ell n \left(\frac{\gamma \lambda_2 a}{2j} \right) \tag{43}$$

and then

$$Z_L = \frac{j\omega\mu_0}{2\pi} \ell n \left(\frac{\gamma \lambda_2 a}{2j} \right) \tag{44}$$

The surface or skin impedance is defined as

$$Z_s = \frac{E_z(a)}{I_z} \tag{45}$$

Using Equations 15a and 34b in Equation 45 one gets

$$Z_s = \frac{j\mu_0 \omega \lambda_2}{2\pi a k_2^2} \quad \frac{H_0^{(1)}(\lambda_2 a)}{H_1^{(1)}(\lambda_2 a)} \tag{46}$$

If it is assumed that σ_1 is very large, which it will always be, then

$$k_1^2 \approx j\mu_0\sigma_1\omega$$

and thus

$$Z_s = \frac{k_1^2\lambda_2}{2\pi a\sigma_1 k_2^2} \frac{H_0^{(1)}(\lambda_2 a)}{H_1^{(1)}(\lambda_2 a)} \tag{47}$$

Now, using Equation 18 in Equation 47 gives

$$Z_s = \frac{\lambda_1}{2\pi a\sigma_1} \frac{J_0(\lambda_1 a)}{J_1(\lambda_1 a)} \tag{48}$$

and since $\lambda_1 \approx k_1 \approx \sqrt{j\omega\mu_0\sigma_1}$ and using the asymptotic expansion for the Bessel's function (Equation 23) finally gives

$$Z_s = \frac{(1-j)}{2\pi a\sqrt{2}} \sqrt{\frac{\omega\mu_0}{\sigma_1}} \tag{49}$$

In summary then, the longitudinal impedance Z_b is

$$Z_b = Z_s + Z_L$$

where

$$Z_s \approx \frac{(1-j)}{2\pi a\sqrt{2}} \sqrt{\frac{\omega\mu_0}{\sigma 1}} \qquad (49)$$

and

$$Z_L \approx \frac{j\omega\mu_0}{2\pi} \ln\left(\frac{\gamma\lambda_2 a}{2j}\right) \qquad (44)$$

The transverse admittance is

$$Y_b = - \frac{2\pi(\sigma_2 - j\omega\varepsilon_2)}{\ell n \left(\frac{\gamma\lambda_2 a}{2j}\right)} \tag{50}$$

The distributed resistance and inductance per unit length are

$$R = \mathcal{R}(Z_b) \tag{51a}$$

$$L = \frac{\mathcal{I}(Z_b)}{-\omega} \tag{51b}$$

and the conductance and capacitance are

$$G = \mathcal{R}(Y_b) \tag{51c}$$

$$C = \frac{\mathcal{I}(Y_b)}{-\omega} \tag{51d}$$

The propagation constant h can now be defined as

$$h = j\sqrt{Z_b Y_b} \tag{52}$$

which is the same as the h defined in Equation 30b. The characteristic impedance Z_0 for the transmission line is

$$Z_0 = \sqrt{\frac{Z_b}{Y_b}} \tag{53}$$

It turns out that in order to obtain the proper values of Z_b and h using the methods of this section the λ_2 of Equation 30a must be altered. Reference 2 discusses the fact that if λ_2 of Equation 30a is used in Equa-

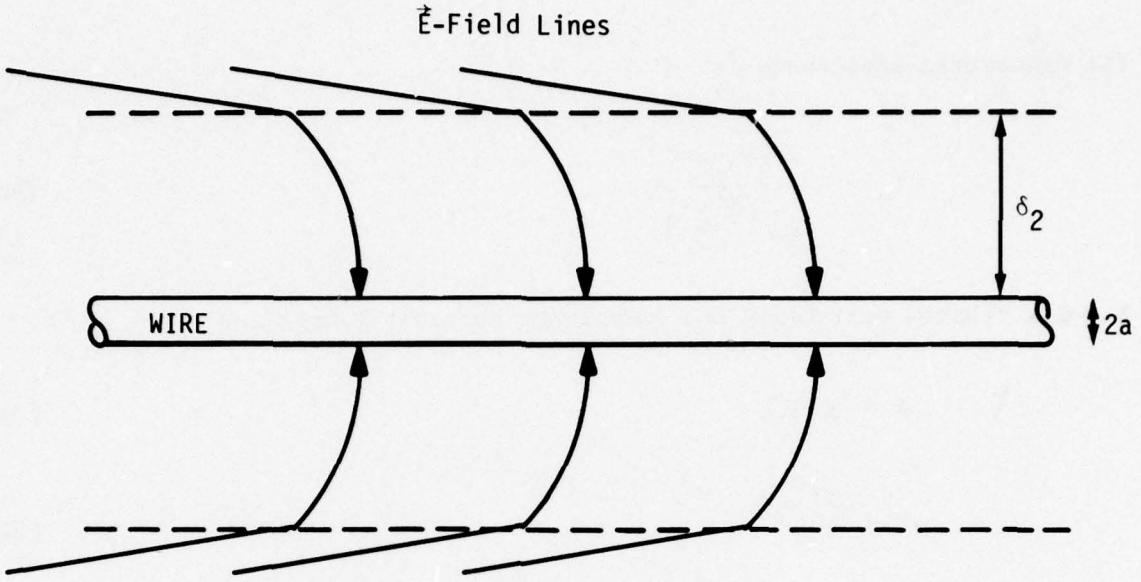

Figure B.3. Electric field near wire.

tion 44 for Z_L then Z_L will have a negative real part. Hence, the following *ad hoc* change should be made before any of the quantities of Section 2 are calculated. Let λ_2 of Equation 30a be changed so that $\lambda_2^* = |c| + jd$. Hence, make the real part of λ_2 positive before using it to calculate Equation 44 or 50.

Even simpler expressions for Z_b and Y_b can be obtained if one uses a coaxial transmission line model. Since the cylindrical conductor is surrounded by earth which is a poorly conducting dielectric, one would expect that the fields produced by the conducting cylinder would be greatly diminished at a skin depth, δ_2, into the earth. An idealized version of the field pattern around the cylinder excited by an axially directed electric field is shown in Figure 3. At the distance $r = a + \delta_2$ a cylinder drawn parallel to, and coaxial with, the wire intersects the fields at nearly right angles, so that such a surface is approximately an equipotential. Hence, if a conducting cylinder were placed at the radius $r = a + \delta_2$ the field path between the wire and the conducting cylinder would not be severely distorted. Thus, a coaxial transmission line has been constructed which is filled with a conducting dielectric, the earth.

$$Z_t = - \frac{1}{2\pi(\sigma_2 - j\omega\varepsilon_2)} \ln\left(\frac{a}{a+\delta_2}\right) \tag{54}$$

$$Z_L = \frac{j\omega\mu_0}{2\pi} \ln\left(\frac{a}{a+\delta_2}\right) \tag{55}$$

and

$$Z_s = \frac{(1-j)}{\sqrt{2}} \frac{1}{2\pi a} \left(\frac{\omega\mu_0}{\sigma_1}\right)^{1/2} \tag{56}$$

In comparing the above expressions with the previously derived impedances we see that Equations 54 and 55 differ from Equations 38 and 44 only in the $\ln$ term. Note also that this is where the starting value for ξ_0 (Equation 29a) comes from.

B.3. BARE WIRE AT AIR-EARTH INTERFACE

The problem of a bare cable lying on the surface of the earth is a difficult problem to solve exactly. This is due to the multiplicity of interfaces which must be considered. However, by the use of the transmission line model developed in Section 2 and by the use of several assumptions the problem as shown in Figure 4a can be solved approximately.

Consider first the total transverse admittance Y_{bs}. It can be argued that the total admittance is the adminttance of the earth in parallel with the admittance of the air. However, because of the high conductivity of the earth, the earth produces an admittance which is much larger than that of the air. Hence, the transverse admittance is just half the transverse admittance of the buried cable, giving

$$Y_{bs} = \frac{1}{2} Y_b \tag{57}$$

where Y_b is from Equation 50.

It has been assumed throughout this report that the permeability of all media is just μ_0. Hence, since μ_0 is the same across the air-earth interface, then the magnetic field lines will show no appreciable deviation from those of the buried cable. Therefore, Z_{Ls} is the same as Z_L of Equation 44. The skin impedance, Z_s, is not altered by the interface so the total longitudinal impedance does not change. The propagation constant is then

$$h = j \frac{\sqrt{Y_b Z_b}}{\sqrt{2}} \tag{58}$$

where Y_b and Z_b are those quantities calculated in Section 2.

B.4. DIELECTRICALLY COATED WIRE IN EARTH

Consider now the cable which is coated with a dielectric of thickness t as shown in Figure 1b. Assume that the thickness t is much less than the skin depth of the dielectric, that is

$$t << \sqrt{\frac{2}{\omega \mu_0 \sigma_3}}$$

Thus, the covering will have little effect on the magnetic flux generation relative to that of the bare wire and the inductive impedance Z_L, will not change much from that of the bare wire in Section 2.

The covering does, however, have a very strong effect on the transverse admittance since the covering will block the flow of conduction current between the wire and the earth. The coated wire can be approximated by a single bare wire of radius $a+t$ for the purpose of determing the transverse admittance from the outer surface to the earth. Hence, from Equation 50

$$Y_{C(SOIL)} = - \frac{2\pi(\sigma_2 - j\omega\varepsilon_2)}{\ell n\left(\frac{\gamma\lambda_2(a+t)}{2j}\right)} \tag{59}$$

The transverse admittance through the covering can be approximated by considering a coaxial transmission line field with the covering dielectric to give

$$Y_{C(COVERING)} = - \frac{2\pi(\sigma_3 - j\omega\varepsilon_3)}{\ell n\left(\frac{a}{a+t}\right)} \tag{60}$$

The total transverse admittance to just the series sum of the above two admittances given by

$$Y_t = \frac{Y_{cs}\, Y_{cc}}{Y_{cs}+Y_{cc}} \tag{61}$$

B.5. DIELECTRICALLY COATED WIRE ON SURFACE

If the coated cable of Section 4 is lying on the surface as in Figure 4b then only the transverse admittance is altered. As for the case of the bare wire on the surface the total transverse admittance is just half that of the buried case, thus giving

$$Y_{ts} = \frac{1}{2} Y_t \tag{62}$$

where Y_t is from Equation 61.

B.6. TWO CONDUCTORS BURIED IN THE EARTH

The case where two conducting cables are buried parallel to one another in the earth, Figure 5a, can be analysed as a three-conductor transmission line. The third conductor is ground which will be taken as

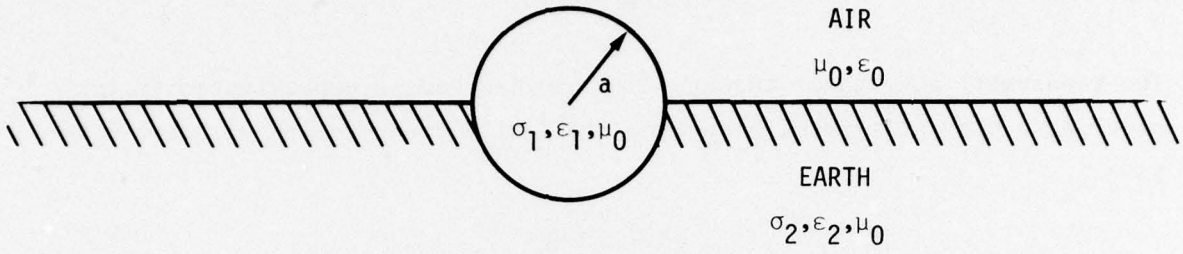

a. Bare cable

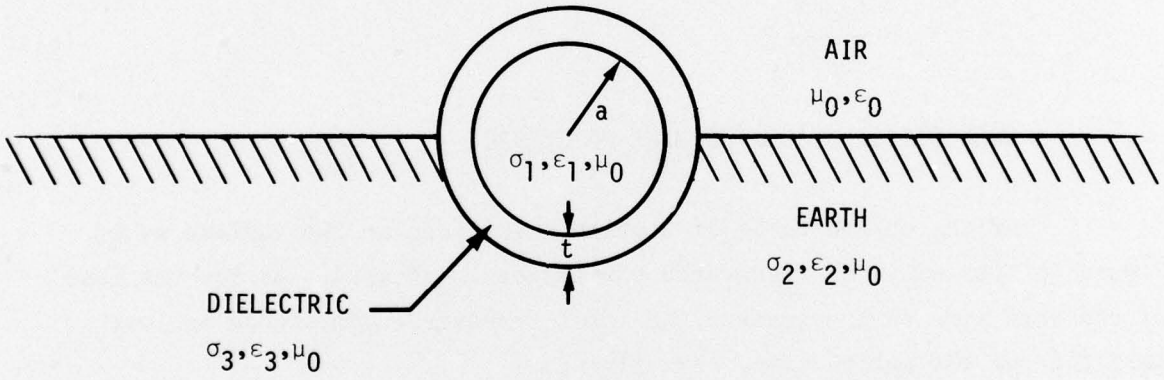

b. Insulated cable

Figure B.4. Surface cable configurations.

a common reference point. In order to determine the two propagation constants of this multiconductor system it is necessary to know the series self impedance Z_{ii} per unit length and the shunt self admittance Y_{ii} per unit length between each conductor and the ground. These self impedance and admittance terms are just the longitudinal impedance and the transverse admittances determined in Sections 2 and 4. In addition, it is necessary to know the mutual admittance Y_{ij} and impedance Z_{ij} per unit length between the two conductors. A drawing of this transmission line model is shown in Figure 6.

Since the self impedances and admittances with the ground were already evaluated in Sections 2 and 5, then all that is left is to evaluate the mutual capacitance, inductance and conductance between the two conductors. For the configuration shown in Figure 5a, Smythe[6] gives the mutual capacitance and conductance as

$$C_{12} = 2\pi\varepsilon_2 \left[\cosh^{-1}\left(\frac{D^2-R_1^2-R_2^2}{2R_1R_2}\right)\right]^{-1} \tag{63}$$

$$G_{12} = 2\pi\sigma_2 \left[\cosh^{-1}\left(\frac{D^2-R_1^2-R_2^2}{2R_1R_2}\right)\right]^{-1} \tag{64}$$

The problem of determining the mutual inductance between the two cables is much more complicated. Short of neglecting the mutual inductance, the best approximation which seems possible is the analysis of the mutual indictance between two thin, tightly coupled wires of length ℓ. This value of M_{12} is given by Schelkunoff and Friis[7] as

$$M_{12} = \frac{\mu_0}{2\pi}\left(\ell n\,\frac{\lambda}{2\pi D} + 0.116 + C_i(\beta\ell) - \frac{\sin\beta\ell}{\beta\ell}\right) \tag{65}$$

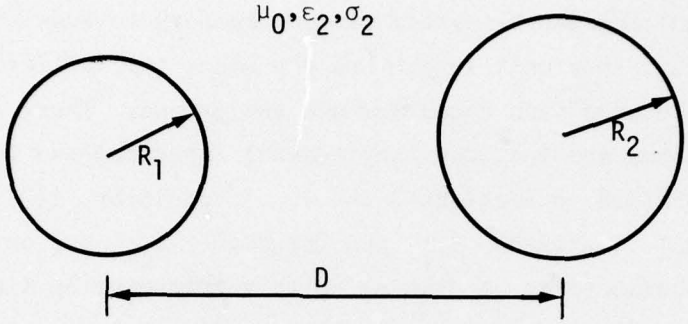

a. Buried

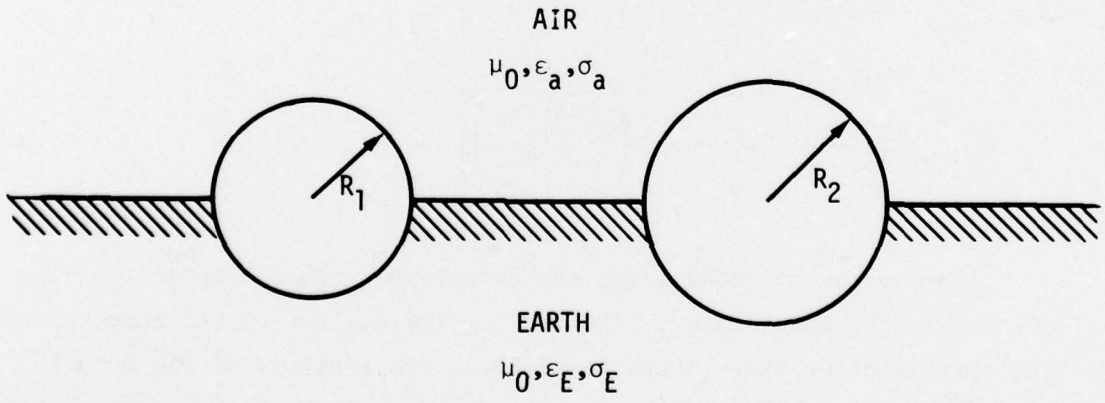

b. Surface

Figure B.5. Two conductor configurations.

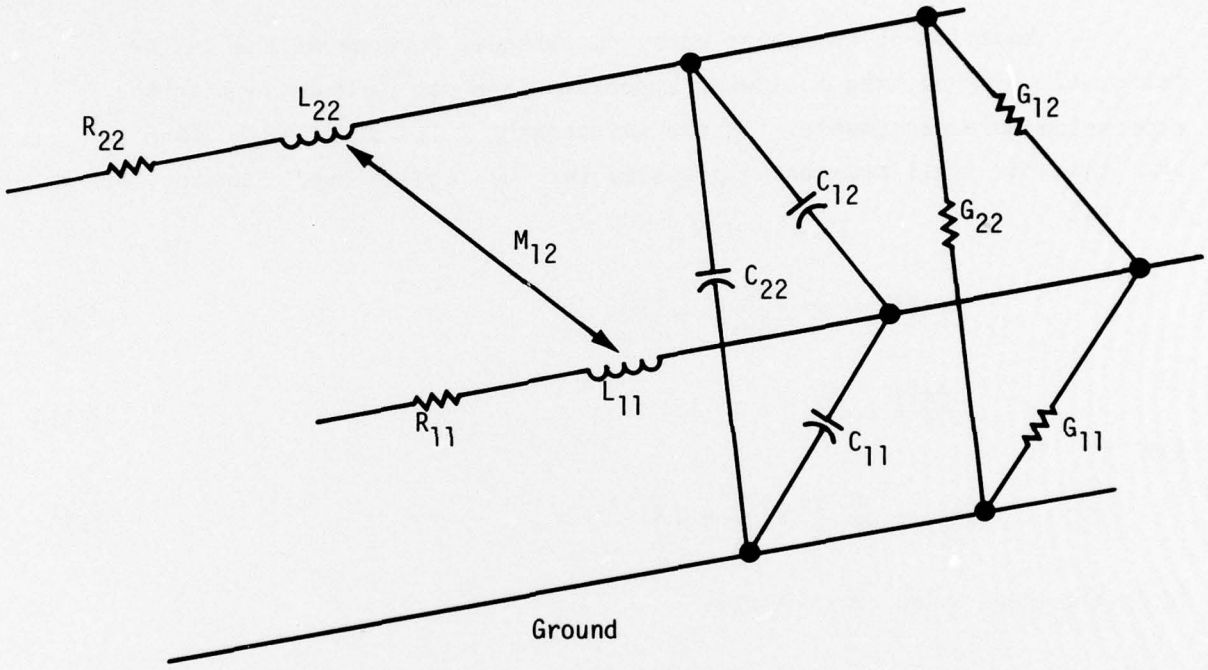

Figure B.6. Equivalent circuit of coupled transmission lines.

where ℓ is the length of the wires, β is $2\pi/\lambda$, and C_i is the cosine integral. This expression is valid only if the wavelength λ and the length ℓ are much greater than the spacing D and the radius of the wires. This criteria will usually be valid for the cables we are attempting to analyse.

Equation 65 is rather messy to evaluate because of the cosine integral. However, the following approximations can be made to make the expression more manageable. If the wavelength λ is much larger than $2\pi\ell$ then the small argument expression for C_i can be used. Hence, for $\lambda >> 2\pi\ell$

$$C_i(\beta\ell) \approx \ell n \frac{2\pi\ell}{\lambda} + 0.577 \tag{66a}$$

$$\frac{\sin\beta\ell}{\ell} \approx 1 \tag{66b}$$

and

$$M_{12} \approx \frac{\mu}{2\pi} \left(\ell n \frac{2\ell}{D} - 1 \right) \tag{67}$$

If on the other hand $\ell << \lambda$ then

$$C_i \to 0 \tag{68a}$$

$$\frac{\sin\beta\ell}{\beta\ell} \to 0 \tag{68b}$$

and

$$M_{12} \approx \frac{\mu}{2\pi} \left(\ell n \frac{\lambda}{2\pi D} - 1 \right) \tag{69}$$

It has been found that a good transmition point between the two approximations, Equations 67 and 69 is when

$$\ell n\ \lambda = -\ 1.116 + \ell n\ 4\pi + \ell n \ell \tag{70}$$

Note that in the determination of the mutual inductance the length of the lines, ℓ, enters into the calculation. Thus, it is necessary to estimate this length but its actual value is not extremely critical since ℓ only appears in the ℓn term.

Once all of the necessary impedances and admittances have been determined it is next necessary to determine the two propagation constants Γ_1 and Γ_2 which are, in relation to z, defined as

$$e^{\Gamma_1 z} \quad \text{and} \quad e^{\Gamma_2 z}$$

as opposed to h of the previous sections which was defined in Equation 5 as

$$e^{jhz}$$

To determine Γ_1 and Γ_2 it is first necessary to form the impedance and admittance matrices[8]

$$\overline{Z} = \begin{bmatrix} R_{11} + j\omega L_{11} & j\omega L_{12} \\ j\omega L_{12} & R_{22} + j\omega L_{22} \end{bmatrix} \tag{71}$$

$$\overline{Y} = \begin{bmatrix} G'_{11} + j\omega C'_{11} & G'_{12} + j\omega C'_{12} \\ G'_{12} + j\omega C'_{12} & G'_{22} + j\omega C'_{22} \end{bmatrix} \tag{72}$$

where

$$G'_{11} = G_{11} + G_{12}$$
$$G'_{12} = - G_{12}$$
$$G'_{22} = G_{22} + G_{12}$$
$$C'_{11} = C_{11} + C_{12}$$
$$C'_{22} = C_{22} + C_{12}$$
$$C'_{12} = -C_{12}$$

The propagation constants Γ_1 and Γ_2 are then the square roots of the two eigenvalues of the matrix

$$\overline{ZY} = \overline{Z} \times \overline{Y} \tag{73}$$

Hence

$$|\overline{ZY} - \Gamma_i^2 \, I| = 0 \tag{74}$$

determines the values of Γ_1 and Γ_2 where I is the identity matrix and the brackets $| \, |$ denote the determinant. Working out the details of Equation 74 one finds that

$$\Gamma_{1,2}^2 = \frac{(a_1+a_4) \pm \sqrt{(a_1+a_4)^2 - 4(a_1a_4-a_3a_2)}}{2} \tag{75}$$

where

$$a_1 = Z_{11}Y'_{11} + Z_{12}Y'_{12}$$
$$a_2 = Z_{11}Y'_{12} + Z_{12}Y'_{22}$$
$$a_3 = Z_{12}Y'_{11} + Z_{22}Y'_{12}$$
$$a_4 = Z_{12}Y'_{12} + Z_{22}Y'_{22}$$

The + sign in Equation 75 will give the common mode and the - sign will give the differential mode. The currents and voltages on the two lines are then

$$\begin{bmatrix} V_1' \\ \\ V_2' \end{bmatrix} = \begin{bmatrix} V_{01}' \\ \\ V_{02}' \end{bmatrix} e^{-\Gamma_{1,2} z} \tag{76a}$$

$$\begin{bmatrix} I_1' \\ \\ I_2' \end{bmatrix} = \begin{bmatrix} I_{01}' \\ \\ I_{02}' \end{bmatrix} e^{-\Gamma_{1,2} z} \tag{76b}$$

where the prime indicates that these are transformed voltages and currents. The true currents and voltages on the line are related to the primed values through the eigenvectors of the matrix $\overline{ZY}$. Hence

$$\begin{bmatrix} V_1 \\ \\ V_2 \end{bmatrix} = \begin{bmatrix} T_{11} & T_{21} \\ \\ T_{12} & T_{22} \end{bmatrix} \begin{bmatrix} V_1' \\ \\ V_2' \end{bmatrix} \tag{77a}$$

and

$$\begin{bmatrix} I_1 \\ \\ I_2 \end{bmatrix} = \begin{bmatrix} T_{11} & T_{21} \\ \\ T_{12} & T_{22} \end{bmatrix} \begin{bmatrix} I_1' \\ \\ I_2' \end{bmatrix} \tag{77b}$$

The eigenvectors,

$$T_1 = \begin{bmatrix} T_{11} \\ \\ T_{12} \end{bmatrix} \tag{78a}$$

$$T_2 = \begin{bmatrix} T_{21} \\ \\ T_{22} \end{bmatrix} \tag{78b}$$

are associated with the eigenvalues Γ_1^2 and Γ_2^2 respectively. These values can be obtained as

$$T_{11} = 1 \tag{79a}$$

$$T_{12} = \frac{\Gamma_1^2 - a_1}{a_2} \tag{79b}$$

$$T_{21} = 1 \tag{79c}$$

$$T_{22} = \frac{\Gamma_2^2 - a_1}{a_2} \tag{79d}$$

The values of the distributed parameters for a coupled two cable buried transmission line have been determined here. The resulting propagation constants Γ_1 and Γ_2 were also calculated. Note that if the mutual terms are zero, then Γ_1 and Γ_2 are just the propagation constants of the individual lines calculated in Sections 2 and 4 multiplied by j or

$$\Gamma_{1,2} = j\ h$$

B.7. TWO CONDUCTORS ON THE SURFACE OF THE EARTH

If the two parallel cables analysed in Section 6 are lying on the air-earth interface as shown in Figure 6b, then it is necessary to alter the elements of the impedance and admittance terms $\overline{Z}$ and $\overline{Y}$. The self terms Z_{ii} and Y_{ii} are just those calculated in Sections 3 and 5 and the mutual terms are similar to those of Section 6 with the following modifications.

Since the wires are on the air-earth interface as in Figure 6b then it can be argued that the mutual capacitance between the wires is just that through the air and that through the earth in parallel, that is

$$C_{12} = 2\pi \left(\frac{\varepsilon_a}{2} + \frac{\varepsilon_g}{2} \right) \left[\cosh^{-1} \left(\frac{D^2 - R_1^2 - R_2^2}{2R_1R_2} \right) \right]^{-1} \tag{80}$$

For most purposes $\varepsilon_a << \varepsilon_g$ and can be ignored. Similarly the mutual conductance is just a parallel combination of the conductance through the earth and through the air, giving

$$G_{12} = 2\pi \left(\frac{\sigma_a}{2} + \frac{\sigma_g}{2} \right) \left[\cosh^{-1} \left(\frac{D^2 - R_1^2 - R_2^2}{2R_1R_2} \right) \right]^{-1} \tag{81}$$

Again, σ_a is generally zero and can be ignored.

The mutual inductance does not change from that of Equation 65, 67 and 69 because the permeability of the air and the earth are taken to be the same.

The propagation constants Γ_1 and Γ_2 are determined in precisely the same manner as outlined in Section 6.

REFERENCES

1. Marston, D.R., and W.R. Graham, Currents Induced in Cables in the Earth by a Continuous Wave Electromagnetic Field, EMP Interaction Note 24,

2. Hill, J.R., and M.R. Wilson, Buried Cable Transmission Line Parameters: A Comparison of Two Theoretical Models, AMRC-N-5, March 1973.

3. Jahnke, E., and F. Emde, Table of Function, Dover, New York, 1945.

4. Stratton, J.A., Electromagnetic Theory, McGraw Hill, New York, 1941.

5. Ramo, S., J.R. Whinnery, T. Van Duzer, Fields and Waves in Communications Electronics, John Wiley, New York, 1965.

6. Smythe, W.R., Static and Dynamic Electricity, McGraw Hill, New York, 1968.

7. Schleikunoff, S.A., and H.T. Friis, Antennas Theory and Practice, John Wiley, New York, 1952.

8. Vance, E.F., Coupling to Cables, DNA Handbook Revision, Chapt. 11, December 1974.

DISTRIBUTION LIST

DEPARTMENT OF DEFENSE

Defense Documentation Center
Cameron Station
12 cy ATTN: TC

Director
Defense Nuclear Agency
ATTN: DDST
ATTN: TISI, Archives
ATTN: SPTD, Major Skarupa
ATTN: SPSS
ATTN: RAEV
3 cy ATTN: TITL, Tech. Library

Commander
Field Command
Defense Nuclear Agency
ATTN: FCPR
ATTN: FCTMD
ATTN: FCTME
5 cy ATTN: FCTMOF

Director
Interservice Nuclear Weapons School
ATTN: Document Control

Chief
Livermore Division, Fld. Command, DNA
Lawrence Livermore Laboratory
ATTN: FCPRL

Dir. of Defense Rsch. & Engrg.
ATTN: S&SS(OS)

DEPARTMENT OF THE ARMY

Commander
Harry Diamond Laboratories
ATTN: DRXDO-NP

U.S. Army Engr. Waterways Exp. Sta.
ATTN: J. D. Day

DEPARTMENT OF THE NAVY

Officer-In-Charge
Naval Surface Weapons Center
ATTN: Code WA501, Navy Nuc. Prgms. Off.

DEPARTMENT OF THE AIR FORCE

AF Weapons Laboratory, AFSC
ATTN: SUL
ATTN: DYC
ATTN: DYV, Maj Mitchell

Headquarters USAF/RD
ATTN: RDQSM

SAMSO/MN
ATTN: Maj D. Shaughnessy
ATTN: MNNH, Maj Gage

DEPARTMENT OF THE AIR FORCE (Continued)

Space & Missile Systems Org.
ATTN: Capt Careway

DEPARTMENT OF ENERGY

University of California
Lawrence Livermore Laboratory
ATTN: Tech. Info. Dept. L-3
ATTN: Harry Reynolds, L-21
ATTN: O. T. Vik, L-24
ATTN: Billy Hudson, L-48
ATTN: Jeff Thomson/Dr. Glenn, L-200
ATTN: J. Morton, L-45

Los Alamos Scientific Laboratory
ATTN: Doc. Control for Robert Thorn
ATTN: Doc. Control for Paul Whalen
ATTN: Doc. Control for Reports Lib.
ATTN: Doc. Control for C. Keller
ATTN: Doc. Control for Robert Brownlee
ATTN: Doc. Control for Harold Agnew
ATTN: Doc. Control for Dr. McQueen, J-DOT
ATTN: Doc. Control for R. Scammon
ATTN: Doc. Control for Mr. Eiler, J-15

Sandia Laboratories
ATTN: Doc. Control for 3141, Sandia Rpt. Coll.
ATTN: Doc. Control for J. W. Allen
ATTN: Doc. Control for Dr. Plimpton, 1112
ATTN: Doc. Control for Dr. Dolce, 1111A
ATTN: Doc. Control for Mr. Cook, 1116

DEPARTMENT OF DEFENSE CONTRACTORS

The Boeing Company
ATTN: R. Bardon

Charles Stark Draper Laboratories, Inc.
ATTN: S. Cohen

Effects Technology, Inc.
ATTN: W. Naumann

EG&G, Inc.
ATTN: W. R. Kitchen

Electromechanical Systems of New Mexico
ATTN: R. A. Shunk

General Electric Company
Tempo-Center for Advanced Studies
ATTN: DASIAC, Mr. Dudash

General Electric Company
Re-Entry & Envir. System Div.
ATTN: J. Wainnas

H-Tech Laboratories, Inc.
ATTN: Dr. Hartenbaum

DEPARTMENT OF DEFENSE CONTRACTORS (Continued)

Jaycor
ATTN: Ralph Stahl

Kaman Sciences Corporation
ATTN: H. Hollister

Lockheed Missiles & Space Co., Inc.
ATTN: E. Summer

Lockheed Missiles and Space Co., Inc.
ATTN: R. Nobles, Dept. 52-11

Mission Research Corp.
ATTN: C. Longmire
5 cy ATTN: Doc. Control

Mission Research Corporation
ATTN: John B. Smyth
ATTN: Victor A. J. van Lint
ATTN: Michael A. Messier

Physics International Co.
ATTN: Coye Vincent

R & D Associates
ATTN: Technical Library
ATTN: Cyrus P. Knowles

DEPARTMENT OF DEFENSE CONTRACTORS (Continued)

Science Applications, Inc.
ATTN: R. I. Miller

Science Applications, Inc.
ATTN: James Cramer

Science Applications, Inc.
ATTN: K. Sites

Science Applications, Inc.
ATTN: L. Scott

SRI International
ATTN: Mr. Keough
ATTN: Mr. DiCarli

Systems, Science and Software, Inc.
ATTN: H. Kratz
ATTN: Dr. Grine
ATTN: Dr. Coleman

Tech Reps, Inc.
ATTN: R. Holmes

TRW Defense & Space Systems Group
ATTN: Dr. Lieberman